Development of a Chemical Surrogate for JP-8 Aviation Fuel

Using a Pressurized Flow Reactor

A Thesis

Submitted to the Faculty

of

Drexel University

by

Alessandro Agosta

in partial fulfillment of the

requirements for the degree

of

Master of Science

in

Mechanical Engineering

May 2002
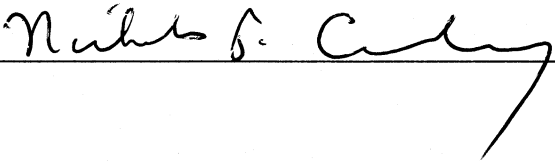
Thesis Approval Form

This thesis, entitled <u>DEVELOPMENT OF A CHEMICAL SURROGATE FOR JP-8</u>

<u>AVIATION FUEL USING A PRESSURIZED FLOW REACTOR</u>

_____and authored

by <u>Alessandro Agosta</u>, is hereby accepted and approved.
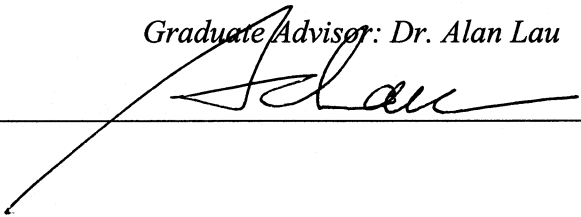
Signatures:

Co-Supervising Professor: Dr. Nicholas P. Cernansky
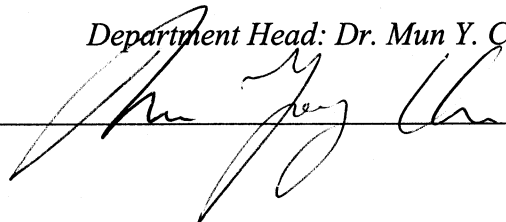
_____

Co-Supervising Professor: Dr. David L. Miller

_____

Graduate Advisor: Dr. Alan Lau

_____

Department Head: Dr. Mun Y. Choi

_____

ACKNOWLEDGEMENTS

I would like to express my sincere and profound gratitude to both my advisors, Professor Nicholas P. Cernansky and Professor David L. Miller for their guidance and support throughout this research project as well as for their friendship during my graduate education at Drexel University. Special thanks are extended to Professor Mun Y. Choi for his invaluable friendship. Through their dedication to research and teaching they have inspired me in new directions for my career.

A big credit goes to the Faculty at Drexel University and, in particular, to Dr. Bakhtier Farouk, Dr. Alan Lau, and Dr. Horacio Sosa. Thanks also to the present and past staff in the Mechanical Engineering Department, particularly Rita Marasa and Kathie Donahue. The technical staff at the Hess Research Lab, particularly George Carenzo, was very helpful with the troubleshooting and upgrade of the experimental facilities. I also owe an appreciation to Hess Lab Manager, Dr. William Danley, for his excellent support throughout both my research and teaching activities.

I wish to thank all my friends and fellow researchers in the Hess Lab for their contributions and support to my research work. In random order, David Lenhert (huge contribution!), Mary Emig, Weiying Yang, Jincai Zheng, and Richard Billmers.

I am very grateful to all my friends and family who have taken good care of me during the last two years. Their true friendship and love was (and is) utterly amazing. I thank especially my friend Simona, whose friendship is one of the best gifts I had in the past two years. And then: my mom Paola, my dad Enzo, and my brother Giampaolo; the magic Italian connection: Andrea and Matteo; Anna and Murat, Ceylan and Ahmet; Carl,

John, Maria, Karen, Stacie, Nick, Marco, Jason, Jean, George, Gi Young, Gwenaelle, Feng, Irina, "Orologio Atomico", Laura, Charlie … and to all people I might have forgotten (sorry!). Thanks also to my friends in Italy and in the rest of the world who showed me that a true friendship goes beyond any geographical barrier: Giancarlo, Paolo C., Valerio, Teresa, Karin, and in particular Erika and "Dr." Paolo G.. Finally, last but not least, a special hug to Taxi and all his family!

TABLE OF CONTENTS

LIST OF TABLES

LIST OF FIGURES

ABSTRACT

Development of a Chemical Surrogate for JP-8 Aviation Fuel
Using a Pressurized Flow Reactor
Alessandro Agosta
Nicholas P. Cernansky
David L. Miller

The next generation of military vehicles will demand higher performance propulsion systems that deliver increased power, fuel efficiency, and lower observable emissions. There is strong evidence that low and intermediate temperature hydrocarbon fuel chemistry controls the important preignition processes through heat release and formation of reactive species. The elucidation of the rate controlling chemical mechanisms during these phases of operations remains an important goal of combustion chemistry as it applies to engine and vehicle systems. This study is an effort to expand the actual knowledge of the chemistry controlling the ignition of single and multi-component mixtures of full boiling range distillate hydrocarbon fuels (diesel and jet fuels) as well as to develop a surrogate for the complex military aviation fuel JP-8.

The oxidation and ignition characteristics of pure alkanes (n-dodecane and isocetane), naphthenes (methylcyclohexane and decalin), and aromatics (α-methylnaphthalene and hexylbenzene) and of their mixtures have been experimentally studied using the Drexel Pressurized Flow Reactor and our CO reactivity mapping technique. A negative temperature coefficient (NTC) region has been clearly identified for both the alkanes and naphthenic compounds through several controlled cool down (CCD) bench scale tests.

The analysis of the interactions controlling the ignition of binary, ternary and larger mixtures of the compounds listed above has been applied to the synthesis of a multi-component surrogate for the worldwide utilized aviation fuel JP-8. The surrogate has been tailored to closely match the hydrocarbon distribution in JP-8: a mixture containing 26% n-dodecane, 36% isocetane, 18% α-methylnaphthalene, 14% methylcyclohexane, and 6% decalin, was shown to accurately reproduce the chemical behavior of JP-8 over different experimental conditions. Due to its compositional reproducibility and tractability, the JP-8 surrogate is suitable for both well-controlled fundamental modeling and experimental studies in lieu of the otherwise complex and chemically undefined parent fuel. A cooperative effort is ongoing with the group of Prof. E. Ranzi at Politecnico di Milano, Italy, to extend their hierarchically constructed semi-detailed kinetic model already available for the oxidation of alkanes and simple aromatic molecules, in order to model the oxidation of the JP-8 surrogate (and thus of the parent fuel) in the low and intermediate temperature regions. The experiments have been carried out over a range of reaction conditions that are representative of actual engine conditions prior to and during the ignition process. Therefore, results from this study provide useful kinetic and mechanistic information to formulate hypotheses on autoignition mechanisms, to determine the relative effect of the various classes of components within multi-component mixtures, and to provide combustion models that can be used in the design and evaluation of combustors and engine systems.

CHAPTER 1 – REAL FUELS AND THEIR SURROGATES

1.1 INTRODUCTION

Although the economic slowdown in the highly developed countries, mainly the United States and the Western European Countries, the world consumption of fuels is expected to constantly increase in the long term. The 2002 Annual Energy Outlook (AEO, 2001) study conducted by the US Department of Energy (DOE) and the National Energy Information Center (EIA) states that the U.S. petroleum consumption is projected to increase by 6.9 million barrels per day in the next twenty years, reaching the 57.5 million barrels per day value in the year 2020.

This study reports projections on fuels consumption based on the results from the EIA's National Energy Modeling System (NEMS). The analysis presents the detailed study of a reference case forecast and a set of alternative cases that assume respectively higher and lower economic growth than in the reference case. Just considering the Transportation sector, which represented more than two-thirds of the petroleum based fuels consumption in the year 2000 (see Figure 1.1), the use of transportation fuels is predicted to increase by 6.0 million barrels per day in the reference case, 4.9 million in the low economic growth case, and 7.1 million in the high economic growth case. The second largest sector is the Industrial sector, which in 2000 accounted approximately for 25% of the consumption of petroleum fuels. For this sector, the reference case forecast of fuel consumption in the year 2020 is estimated to be higher than in 2000 by 1.3 million barrels per day, while being 0.8 million greater in the low economic growth case, and 2.0 million greater in the high economic growth case. The other two sectors of petroleum-

based fuels considered in this study are the Residential and Commercial sectors. As shown in Figure 1.1 for the reference case, the Residential fuel use, which represents a considerably smaller portion of the whole consumption, is projected to monotonically decrease from approximately 1.46 million barrels per day in 2000 to 1.2 million barrels per day in 2020, resulting in a projected annual decline of about 0.7%. Finally, the Commercial sector is seen almost steady in the next twenty years, growing at a modest 0.4% rate per year.

Although these statistics are inevitably subject to change, they provide an essential insight on the current and future applications of the primary source of energy on the earth, the petroleum-based fuels. Moreover, they lead us to focus our attention to the Transportation sector, which is, and will be, the largest sector of fuel consumption by far. Figure 1.2 shows the projected trends of growth in this sector. The majority of this growth stems from increased consumption of "light products", mainly gasoline, diesel, and jet fuels.

The oxidative behavior of jet fuels, and in particular the military jet fuel JP-8, is the subject of this study. As shown by the EIA's reference case forecast, the already large class of jet fuels will expand in the future. Both on the environmental, economical and chemical platforms, the current and next generations of military and civil aircrafts require higher performance jet fuels. For these reasons, the study of jet fuels is of extreme interest. An overview of jet fuels is presented in the next section followed by a more detailed analysis of the relevant fuel specifications and surrogates.

1.2 JET FUELS

Since the end of the First World War, aviation has continuously grown at a very fast rate, nowadays becoming an essential element of our modern society. It provides the fastest means of transportation, both for people and goods, shortening the distances between different countries and cultures.

The growth of aviation is in turn reflected in the increase of jet fuel consumption over the years. As shown in Table 1.1 and in Figure 1.3, considering only the past decade, the world consumption of jet fuels has increased by more than 10%, especially in the Western European Countries, Oceania, and North America.

Table 1.1 Jet Fuels - World Consumption

AREA	1990	1992	1994	1996	1998
NORTH AMERICA	69	66	69	72	74
WESTERN EUROPE	27	28	31	34	38
EASTERN EUROPE & FORMER CIS	24	18	12	11	12
FAR EAST & OCEANIA	20	25	31	36	35
OTHERS	18	17	20	20	19
TOTAL	**158**	**154**	**163**	**173**	**178**

Fuels consumption in [Million Gallons / day]
Source: Chevron, (2000) - "Aviation Fuels Technical Review (FTR3)", Chevron Products Company, USA.

Mainly due to the difficulties in the growth of the air travel market after the September 11th events, jet fuel consumption is projected to increase at a slower rate through the decade 2000-2010 than it did in the 1990s. However, according to the reference case forecast prepared by the EIA, the recovery of the economic growth and the low projected jet fuel prices will reflect into a 3.5% projected annual increase in air travel, in turn causing jet fuel use to increase at a faster rate in the 2010s. Actually, considering the US market only, which is by far the largest single market, the consumption of jet fuel is expected to be 46.2 million gallons per day higher in 2020 than in 2000 as is shown in Figure 1.3.

Over the years, both civil and military aviation has required the continuous development of fuels in order to match the need for higher propulsion performances, lower cost, increased safety, and reduced emissions. Since the beginning of aviation history, petroleum-type fuels emerged as the most valuable type of propellants, mainly because of their volumetric energy contents, which are higher than those of gases, and their ease of distribution and handling with respect to solid fuels. Among liquid fuels, the liquid hydrocarbons mixtures offer the best combination in terms of performance, cost and availability. So, restricting the focus to the liquid hydrocarbons, in the 1930s kerosene was the first choice for jet propulsion, mainly because of its common availability and its average cost. Since 1940s, however, the United States Air Force (USAF) started to use the so-called 'wide-cut' fuel type, driven by availability concerns, especially during periods of war. The 'wide-cut' fuels are basically mixtures of hydrocarbons with boiling ranges intermediate between those of the gasoline and the kerosene fuels and are exemplified by the JP-4 fuel.

A summary of the characteristic properties, such as the fuel flash point or the average Cetane Number, for JP-4 and the other important civilian and military jet fuels, is given in Table 1.2. As can be inferred from Table 1.2, the 'wide-cut' type JP4 is well suited for cold weather because of its low freezing point. However when focusing on the Reid vapor pressure (or on the distillation range), JP4 shows a greater volatility than the kerosene-type fuels. Indeed the more volatile JP4 aviation fuel is characterized by high Reid vapor pressure (RVP_{JP4} = ~23 kPa comparing to ~1 kPa for the kerosene-type fuels) and low boiling temperature limit. Due to its high volatility, JP4 shows several operational disadvantages when compared to the kerosene-type fuels. As an example, it has greater evaporative losses at high altitudes. Because of these disadvantages, the USAF decided to reintroduce the kerosene-type fuels on its military airplanes starting from the 1970s (Chevron, 2000).

Nowadays there are three main aviation fuels, all of them of the kerosene-type: Jet A (European Jet A1), JP-5, and JP-8 (JP-8+100). Jet A and Jet A1 are the most common civilian jet fuels. The main difference between these two fuels is represented in Table 1.2 by their freezing temperatures. The low-cost Jet A has a higher freezing temperature limit than the Jet A1, so it is less suitable to be used in cold weather or on polar routes such as the trans-Atlantic routes. On the other hand the less restrictive lower freezing temperature limit of Jet A accounts for a reduced cost in the Jet A production, since it is possible to use a broader cut during the distillation process.

JP-5 is a high flash point kerosene fuel whose introduction by the United States Navy dates to the 1950s. Having a higher flash point than other military fuels, JP-5 allows for higher safety on the aircraft flying especially from aircraft carriers.

JP-8 is the kerosene-type fuel introduced in 1979 to replace the wide-cut type JP-4 for the US Air Force. Very similar to commercial Jet A, JP-8 contains a larger additive package to enhance its performance. This package includes anti-icing compounds (FSII), corrosion inhibitor compounds (CI), and anti-static compounds (SDA). In 1995 the US Air Force completed the conversion from JP-4 to JP-8. A natural development of JP-8, which has a low thermal stability limit, is JP-8+100. Since the second most important role of a jet fuel (after providing propulsion) is to act as a coolant for the engine subsystem and the airframe, the thermal stress for the fuel is extremely high (Edwards, 1993). For this reason JP-8+100 is a more complex version of JP-8 that includes another group of additives, mainly antioxidants, dispersants/detergents, metal deactivators, and solvents, that specifically improve the fuel thermal stability. It was introduced in 1998.

Finally, nowadays JP-8 is becoming of high interest not only for military aircraft, but also for ground vehicles. In fact, the U.S. Department of Defense (DOD) directive 4140.25 prescribes using JP-8 as the primary fuel support for land-based air and ground forces to improve the efficiency of its tactical bulk fuel distribution system. Therefore, the study of the oxidative behavior of JP-8 is of extreme importance to determine the feasibility of using JP-8 in lieu of diesel.

Table 1.2 Typical Aviation Fuels Properties

PROPERTY	JP-4 (NATO F-40)	JP-5 (NATO F-44)	JP-8 (NATO F-34)	JET A (/A1) (NATO F-35)
TYPE OF FUEL	WIDE-CUT	KEROSENE	KEROSENE	KEROSENE
APPROX. FORMULA	$C_{8.5}H_{17}$ [1]	$C_{12}H_{22}$ [1]	$C_{11}H_{21}$ [1]	$C_{11}H_{21}$ [1]
BOILING RANGE, [°C]	60-240 [2]	180-260 [2]	165-265 [2]	170-300 [3]
FREEZING POINT, [°C]	-62 [2]	-50 [2]	-51 [2]	-40 (Jet A) [3] -47 (Jet A1) [3]
FLASH POINT , [°C] (MINIMUM)	-23 [2]	60 [3]	38 [3]	38 [3]
REID VAPOR PRESSURE, [kPa] (RVP @ 38 °C)	~21 [3]	~1 [4]	~1 [3]	~1 [3]
CETANE NUMBER, AVG.	23 [4]	42 [4]	45 [4]	—
AVERAGE DENSITY, [g/cm³]	0.755 [4]	0.818 [4]	0.797 [4]	—
K. VISCOSITY (@ 40 °C), [cSt]	0.56 [4]	1.5 [4]	1.2 [4]	—

Sources:
[1] *Martel, C.R., (2000) - "Molecular weight and average composition of JP4, JP5, JP8 and Jet A" – Chemical Propulsion Information Agency Airbreathing Propulsion Manual, Columbia, MD.*

[2] *Coordinating Research Council, (1983) - "Handbook of Aviation Fuel Properties", Rept. 530, Coordinating Research Council Atlanta, GA.*

[3] *Chevron, (2000) - "Aviation Fuels: Technical Review", Chevron Product Company, Chevron USA Inc..*

[4] *US Army Tank-Automotive RD&E Center, (2000) - "Fuel User Guide – Average Survey Data", Fuels and Lubricants Team, Warren, MI.*

1.3 REAL AVIATION FUELS SPECIFICATIONS

Several kinds of aviation fuels are commonly available nowadays for specific applications. As an example, JP-10 and JP-9 are two typical aviation fuels specifically developed for the high demands of missile propulsion. In order to maximize their volumetric content of energy, these fuels are composed of almost pure high-density naphthenes or simple blends. In particular, JP-10 is composed of exo-tetrahydrodicyclopentadiene only, while JP-9 can be approximated as a mixture of methylcyclohexane, perhydronorbonadiene, and exo-tetrahydrodicyclopentadiene.

Nevertheless, the majority of hydrocarbons aviation fuels are mixture of more than several hundreds different compounds. The exact number of compounds in a specific fuel and their identity is unknown, since none of the current analytical techniques is powerful enough to detect and separate each molecular species. Moreover, most of the individual compounds occur at level below 1% by volume.

A mass spectrum of JP-8 has been collected using a Finnigan mass spectrometer from the Chemistry Department at Drexel University and it is shown in Figure 1.5. The high number of peaks in the spectrum demonstrates the difficulty of identifying all the different compounds that are present in the fuel. Even the most recent analysis by Edwards (2001) and Briker (Briker et al., 2001), a gas chromatography analysis coupled with flame ionization mass spectrometry detection, produced an unsatisfactory fuel compositional distribution for both Jet A and diesel fuel.

Therefore real jet fuels are formulated to meet general property limits, such as the maximum freezing point or the flash point, rather than a specified chemical composition. Nevertheless, for each particular fuel, common standards exist and limit the upper (or

lower) volumetric percentage composition of certain hydrocarbons, to insure proper quality and safety standards in the engines as well as fuel systems performances.

For example, in every jet engine, during the combustion process, small carbonaceous particles form, as it can be noticed by the visible smoke traces emitted by some engines especially during take-off. These particles can cause critical problems eventually leading to engine failures, such as turbine blades erosion or the formation of cracks inside the combustor zone. So, since aromatic hydrocarbons and in particular of the naphthalene type are a high source of these carbonaceous particles, standard aviation fuels specifications limit the maximum aromatics content up to 25% in the jet fuels, including a maximum 3% of the naphthalene type. The aromatics percentage distribution by volume inside JP-8 has been reported in the "Survey of Jet Fuels (1990-1996)" (Defense Logistic Agency, 1998) conducted by the US Defense Energy Support Center considering JP-8 purchases by the US Air Force bases over the years 1990 to 1996 and it is presented in Figure 1.4. The results show an aromatic content distribution with a mean of 18.2% and a large standard deviation of 3.1%. Nevertheless all the batches tested satisfied the 25% maximum limit on aromatics content.

However, it can also be inferred from Figure 1.4 that the aromatic content in JP-8 varied greatly from purchase to purchase, thus resulting in the impossibility of defining a precise composition of the fuel. In order to study the combustion behavior of JP-8, a fuel with well defined and reproducible composition is required for both experimental and modeling work. A fuel with a defined composition and that shows a behavior similar to that of a parent fuel is called a "surrogate". Surrogates are usually constituted of 1 to 15 hydrocarbons blended in a specific and reproducible composition. An overview of the

different kinds of surrogates and of their role on the study of combustion is presented in the next section.

1.4 SURROGATES TO REPRESENT COMPLEX REAL FUELS

Several surrogates have been proposed to represent complex real fuels, both of the aviation and automotive type. A surrogate is a mixture of a limited number of hydrocarbons with a well defined and reproducible composition that can be used in place of the real fuel both for experimental and computational applications. In fact, surrogates of real fuels are of extremely high interest since they can be utilized to study the effect of chemical composition and fuel properties in lieu of their parent fuel. Moreover they can provide essential information for the development of numerical codes and kinetic models. In both cases the final goal is to improve the efficiency of the real fuel itself and to aid the design and development of combustors.

Single-component and multi-component surrogate mixtures are typically classified either as "physical" or "chemical" surrogates, depending on the real fuel properties or behaviors that are being simulated. However, a few other surrogates fall in between these two categories since they are designed to match some specific physical properties and to partially simulate the chemical behavior of a real fuel in a particular application. Real fuel surrogates can be defined following Edwards and Maurice (2001):

¦ Physical surrogate: a mixture whose physical properties, such as density, viscosity, or the distillation points, match those of the real fuel. Considering a single-component surrogate, n-dodecane is characterized by density, viscosity, specific heat and

thermal conductivity values that are similar to those of JP-7 and JP-8 / Jet A, over the temperature range 100-650ºC (Edwards, 1993). A multi-component physical surrogate of JP-8 has been recently studied by Sarofim at University of Utah (Sarofim et al., 2002).

┊ Chemical surrogate: a mixture with a chemical-class composition and average molecular weight that strictly match those of the real fuel. Thus the surrogate has the right proportion of aromatics, naphthenes, olefins and paraffins and similar ratio of hydrogen to carbon atoms. A chemical surrogate would have a similar oxidative behavior even if, on a theoretical platform, the surrogate would not adequately simulate fuel chemistry that is dependent upon trace species (Edwards, 2001). For example, soot emissions dependent upon trace fuel species would not be simulated by this type of surrogates.

This thesis is an effort to develop a chemical surrogate for the military aviation fuel JP-8. Other efforts have been conducted at Drexel University to synthesize a chemical surrogate for typical gasoline fuel, called RON 92 (Khan, 1998; Lenhert, 2002).

┊ Comprehensive surrogate: a mixture that has approximately the same physical and chemical properties of the complex real fuel. These surrogates are usually more close to the physical surrogate class and match only some particular aspect of the oxidative behavior of the real fuel, such as the sooting tendency (Sarofim et al., 2002).

1.5 HYDROCARBON BLENDING: OCTANE NUMBER AND CETANE NUMBER

The concept of surrogate fuels can be applied to both gasoline and diesel fuels. The easiest way to create a surrogate mixture is to blend only two pure compounds. When considering a gasoline fuel surrogate, pure n-heptane is usually mixed with pure isooctane to obtain a blend which is referred to as a Primary Reference Fuel (PRF) Blend.

One of the most important characteristic of a gasoline fuel blend is to reproduce the auto-ignition resistance of the actual fuel, since this property is of great practical importance for avoiding the problem of engine knock. In the 1920s, in order to characterize the auto-ignition resistance of a fuel surrogate compared to that of the parent fuel, the Cooperative Fuel Research (CFR) Committee proposed to use a dimensionless parameter called Octane number (ON). Considering the octane scale introduced by Edgar in 1926 (Guibet and Faure-Birchem, 1999), n-heptane was assigned an Octane number of 0 since it showed a very high tendency to autoignition, whereas the much less reactive 2,2,4-trimethylpentane (isooctane) was chosen as the second standard fuel for gasoline surrogates and it was assigned a conventional Octane number of 100 due to its high resistance to knock. Using this scale, the octane number of a fuel is the volume percentage of 2,2,4-trimethylpentane blended with n-heptane to create a surrogate fuel that shows the same autoignition resistance performance as the test fuel when tested using a standard procedure defined by the CFR Committee.

For gasoline fuel it is important to resist autoignition since it would cause the knock problem, however a diesel fuel should have a good tendency to autoignite. For a diesel fuel this characteristic is expressed by the Cetane number (CN). In this case the higher the Cetane number, the higher the tendency of the fuel to auto-ignite.

The Cetane number of a fuel is obtained by comparing its ignition quality in a standard engine with the behavior of a blend of two reference hydrocarbons. When the idea of the Cetane number was initially introduced, the two selected reference fuels were the highly reactive n-hexadecane (cetane), with a CN equal to 100, and a-methylnaphthalene, which is a bicyclical aromatic compound and, thus, it is extremely resistant to oxidation, with a CN of 0. Using these two reference compounds, a fuel has a Cetane number CN = x if it behaves like a volumetric blend of x % of n-hexadecane and (100 - x) % of a-methylnaphthalene. Or, in other words, a surrogate fuel characterized by a Cetane number CN should present the same ignition behavior of the corresponding real fuel if they have the same Cetane number.

Nowadays the lower Cetane reference fuel a-methylnaphthalene has been replaced by the isoparaffin 2,2,4,4,6,8,8-heptamethylnonane (isocetane) with a Cetane number of 15, mainly due to the cost, instability and very bad ignition behavior of the a-methylnaphthalene in the CFR test engine. However, it should be noticed that usually Cetane numbers are uncertain within ±3 units (Griffith et al., 1998). Values of the Cetane numbers of several representative hydrocarbons, including those investigated in this study, are reported in Appendix A. Several relations between the hydrocarbon structure (linear vs. branched) or the hydrocarbon class, and the corresponding Cetane number can be identified. Among the different classes of hydrocarbons, the Cetane number generally increases as follows: $CN_{n-alaknes} > CN_{olefins} > CN_{cycloalkanes} > CN_{aromatics}$. Ring structures tend to lower the Cetane number. Moreover, when considering a particular class, the CN increases with the length of the straight carbon chain. Thus large n-alkanes have greater Cetane numbers than smaller n-alkanes or branched iso-alkanes. Naphthenes usually have

Cetane numbers from 40 to 70, whereas aromatics range from zero to 60. An aromatic compound with a single ring and a long alkyl side chain will be in the upper part of this range, whereas molecules with two or three aromatic rings fused together have Cetane numbers below 20. An investigation of the relationship between the Cetane numbers of paraffinic hydrocarbons and their structures has been conducted by Griffiths (Griffiths et al., 1998). Their reduced kinetic model showed that when considering diesel-fuel type, full boiling range alkanes, the ratio of primary to secondary hydrogen atoms in the molecule determines the rate of ignition of the specific compounds and, in turn, its Cetane number.

The method applied to measure the Cetane number of a mixture (mono or multi-component) is still based on the experimental CFR engine test, and the procedure is reported in ASTM D 613. The following equation 1.1 is applied to calculate the Cetane number of a mixture of i components, with the volumetric constraint represented by equation 1.2:

$$CN_{Mixture} = \sum_i V_i \cdot CN_i \tag{1.1}$$

$$\sum_i V_i = 1 \tag{1.2}$$

Equation 1.1 is based on the assumption of linear blending. However, usually the Cetane number (as well as the Research ON and Motor ON) of a multi-component mixture – and thus the reactivity and the autoignition behavior of the mixture itself – is not related to the mixture composition by a linear equation. This is mainly due to the fact that each particular component in a blend interacts with the other components present in the pool.

When a mixture does not show a linear behavior with respect to its composition, it can behave either synergistically or antagonistically. A hydrocarbon mixture shows a synergistic behavior if it less reactive than the ideal linear mixture of its components. On the other hand a mixture is considered to behave antagonistically if it is more reactive than the corresponding ideal blend (Wilk, 1989).

The prediction of mixture behavior still presents practical problems whose solution will require a better understanding of the chemical kinetics of the hydrocarbons involved (Pilling, 1997). In order to take into account the compositional non-linear behavior of a particular mixture, different approaches have been investigated. One of the most common is the "Blending Bonus" approach (Owen and Coley, 1995), which is based on equation 1.3:

$$P_{blend} = V_1 \cdot P_1 + V_2 \cdot P_2 + V_3 \cdot P_3 + BONUS \qquad (1.3)$$

Thus, applying equation 1.3, a property P_{blend} (RON, MON, CN, etc.) of a blend is described by a linear equation with respect to the blend volumetric composition, plus a term called "BONUS" that represents the deviation from linearity. The value of the bonus can be calculated by application of equation 1.4, which is based on the average olefins (O_{ave}) and aromatics (A_{ave}) contents of the mixture and on its blending RON calculated using the linear blending assumption.

$$\begin{aligned} BONUS = {}& 0.43 \cdot RON - 0.004 \cdot O_{ave}^{\,2} + 0.004 \cdot A_{ave}^{\,2} \\ & - 0.01 \cdot RON^2 - 0.005 \cdot O_{ave} \cdot A_{ave} - 55.18 \end{aligned} \qquad (1.4)$$

Even though it considers the different effect of both olefins and aromatics, this method does not take into account the non-linearity introduced by the naphthenic hydrocarbons which can represent a significant portion of the whole blend in the case of jet fuels. Moreover this method usually returns a large error (Owen and Coley, 1995).

Another method to predict the correct behavior of a mixture is based on the concept of Blending Cetane number (or the equivalent Blending Octane number) (Rose and Cooper, 1955). The $CN_{blending}$ parameter represents the autoignition tendency of a particular fuel when it is blended with a base fuel in a specific volume fraction. Usually the base compound represents the 80% or the 50% of the whole binary mixture. Equation (1.1) is still valid to calculate the overall Cetane number of a mixture, but the values for the Cetane numbers for non-linear components of the blend need to be replaced with their correspondent Blending Cetane numbers. Unfortunately, due to dependence of the Blending Cetane number on the particular base compound selected and on its volume fraction, the application of this method results in accurate predictions only for the case of low departures from linearity of the whole mixture. Moreover the data available for Blending Cetane numbers are extremely sparse.

Finally, considering the somewhat approximate and arbitrary nature of Cetane number (Pilling, 1997), a reasonably close approximation for the CN of a fuel is represented by the Cetane Index (CI). This parameter requires a few very simple measurements compared to the determination of CN using a CFR engine test. It is based on the fuel volatility and density at T = 298 K. Thus, by knowing the fuel density at ambient temperature, only few points of the fuel distillation curve are required to obtain

the CI value. ASTM D 976 requires a single temperature point, T_{50}, the 50% distillation point on the ASTM D 86 distillation curve. A correlation between the calculated values of $CI_{ASTM\ D\ 976}$ and the corresponding measured Cetane numbers (ASTM D 613) is reported by Guibet (Guibet and Faure-Birchem, 1999). This correlation shows that for 75% of the tested samples the difference between the CI and the CN ratings is of more than 2 units when considering CN values in the range 30 to 60. Therefore a more accurate measure of the Cetane index has been defined by the protocol ASTM D 4737 or ISO 4264. This method requires the measurement of 3 temperature points, specifically T_{10}, T_{50}, and T_{90}, and it is replacing the single point method. Using ASTM D 4374, the calculated values of the CI for a fuel differed by less than 2 units from the corresponding CN in 65% of the cases for CN values in the range 32.5 to 56.5 (Guibet and Faure-Birchem, 1999).

In conclusion, all the methods applied to evaluate the autoignition tendency of a multicomponent fuel mixture (CN, CI, etc.) are only approximate, especially when considering large mixtures. As a qualitative explanation, the compositional non-linearity of a hydrocarbons mixture can be related to the chemical interactions among the compounds in the pool. The effects of radical production or destruction for each compound can affect the rates of branching or termination reactions. Therefore, more detailed studies of the chemistry underlying the oxidation of hydrocarbons, not only alkanes, are needed to really understand the complex behavior of hydrocarbons mixtures (Pilling, 1997).

Trends in Petroleum Fuels Consumption: 1999-2020
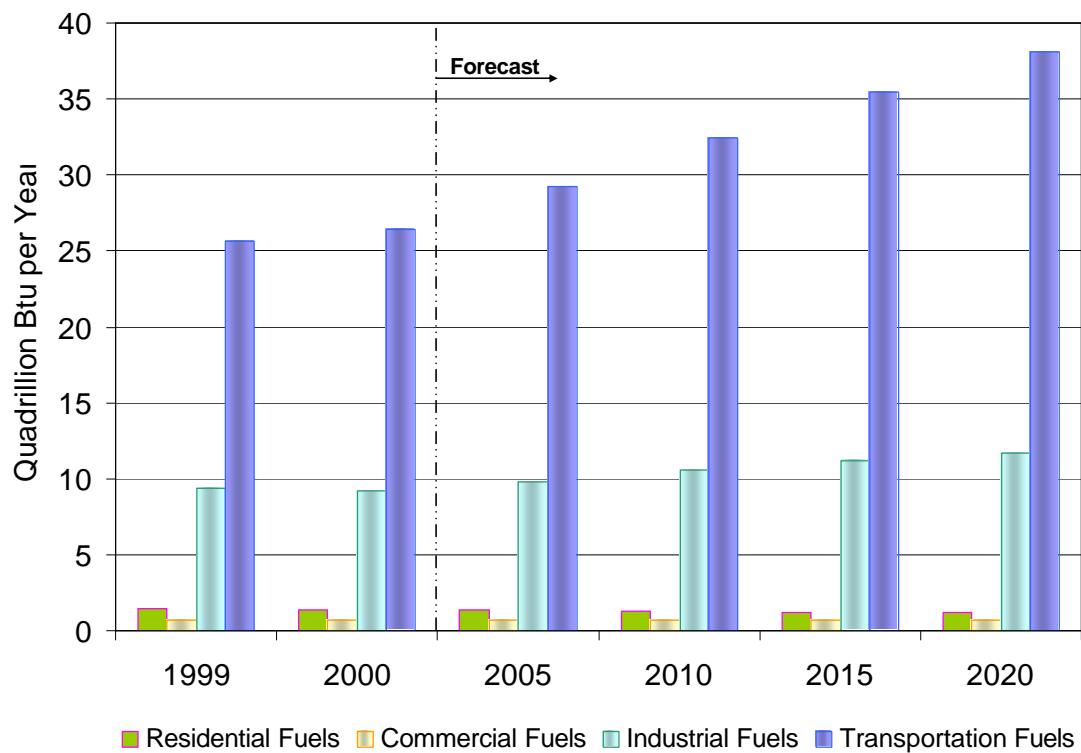
Source: "Annual Energy Outlook 2002 With Projections to 2020"
US Department of Energy and National Energy Information Center DOE/EIA-0383(2002) - December 2001.

Figure 1.1 Trends in Petroleum Fuels Consumption: 1999-2020

**Trends in Transportation Fuels Consumption:
1999-2020**
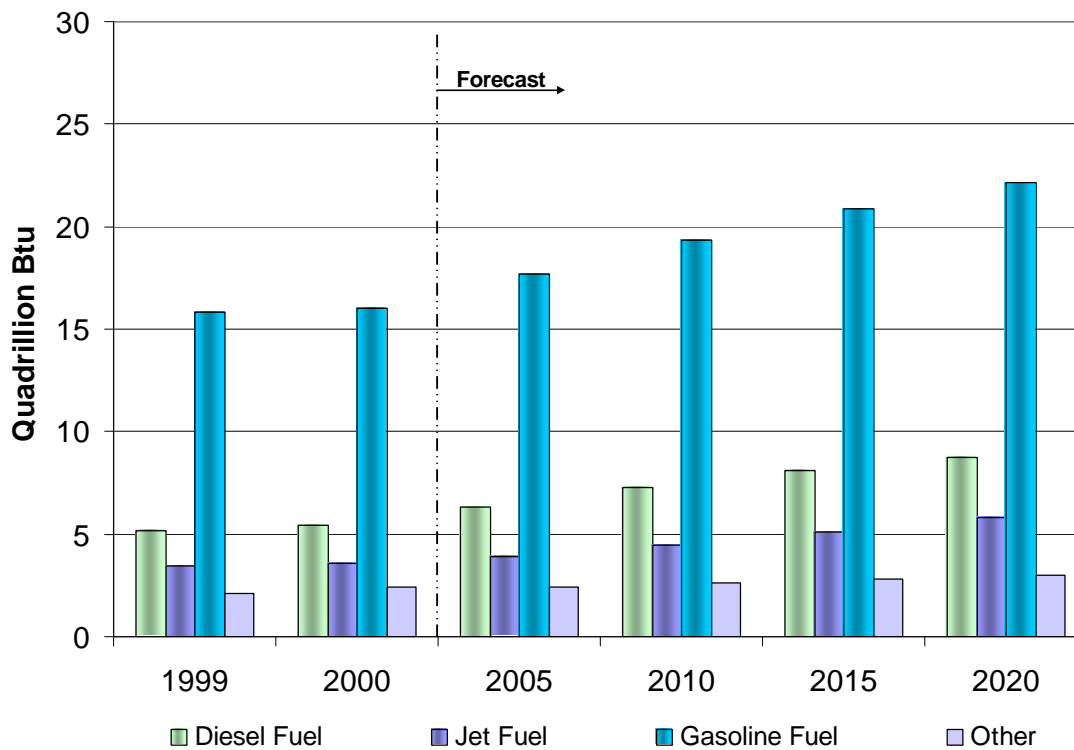
Source: "Annual Energy Outlook 2002 With Projections to 2020"
US Department of Energy and National Energy Information Center DOE/EIA-0383(2002) -
December 2001.

Figure 1.2 Trends in Transportation Fuels: 1999-2020

Trends in Jet Fuels Consumption: 1990-2020
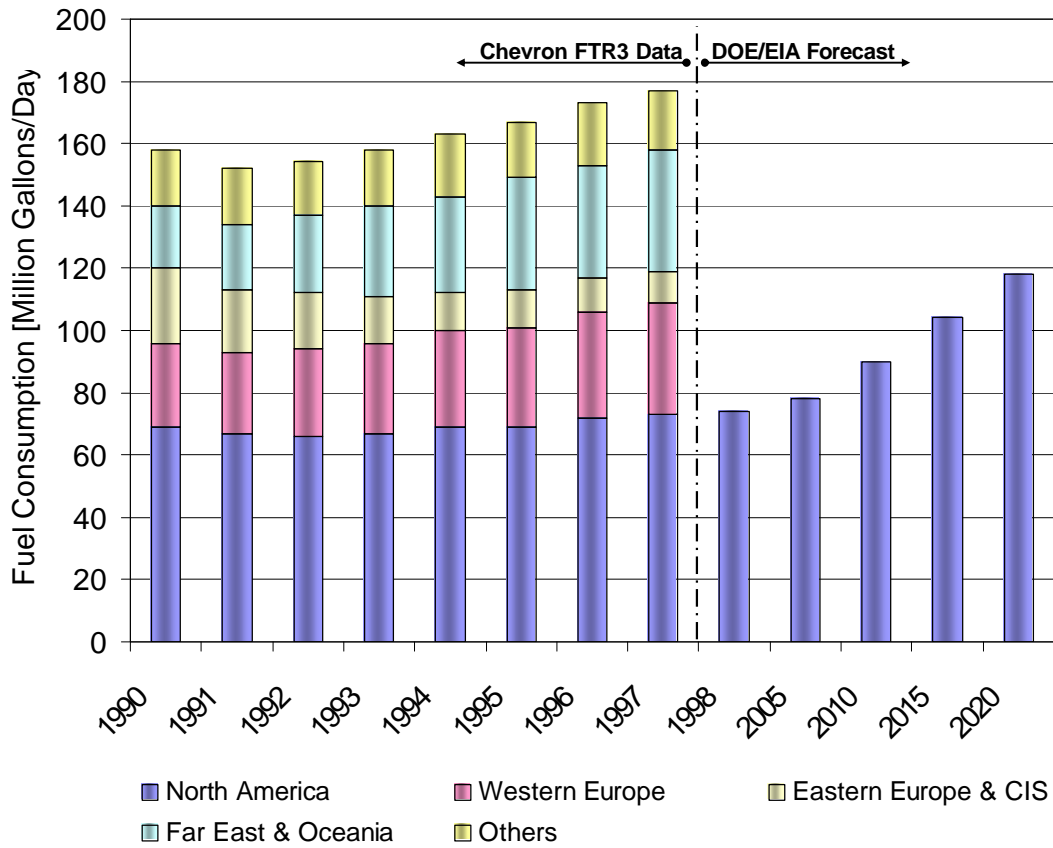
Figure 1.3 Trends in Jet Fuels Consumption: 1999-2020

Aromatics Content in JP8
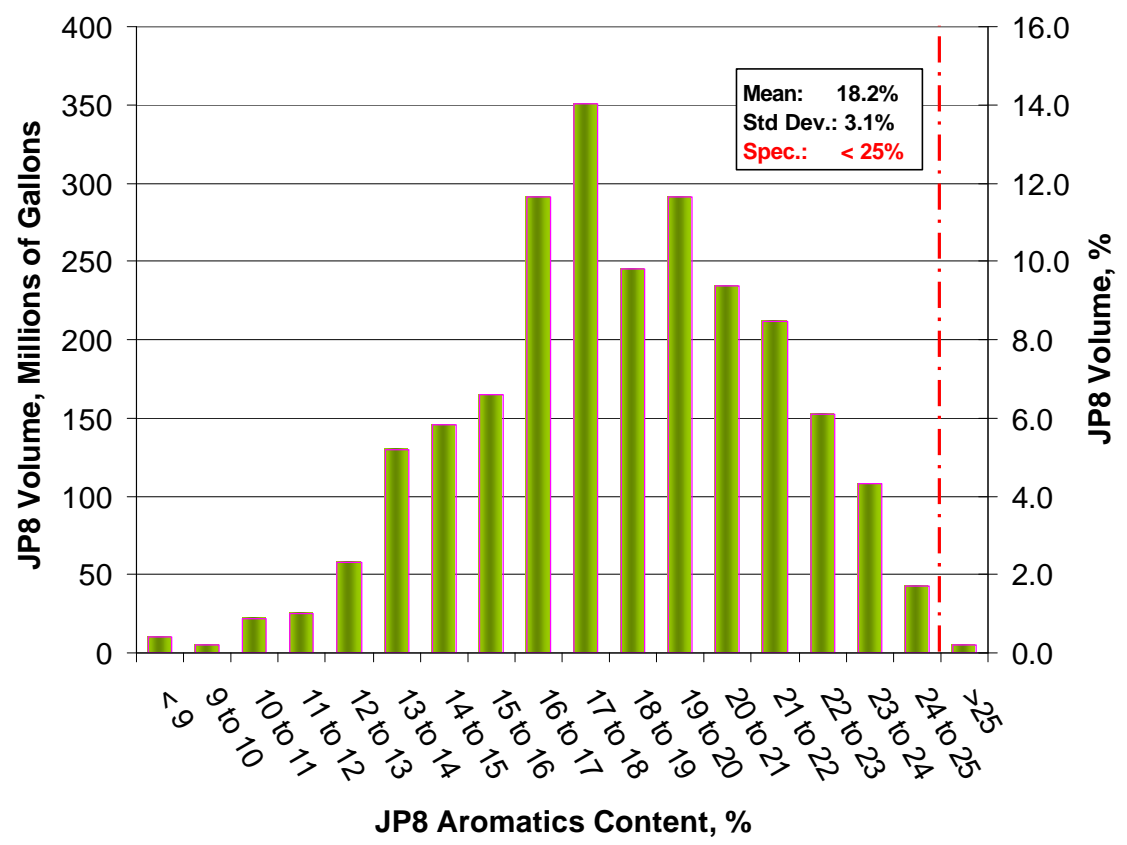
Figure 1.4 JP-8 Aromatics Content
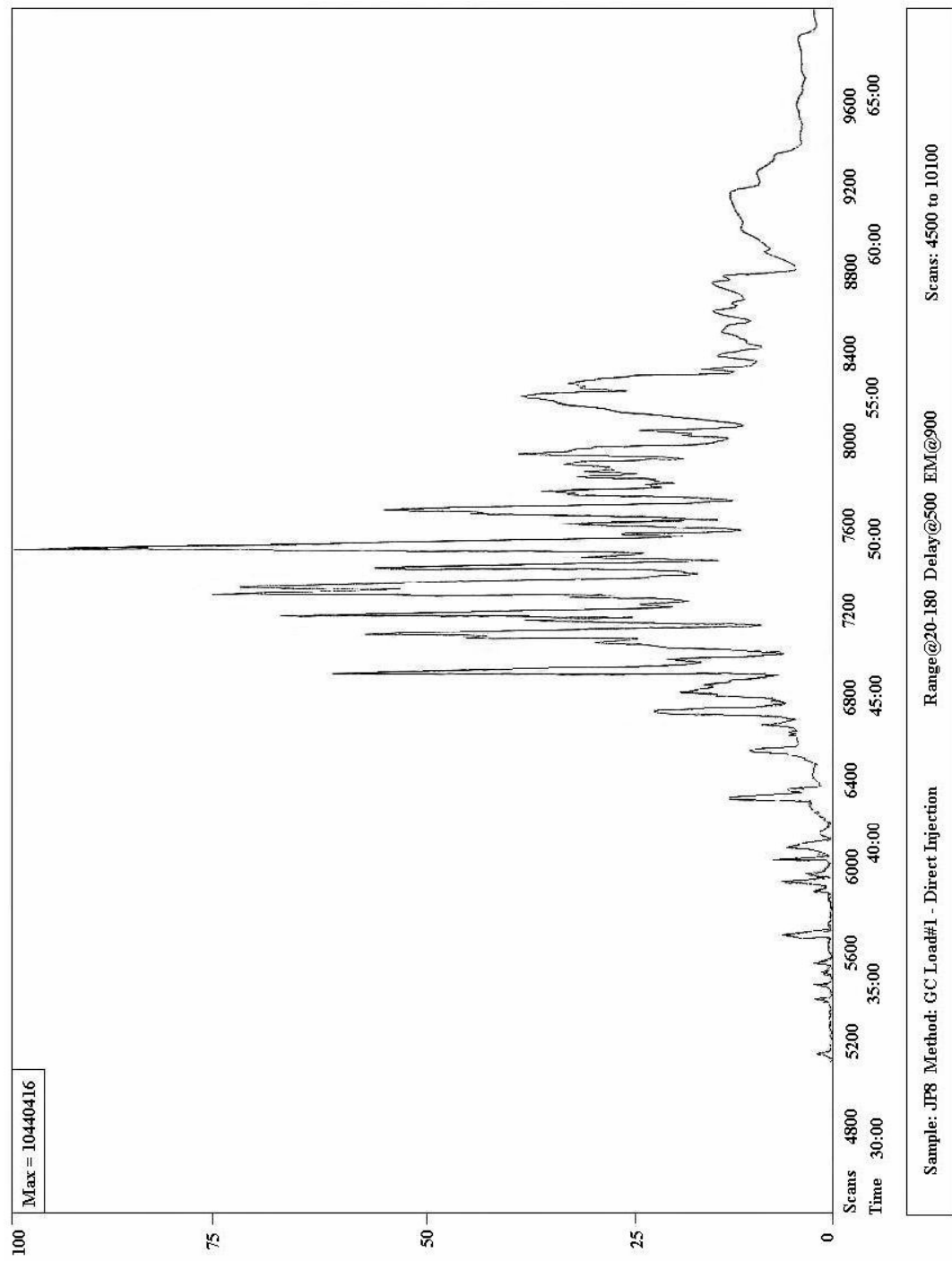
Figure 1.5 JP-8 Mass Spectrum

CHAPTER 2 – BACKGROUND AND LITERATURE SURVEY

2.1 INTRODUCTION

Since the beginning of the 20th century, the study of hydrocarbon oxidation has proceeded through the measurement of combustion processes at different conditions of temperature, pressure, concentration, etc. followed by the development of chemical kinetic models. Once fully developed and tested, these models are applied to predict the behavior of a system under conditions that otherwise would not be easily reached experimentally. For example such models have been applied to solve very well known problems, such as the knock in spark ignition engines, or the cold start and the pollutant emission control in diesel engine. Especially considering that combustion is the predominant source of energy in our life, it is clear that the search for new solutions to all of these problems is of great practical importance.

The word combustion covers an extremely broad variety of phenomena such as explosions, cool flames, or detonations, which occur over a wide range of temperatures. This study focuses on the low and intermediate temperature regions of combustion, where the interesting phenomenon of autoignition takes place. In fact, autoignition is of practical importance in a large range of applications. For example, it is a desired way of achieving combustion in diesel engines, while it can produce "knock" in spark ignition engines with the potential for severe engine damage. The importance of the chemical studies in the low and intermediate temperature regions is to provide a better understanding of the hydrocarbon oxidation processes with the ultimate goal of controlling the autoignition phenomenon.

In the next sections an overview of the low and intermediate temperature chemistry for different classes of hydrocarbons is presented, since it is the basis for understanding the results of this experimental study.

2.2 THE OXIDATION OF ALKANES AND THE NEGATIVE TEMPERATURE REGION

The foundation of modern interpretations of the chemistry underlying gas-phase hydrocarbon oxidation is provided by the theory of Semenov (1935), which is based on the concept of free radicals. Reformulated in the light of the pioneering experiments of Knox and Wells (1963) and Zeelenberg and Bickel (1961), this theory identifies the following major steps in the oxidative process of hydrocarbons (Pilling, 1997):

- Primary initiation: radicals are formed from the parent molecules.

- Chain propagation: no change in the number of radicals.

- Chain Branching: multiplication of the number of radicals.

- Degenerate Branching: new radicals are formed from a "stable" intermediate species.

- Radical Chain Termination: removal of radicals from the system.

Nowadays, the development of powerful methods for chemical analysis, such as gas chromatography, allows the measurement of the products and intermediates of oxidation, and the study of how these species depend on the system parameters, including the dominant effects of temperature and pressure. This provides an extremely useful step for elucidating the chemistry of hydrocarbon oxidation. Considering the alkane group

with a number of carbon atoms greater than 4, the analysis of the products of combustion resulted in the definition of general mechanisms for the oxidation in the low and intermediate temperature regions and provided an explanation for the transition between these two regions.

Below approximately 400 K, alkanes do not tend to react. When the temperature increases to ca 500 K, the parent alkane (RH) starts to react with molecular oxygen following the path indicated by the following reaction (R1) and forming a hydroperoxy radical ($HO_2\bullet$):

$$RH + O_2 \leftrightarrow R\bullet + HO_2\bullet \tag{R1}$$
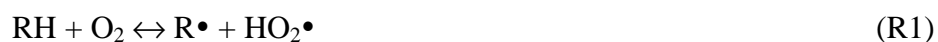
Reaction R1 represents the primary initiation but, since it is very endothermic, it is of little interest after some free radicals have been produced. After this initiation, much more important reactions (R2) between the parent alkane and a hydroxyl radical ($HO\bullet$), formed from further reactions of either the alkyl radical ($R\bullet$) or the $HO_2\bullet$ radical in R1, control the progress of the oxidation.

$$RH + HO \leftrightarrow R\bullet + H_2O \tag{R2}$$

Once the alkyl radical $R\bullet$ is formed, it can follow two different paths of reaction. It can form the activated complex $RO_2{}^*$, which is the product of the reaction (R3) between R and molecular oxygen, or it can decompose to an alkene and a smaller alkyl radical, through reaction R4.

$$R\bullet + O_2 \leftrightarrow RO_2\bullet^* \qquad\qquad\qquad (R3)$$

$$R\bullet \rightarrow \text{ smaller } R\bullet + \text{alkene} \qquad\qquad\qquad (R4)$$

Then, two possible reaction pathways for the activated complex are reaction R5, and R6.

$$RO_2\bullet^* \leftrightarrow \text{conjugate alkene} + HO_2\bullet \qquad\qquad (R5)$$

$$RO_2\bullet^* \leftrightarrow \bullet QOOH \qquad\qquad\qquad (R6)$$

Reaction R5 produces the conjugate alkene and a hydroperoxyl radical ($HO_2\bullet$). Both R4 and R5 are termination reactions since they lead to the formation of inert radicals, $HO_2\bullet$ and small $R\bullet$ (Pilling, 1997). Reaction R6 represents a propagation reaction and consists of the addition of oxygen to the original alkyl radical $R\bullet$ to form an alkyl peroxy radical ($\bullet QOOH$) via the abstraction of a hydrogen atom and internal isomerization (Wagner et al., 1990; Bozzelli and Dean, 1990). The alkyl peroxy radical $\bullet QOOH$ can now follow two pathways.

$$\bullet QOOH \leftrightarrow QO + HO\bullet \qquad\qquad\qquad (R7)$$

$$\bullet QOOH + O_2 \leftrightarrow \bullet O_2QOOH \qquad\qquad\qquad (R8)$$

First, $\bullet QOOH$ can undergo a cyclization to form a stable epoxide (QO, a cyclic ether) and a hydroxyl radical (HO$\bullet$). Cyclic ethers are among the major products of alkane's oxidation in the low temperature region. However, the isomerized alkyl peroxy radical can also add another molecular oxygen (R8), creating an unstable intermediate,

•O₂QOOH, that undergoes an isomerization process to form a molecular hydroperoxide, ROOH and a hydroxyl radical (R9). ROOH is the degenerate branching agent since it decomposes (R10) to form RO• and another HO•, thus increasing the number of free radicals acting in the system.

$$\bullet O_2QOOH \rightarrow ROOH + HO\bullet \qquad\qquad\qquad (R9)$$

$$ROOH \rightarrow RO\bullet + HO\bullet \qquad\qquad\qquad (R10)$$

Therefore, on the one hand reaction R9 and R10 – thus reaction R6 and R8 too – are responsible for the branching process that ultimately will lead to the autoignition phenomenon. On the other hand, reactions R4 and R5 lead to the termination of reactivity.

Reactions R3 and R4, R5 and R6 can be summarized by the following general pathway, R11, which reflects the chemical competition between the formation of the alkyl radical R• and the peroxy radical RO₂•:

$$R\bullet + O_2 \leftrightarrow RO_2\bullet \qquad\qquad\qquad (R11)$$

This reaction is reversible. In the low temperature region R11 is self-catalyzed and shifted to the right, thus it favors the branching process, which in turn is reflected into the increase of the system temperature and of the overall reaction rate.

Although the reaction rate of many chemical systems is characterized by a monotonic increase as the temperature increases, when considering the oxidation of particular classes of compounds such as the alkanes, it is possible to note that in a

particular range of temperature the overall reaction rate decreases as the temperature is increased. First detected in the early '30s by Pease in the study of oxidation of propane and n-butane in both flow and static systems (Pilling, 1997), this behavior is often referred to as the negative temperature coefficient (NTC) region. The NTC behavior can be explained to occur through the reversibility of reaction R11. In fact, in the intermediate temperature region reaction R11 is shifted to the left, or in other words, reaction R5 is favored with respect to R6 (Benson, 1981). Since R5 is a termination reaction, in the intermediate temperature region the overall reactivity of the system decreases with increasing temperatures. Therefore the start of NTC region is the turnover temperature between the low temperature region, which is dominated by the peroxy chemistry, and the intermediate temperature region, which is characterized by the HO_2 and H_2O_2 chemistry.

If the temperature of the system is further increased, the phenomenon of "hot-ignition" occurs, defining the end of the intermediate temperature region and the beginning of the high temperature region (Bartok and Sarofim, 1991). Now the overall reaction rate increases again as the temperature of the system is increased. Hot ignition is characterized by the decomposition of hydrogen peroxide H_2O_2 into two hydroxyl radicals HO•, which results in the increase of the overall reactivity.

It is interesting to note that the equilibrium in reaction R11 is controlled by many factors, among them is of course the temperature, but the pressure is also important. As the pressure in the system is increased, the NTC region tends to become narrower and the turnover temperatures between the three oxidative regimes change. As noted by Pilling (1997), for example, at 800 K the oxidation in a glass-bulb system at P < 0.1 bar can be

dominated by the H + O$_2$ high temperature chemistry, while at the same temperature in an engine, at much higher pressure, low temperature chemistry can dominate. Moreover, the low-to-intermediate temperature boundary is so sensitive to pressure (and thus to O$_2$ concentration) that turbulent flow reactors, which use highly diluted oxidant streams, need to operate at rather low temperatures to be in the low temperature region, even if their pressure is several bar.

When considering the oxidation of alkanes, several compounds have been extensively investigated including propane, butane, pentane, and of course the two gasoline primary reference fuels, n-heptane and isooctane. A simplified general model for the oxidation of alkanes has been presented by Scacchi and coworkers (2000). In this study, the analysis of the reactivity of free radicals and of the relative rates of generic reactions versus temperature is presented.

Nowadays the scientific community has started to focus its attention on the oxidation of C$_n$ alkanes, with n > 8, too. The oxidative behavior of n-decane has been investigated by Dagaut (Dagaut et al., 1994) at high pressure and from low to high temperatures using a jet stirred reactor. Bikas and Peters (2001) constructed and validated a semi-detailed mechanism for the low and intermediate temperature chemistry of n-decane, based on the work of Dagaut.

The oxidation of n-dodecane has been investigated by Sahetchian (Sahetchian et al., 1995; Blin-Simiand et al., 2001) indicating the presence of several peroxidic species during the gaseous phase combustion of the fuel in a flow system. Different hydroperoxides were formed at different experimental conditions. The formation of

ketoperoxides (bearing three oxygen atoms) was shown and modeling studies confirmed the large influence of the production and decomposition reactions of these ketohydroperoxides on preignition chemistry. An experimental study and a modeling effort of n-dodecane ignition have been conducted by Sahetchian (Sahetchian et al., 1995) in a diesel engine. Through continuous sampling of the combustion chamber gases, the concentrations of hydroperoxides and molecular hydrogen were monitored. Moreover the ignition delay of n-dodecane spray in an oxidation chamber filled with air has been conducted between 715 K and 760 K and over pressures from 15 to 25 bar. Time-dependent evolutions of average concentrations showed that RO_2H reaches a maximum first, then H_2O_2, and lastly the H atoms.

Finally, the oxidation of n-hexadecane has been studied for the first time in a jet stirred reactor at 1 atm in the high temperature region by Dagaut (Dagaut et al., 2001). A detailed kinetic reaction mechanism consisting of 242 species and 1801 reactions was built and validated by comparison with the experimental data. Results showed that n-hexadecane follows the general oxidation paths of lighter alkanes. At low fuel conversions and low temperatures (T < 1000 K), n-hexadecane mostly reacts via H atom abstraction, while at high fuel conversion and higher temperatures (T > 1000 K), thermal decomposition dominates in stoichiometric and fuel-rich conditions. However, in fuel-lean conditions, the abstraction of H-atoms by O and HO still dominates.

2.3 THE OXIDATION OF AROMATICS

The first studies on the oxidation of aromatic compounds were conducted by Burgoyne in the 1930s (Roubaud et al., 2000) using a static reactor and focused mainly on the low temperature oxidation of benzene and toluene. The results of these studies showed the extreme resistance of the highly unsaturated benzene ring to undergo oxidation in the temperature range between 500 K and 900 K. Nevertheless, Burgoyne successfully measured the principal products of benzene and toluene oxidation at temperatures of about 750 K, among which after CO and CO_2 where phenols and acids. In successive studies he also observed cool flames and NTC behavior in the oxidation of n-butyl benzene, and recognized the increase in reactivity in the alkyl benzenic compounds as induced by the increase in the number and length of the alkyl side chains. Later, the results obtained from Burgoyne were confirmed by Salooja (1965), when he studied the autoignition behavior of several monocyclic aromatic compounds.

First in 1968, Barnard and Sankey (Pilling, 1997) showed that among the xylene compounds (dimethylbenzenes), *o*-xylene was much more reactive in the low temperature region than the corresponding isomers *p*-xylene and *m*-xylene.

Recently, the oxidation of aromatic compounds has received comparatively more attention by the researchers than in the previous years since aromatic compounds are major constituents of gasoline, diesel and aviation fuels and their chemistry is not well characterized. As shown in Chapter 1, aromatic compounds can represent up to the 25% of the volumetric composition in typical aviation fuels. Moreover, nowadays the aromatics are replacing the banned lead-based knock suppressors in gasoline since they have very high octane numbers.

In 1986, an extensive study was conducted by Brezinsky and coworkers (1986) on methyl, ethyl, n-propyl and n-butyl benzene using a plug flow reactor. All these n-alkyl monocyclic aromatics were studied at atmospheric pressure and in the high temperature region and the results confirmed that the oxidation of this class of hydrocarbons is controlled by the side-chain chemistry.

Few years later, Shaddix (Shaddix et al., 1997) investigated the oxidation of a-methylnaphthalene at atmospheric pressure and temperatures of about 1200 K. a-methylnaphthalene appeared to follow the high temperature oxidation behavior of toluene, which is its monocyclic analog.

Finally, in 2000, Roubaud (Roubaud et al., 2000) compared the reactivity of several low alkyl benzenes at high pressure and low temperatures and studied their autoignition behavior. The 11 alkyl benzenes studied were classified in two groups. The first group, the "toluene group", included compound such as toluene, *m*-xylene, *p*-xylene and 1,3,5-trimethylbenzene, which ignited only at high temperatures (more than 900 K) and pressures (16 bar). On the contrary, the second group, the "*o*-xylene group", was characterized by compounds that ignited at much lower temperatures and pressures showing oxidative behaviors similar to those of alkanes and alkenes. This group included ethylbenzene, *o*-xylene, 1,2,3-trimethylbenzene, 1,2,4-trimethylbenzene, n-propylbenzene, 2-ethyltoluene, and n-butylbenzene. Analyzing the ignition characteristic and global reactivity (G.R.) of these fuels, the author showed that the decrease in the resistance to low-temperature oxidation and autoignition showed by the *o*-xylene group is related to proximity rather than the number of aliphatic carbon atoms in the molecule. In fact, for example *o*-xylene, 2-ethyltoluene or 1,2,3-trimethylbenzene, all showed higher

reactivity than *m*-xylene, *p*-xylene or 1,3,5-trimethylbenzene. Finally, ethylbenzene, even if classified in the more reactive *o*-xylene group, in reality can be considered an element of transition between the two groups, having an ignition temperature limit of 861 K at 17 bar in the rapid compression machine used by Roubaud.

2.4 THE OXIDATION OF CYCLOALKANES

Hydrocarbons characterized by saturated carbon atoms assembled in a ring structure are called naphthenes or cycloalkanes. Few studies have focused on the oxidation behavior of this class of compounds even if cycloalkanes are major constituents of conventional automotive and jet fuels.

The oxidation of cyclohexane and cyclopentane has been investigated by Walker and reported by Pilling (1997). Considering the rate of attack for OH and H to the $-CH_2-$ groups of both cyclohexane and cyclopentane, Walker showed that this group behaves like the $-CH_2-$ groups present in the alkanes. Moreover, he showed that conjugate alkenes are the initial products of oxidation and benzene (and substituted benzenes) represents the majority of the secondary products. Therefore, the oxidation of compounds such as cyclohexane or substituted cyclohexanes leads to the formation of high pollutant aromatic products.

Very few studies have investigated the chemistry of alkyl substituted cycloalkanes, such as methylcyclohexane. As noted by Pilling, however, when considering methylcyclohexane, its chemistry should reflect the chemistry of the correspondent cyclohexane. Thus the attack at the alkyl chain will be followed by the

intermediate formation of the correspondent olefin (cyclohexene) and R radicals (CH_3) by homolysis, and the final production of benzene.

Recently, the atmospheric oxidation of methylcyclohexane (MCH) has been investigated by Zeppieri (Zeppieri et al., 1997) using a flow reactor at temperatures above 1000 K. Major intermediate products of the vapor-phase pure methylcyclohexane pyrolysis were ethane, methane, propene, and 1,3-butadiene, while toluene was not present. A simple model for the high temperature oxidation was postulated starting from a base typical for aliphatic compounds. Thus the main paths for the MCH pyrolysis were the hydrogen abstraction and the C-C homolysis, with the resulting radicals undergoing ß-scission of both C-C and C-H bonds.

Several mixtures of methylcyclohexane and toluene were also oxidized. The results showed that the two fuels mechanisms of decay were not affected by the presence of the other fuels. Nevertheless, since MCH is less stable than toluene, when the initial MCH concentration for a given mixture was increased, then the rate of MCH and toluene consumption also increased as a consequence of the larger radical pool available in the mixture. The results obtained by Zeppieri et al. (1997) were also compared with the measurements of Kaiser et al. (1992) of the oxidation of methylcyclohexane in a test engine. The products of the MCH oxidation were extrapolated from the intermediates and qualitatively matched the exhaust species measured from the engine.

2.5 FUELS BLENDS AND SURROGATES: LITERATURE SURVEY

Over the years, a considerable amount of research has addressed the chemistry of the small hydrocarbons (carbon number = 8). Typical studies in the low and intermediate temperature regions were conducted using the gasoline reference fuels, n-heptane and iso-octane, and their blends. As noted by Edwards (1993), the fundamental combustion behavior of the high-order hydrocarbons, mainly compounds with more than 8 carbon atoms, has received comparatively little study.

In 1973, Barnard and Harwood (1973a, 1973b) studied the low and intermediate temperature oxidation of both iso-octane and n-heptane using sub-atmospheric conditions in a static reactor. They noticed a two stage ignition for n-heptane while iso-octane showed a very weak and slow combustion process. Later in the 1980s, Lignola and coworkers (Lignola et al., 1984; Lignola and Reverchon, 1986) reexamined the oxidation of these two primary reference fuels. However this time the use of a jet stirred flow reactor allowed operations at pressures up to 12 atmospheres where iso-octane showed the classical two-stage ignition behavior.

More recently, the ongoing research effort at Drexel University exploring low and intermediate temperature hydrocarbon chemistry examined iso-octane, n-heptane and their blends. In 1998, Khan studied several mixtures of the two gasoline reference fuels comparing the auto-ignition behavior of these surrogates with those of real fuels such as Indolene. This study showed that a blend of two compounds is not enough accurate to reproduce the behavior of complex real fuels, even if it matches the real fuel MON/RON values. In particular this study showed that the simple primary reference fuels surrogates ignited earlier than the industry standard fuel (ISF), Indolene. The real fuel oxidation

behavior was finally reproduced using a surrogate fuel composed of 4 different hydrocarbons, specifically the two reference fuels plus 1-pentene (an olefin) and toluene (an aromatic). A difference in the olefinic chemistry was observed between the PRFs and ISFs, which suggested the importance of small hydrocarbon chemistry in the oxidation of ISFs.

Since complexity increases with the number of constituents, only a few studies have focused on the combustion aspects of complex mixtures of hydrocarbons. In a study of the autoignition chemistry of gasoline PRFs and of paraffin/olefin mixtures, Leppard (Leppard, 1989; Kowalski, 1992) identified a synergistic behavior for binary mixtures of paraffins and olefins. Leppard also related this inhibiting behavior to the alkenes acting as radical scavengers in the low temperature chemistry of the alkanes, and the alkanes slowing the faster alkenes high temperature chemistry.

In 1989, Wilk et al. studied the autoignition tendency of several compounds representative of the main hydrocarbons classes and their binary mixtures with n-heptane. The alkenes inhibited the alkane chemistry of n-heptane in the low temperature region but promoted the oxidation in the intermediate temperature region. The aromatic and branched alkane compounds all showed inhibiting behavior. Furthermore this study related the amount of CO produced by the combustion of the mixtures to their Octane number, providing a simple correlation to predict the non-linear behavior of binary hydrocarbons mixtures. A comparable cetane correlation was developed based on the experimental data for n-heptane, n-octane and n-decane but, due to difficulties in running experiments with heavy fuels, this correlation was not tested with standard diesel or aviation fuels.

For several years the kinetic study of full boiling distillate fuels like aviation fuels have been considered prohibitive due to their high order of complexity. Maurice and Lindstedt (2000) reduced the complexity of the kerosene-type aviation fuels using a surrogate model of 89 mole % n-decane and 11 mole % of various aromatics, including benzene, toluene, ethylbenzene, and ethylbenzene/naphthalene as an input to a detailed kinetic model. The n-decane/benzene surrogate oxidation matched the major species profiles of the parent fuel, but failed to predict benzene concentrations, which were matched by the n-decane/alkyl-aromatics. Moreover no differences were observed between the various alkyl-benzene surrogates analyzed. Wood and coworkers (Wood et al., 1989) performed experimental combustion studies with JP-4 and JP-5 surrogates. These surrogates are listed in Table 2.1 and 2.2 and were developed with the goal of establishing a set of surrogate fuels for modeling and for the study of fuel property and chemical composition effects. The following five criteria were enumerated for selecting the surrogate components:

1. limit of 10 to 15 pure hydrocarbon species.

2. match compound class in parent fuel.

3. match distillation curve in parent fuel.

4. high purity components.

5. minimum component cost.

Wood and coworkers reported that the physical and chemical properties of the surrogates were in good agreement with those of the parent fuels, except for the smoke point. Moreover, in their combustion tests in a swirl-stabilized laboratory combustor, the surrogates represented the combustion properties of the distillate fuels, including soot concentrations (Edwards and Maurice, 2001). This indicates that the fuel hydrogen content, which was maintained between the surrogates and the parent fuels, may be a good predictor of the soot levels.

Later in 1993, Schulz et al. (1993) developed a surrogate for JP-8 (see Table 2.3). This surrogate reproduced the general oxidative behavior of the JP-8, but could not reproduce the deposition levels in thermal stability testing. This fact has been related by Edwards and Maurice to the key role that trace species, such as metals and heteroatoms, play in the deposition process (Edwards and Maurice, 2001).

Finally, two JP-8 surrogate fuels have been developed by Sarofim and coworkers (Sarofim et al., 2002) in their work on fire simulation. Six pure hydrocarbons were blended in such a way as to create a surrogate that could reproduce the distillation curve of the parent fuel, as well as its sooting propensity. It was determined that a six-component surrogate provides sufficient flexibility to simulate the major properties of interest to pool fires of real jet fuels. These two surrogates are listed in Table 2.4 and 2.5.

Table 2.1 JP-4 Surrogate – Wood et al. (1989)

COMPOUND CLASS	JP-4 VOLUME, %	JP-4 SURROGATE COMPONENT	VOLUME, %
PARAFFINS	61.2	N-HEXANE	5.5
		N-HEPTANE	8.0
		N-OCTANE	8.0
		N-NONANE	10.0
		N-DECANE	10.0
		N-DODECANE	10.0
		N-TETRADECANE	10.0
MONOCYCLOPARAFFINS	24.2	CYCLOHEXANE	8.0
		METHYLCYCLOHEXANE	8.0
		CYCLOOCTANE	8.0
DICYCLOPARAFFINS	4.9	DECALIN	5.0
ALKYLBENZENES	8.2	TOLUENE	8.0
INDANS & TETRALINS	1.1	TETRALIN	1.0
NAPHTHALENES	0.4	a-METHYLNAPHTHALENE	0.5
Source: Wood, C.P., McDonell, V.G., Smith, R.A., Samuelsen, G.S.,(1989) - "Development and Application of a Surrogate Distillate Fuel", Journal of Propulsion and Power Vol.5, No.4.			

Table 2.2 JP-5 Surrogates – Wood (1989)

COMPOUND	BLEND 1, VOLUME %	BLEND 2, VOLUME %
N-DECANE	2.5	2.5
DECALIN	11.5	11.5
N-UNDECANE	0.0	5.0
N-PENTYLCYCLOHEXANE	11.0	0.0
1,3-DIISOPROPYLBENZENE	3.0	3.0
TETRALIN	9.5	9.5
N-DODECANE	25.0	31.0
1-PHENYLHEXANE	5.0	5.0
N-TRIDECANE	10.0	15.0
N-HEPTYLCYCLOHEXANE	11.0	0.0
a-METHYLNAPHTHALENE	1.5	1.5
N-TETRADECANE	5.0	11.0
N-PENTADECANE	5.0	5.0

Source: Wood, C.P., (1989) - "The Development and Application of Surrogate Blends in Simulating the Combustion Performance of Distillate Aviation Fuels", M.S. Thesis, Dept. of Mechanical Engineering, University of California, Irvine.

Table 2.3 JP-8 Surrogate – Schulz et al. (1993)

COMPOUND	MASS, %
METHYLCYCLOHEXANE	5.0
m-XYLENE	5.0
CYCLOOCTANE	5.0
DECANE	15.0
BUTYLBENZENE	5.0
TETRAMETHYLBENZENE	5.0
TETRALIN	5.0
DODECANE	20.0
METHYLNAPHTHALENE	5.0
TETRADECANE	15.0
HEXADECANE	10.0
ISOOCTANE	5.0

Source: Schulz, W.D., Heneghan, S.P., Locklear, S.L., Geiger, D.L., Anderson, S.D., (1993) - "Static Tests of Jet Fuel Thermal and Oxidative Stability", Journal of Propulsion and Power, Vol.9, No.1.

Table 2.4 JP-8 Surrogate #1 – Sarofim et al. (2002)

COMPOUND	VOLUME, %
ISOOCTANE	10.0
METHYLCYCLOHEXANE	20.0
m-XYLENE	15.0
N-DODECANE	30.0
TETRALIN	5.0
N-TETRADECANE	20.0

Source: Sarofim, A.F., Eddings, E.G., Yan, S., Violi, A., and Ranzi, E., Faravelli, T., Granata, S., (2002) - "Experimental Formulation and Kinetic Model for JP-8 Surrogate Mixtures", 2nd MCS.

Table 2.5 JP-8 Surrogate #2 – Sarofim et al. (2002)

COMPOUND	VOLUME, %
ISOOCTANE	5.0
METHYLCYCLOHEXANE	5.0
TOLUENE	20.0
N-DECANE	25.0
N-DODECANE	25.0
N-TETRADECANE	20.0

Source: Sarofim, A.F., Eddings, E.G., Yan, S., Violi, A., and Ranzi, E., Faravelli, T., Granata, S., (2002) - "Experimental Formulation and Kinetic Model for JP-8 Surrogate Mixtures", 2nd MCS.

CHAPTER 3 – EXPERIMENTAL FACILITY AND METHODOLOGY

3.1 INTRODUCTION

Several kinds of devices are commonly used to investigate the chemistry of hydrocarbon combustion, depending on the temperature-pressure ranges to be studied. For low temperature and approximately atmospheric pressure conditions, a closed constant volume static vessel is a typical experimental device. A flow reactor is usually employed for intermediate temperatures and pressures, when the reactions proceed at a rate too fast for the use of a simple static reactor.

Whilst in the earliest chemical kinetic studies the applied flow systems were mainly laminar flow tubes operated at constant atmospheric pressure, nowadays typical flow devices are Pressurized Flow Reactors (PFR), as currently operated at Drexel University and at Princeton University, or Stirred Flow Reactors, such as the Jet Stirred Flow Reactor (JSFR) operated by Dagaut et al. (2001). Both these devices are much more flexible than the laminar flow reactors since they realize turbulent flow conditions and they allow for the study of the effect of pressure on the hydrocarbon oxidation.

Finally, since the combustion of hydrocarbons covers a wide temperature range, a typical source of kinetic data at high temperatures and pressures is the study of reactions in shock tubes. Usually the temperature range in a shock tube study is between 1500 K and 2500 K and, considering the high pressure, these conditions are almost close to those in the post-ignition period in a real engine.

This study was conducted using the pressurized flow reactor facility in Frederic O. Hess Laboratories at Drexel University. The detailed description of the facility has

been provided elsewhere by Koert (Koert, 1990; Koert and Cernansky, 1992) and only the necessary information and important modifications about the facility will be described here. The sampling and chemical analysis system and the experimental methodology will also be addressed in this chapter. Moreover, this chapter includes the description of a new fuel calibration and delivery method and of a parametric statistical data analysis method that has been developed to perform the comparison of the experimental results.

3.2 THE PRESSURIZED FLOW REACTOR FACILITY

The Drexel Pressurized Flow Reactor (PFR) is a modern bench scale experimental test facility developed in the 1990s by Koert (Koert, 1990; Koert and Cernansky, 1992) in order to study the chemical kinetics controlling hydrocarbon oxidation, mainly in the low and intermediate temperature regions at pressures up to 20 atm.

The PFR has a temperature range up to 1000 K, which is effective to characterize the low and intermediate temperature regimes, and it is maintained at nearly adiabatic conditions so that the heat transfer effects can be ignored. As noted by Pilling (1997), even if this condition of nearly adiabatic operations may seem remote from any practical application, in reality it can be approached in a practical application whenever the chemical time scale is considerably shorter than the heat loss time scale.

In the PFR, a stream of pre-vaporized fuel is diluted using nitrogen. Then, as it enters the adiabatic quartz reaction duct, it is mixed into a stream of oxygen diluted with nitrogen in order to slow down the chemistry. Moreover, the high flow rate reached inside the reactor allows establishing a turbulent regime and, thus, neglecting the surface effects since the overall residence time is much shorter that the time it takes for the chain carriers to diffuse radially to the wall.

The reactor duct is heated by means of two sets of manually controlled heaters, and it is insulated as described in the Section 3.3. A computer controlled probe is moved inside the reactor and the extracted samples are delivered to the gas analyzer devices described in the Chemical Analysis section. A schematic of the PFR device is presented in Figure 3.1.

3.3 REACTOR FLOW SYSTEMS

The reactor duct is a 2.25 cm I.D., 40 cm long, quartz tube. The temperature is kept as constant as possible along the reactor length by insulation and by the use of multiple bead heaters that can be manually controlled from the PFR Bead Heater Control Panel shown in Figure 3.1.

As suggested in the previous study of Khan (Khan, 1998), the multiple heating element system has been developed and it maintains a much improved temperature profile. The PFR has been divided in three main sections, the inlet, the test and the outlet section, and the temperature of each of these sections can be monitored and adjusted by changing the temperature set point on the corresponding bead heater. The current temperature set points for the bead heaters during the experiments are shown in Table 3.1.

Table 3.1 Bead Heaters Temperature Set Points

PFR SECTION	SWITCH	TEMPERATURE
INLET SECTION	1 → ON 2 → ON 3 → ON	700 ℃ 700 ℃ 700 ℃
TEST SECTION	4 → ON 5 → ON 6 → OFF	550 ℃ 550 ℃ —
OUTLET SECTION	9 → ON	500 ℃
NITROGEN-FUEL SECTION	7 → ON 7 → ON 8 → OFF	300 ℃ [1] 400 ℃ [2] —

[1] *Set Point for low boiling temperature fuels*
[2] *Set Point for high boiling temperature fuels*

The fourth row in Table 3.1 represents the Nitrogen-Fuel section, which refers to the external line between the mixing nozzle and the fuel pump delivery system (line 2, Figure 3.2). Along this line the liquid fuel delivered by the pump is vaporized and at the line end it is mixed with a stream of nitrogen to achieve the desired experimental conditions. Two different fuel lines (line 1) can be used depending on the fuel viscosity: a larger diameter line is employed to reduce the stress on the pump for highly viscous fuels such as a-methylnaphthalene, while a smaller diameter line is commonly utilized for the other fuels.

Controlling the temperature along line 2 is of great importance and its temperature set points must range between a lower temperature limit, which reflects the fuel boiling point, and a higher temperature limit, which represents temperatures where significant decomposition of the fuel occurs. For low boiling fuels a set point of 300 ℃ has been used (Khan, 1998). However this value is close to the boiling points of the full boiling range fuels investigated in this study. Therefore, a new set point at 400 ℃ was chosen that allows the effective vaporization of the heavy fuels without inducing fuel cracking. In fact, fuel pyrolysis in the fuel delivery system is unacceptable. Prior to each experiment, a comparison of the spectrum of a sample of the fuel-nitrogen stream coming out from the PFR to the tabulated fuel spectrum is performed using the FTIR analysis to be sure that the fuel has not pyrolized in the delivery system.

Once the reactor reaches the experimental set point, the temperature along the reactor is monitored using the 'Temperature Profile' LabVIEW® code developed by Lenhert (2002). This code automatically moves the probe inside the reactor duct every 30 s, starting from the outlet and moving it towards the nozzle with a 0.5 cm step. The

collected temperature data can be saved and then exported into an Excel spreadsheet. A typical temperature profile which extends from the inlet (position x = 5 cm) to the outlet (position x = 38 cm) of the reactor is shown in Figure 3.3. The temperature along the reactor is nearly constant, particularly along the test section, which usually extends from x = 12 cm to x = 36 cm, while the overall maximum temperature variation is less than 3 °C. The drop off at approximately x = 35 cm is due to heat losses related to reduced insulation at the intersection between the reactor duct and the exhaust line (Figure 3.2).

3.4 SAMPLING METHOD

Samples of the reacting gases are obtained at different locations along the reactor via a stainless steel probe whose position is computer controlled. Because of turbulent gas flows in the reactor and because of the rapid initial mixing of the fuel and the oxidizer, radial gradients in the PFR can be neglected and samples taken along the centerline of the test section characterize the chemistry of the reactions.

Moving the probe to different positions along the PFR while maintaining the inlet temperature constant, it is possible to collect samples which correspond to different residence times and, in turn, different reaction times, thereby obtaining information on the evolution of the reactant and product species. On the other hand, moving the probe and keeping the residence time constant it is possible to monitor the fuel reactivity behavior during a controlled cool down experiment. In both cases the probe motion is automatically controlled using the 'Probe Automove' LabVIEW® code developed by Koert (1990) and modified by Lenhert (2002).

A pressure drop across the probe orifice and the probe water-cooling system (Figure 3.1) extracts the reacting gases in such a way that further reactions are rapidly quenched. The extraction line is also heated to approximately 70 ℃ in order to keep the products at a temperature high enough to avoid condensation of important species such as formaldehyde. The temperature along the extraction line has been monitored by adding three thermocouples to the original design developed by Koert (1990).

The original 2 m length Teflon line between the probe and the FTIR has been replaced by a 0.55 m flexible metal line (line 5, Figure 3.2) plus a 1.6 m rigid metal line (line 6). Both lines are heated and insulated to maintain sample temperature = 70 ℃. The temperature control of this line is realized via heating tapes and it is controlled manually. Typical temperature values are on the order of 100 ℃ during an experiment and 120 ℃ during the flow rate calibration of a high boiling point fuel. The higher temperature value during the calibration process is maintained in order to prevent even the smallest amount of condensation by the fuels.

Continuous samples, extracted from the PFR at constant flow rate, can be analyzed online using a Fourier Transform Infrared (FTIR) device for a quantitative analysis of the products of combustion and using a Non-Dispersive Infrared (NDIR) device for CO and CO_2 production. The CO concentration is used to map the overall reactivity of the fuel as it is explained in the "Chemical Analysis" section. Samples can also be stored in a constant temperature storage unit capable of holding up to 15 gas samples for later GC/MS analysis.

A schematic of the entire extraction line, which runs from the probe exit to the NDIR inlet, is presented in Figure 3.1. The overall length of the extraction line, that is the

sum of line 5 and 6, is approximately 4 m. The volumetric flow rate inside this line is kept constant at 3 l/min and it is regulated by the rotameter of the NDIR. Due to the length of the extraction line, there is a time delay between the measurement of CO and CO_2 for a specific sample in the NDIR and the measurement of that specific sample temperature by the thermocouple mounted on the tip of the probe. Applying the equations of ideal fluids without losses, it is possible to calculate the residence time of the gases extracted from the PFR and flowing into lines 5 and 6. This time has been estimated to be less than 5 s. The reactor cooling rate during a typical controlled cool down experiment is on the order of 3 °C/min at the start and end of reaction, while it decreases to approximately 2 °C/min in the temperature region close to the start of NTC – due to the larger amount of heat released (see Section 3.7). Therefore in the worst case the temperature change during the 4 s time delay is about 0.05 °C, and this is small enough that the CO/CO_2 and the temperature measurements can be considered to be simultaneous.

3.5 CHEMICAL ANALYSIS

The samples extracted from the reactor can undergo three different types of chemical analysis using different techniques and devices: Fourier Transform Infrared (FTIR) Spectroscopy, Non-Dispersive Infrared (NDIR) Spectroscopy, and Gas Chromatography eventually coupled with Mass Spectroscopy (GC-MS).

Infrared Spectroscopy is a powerful tool for identifying types of chemical bonds in a molecule by producing an infrared absorption spectrum that is like a molecular "fingerprint". The term Fourier Transform Infrared Spectroscopy (FTIR) refers to a fairly recent development of this technique in the manner in which the data is collected and converted from an interference pattern to a spectrum.

The physical principle of this analysis is based on the property of both organic and inorganic compounds of absorbing electromagnetic energy in the infrared (IR) portion of the electromagnetic spectrum. Absorption in the IR region results in changes in the vibrational and rotational status of the molecules and the absorption frequency depends on the vibrational frequency. However, not all molecular vibrations result in the absorption of infrared energy. Indeed a molecular vibration changes in the presence of IR radiation only if the dipole moment of the molecule changes.

In an Infrared Spectrometer a beam of IR radiation is passed through a gas sample inside a closed cell and is continually compared with a reference beam while the frequency of the IR beam is changed, generating a plot of the infrared absorption versus the frequency ?, the wavelength ?, or the wavenumber ?. While inorganic compounds usually have 'simple' spectra, organic compounds have very detailed spectra which include so many different absorption bands (or peaks) that an IR spectrum of a pure

compound is generally so unique that it can be considered the molecular 'fingerprint'. For these reasons and since the strength of the absorption is related to the concentration, the FTIR analysis is a very useful technique for identifying chemicals, and eventually it can be utilized to conduct a quantitative analysis of some components or functional groups of an unknown mixture. Unfortunately, since many peaks fall very closely together in a mixture spectrum, it can be tough to distinguish one particular compound from another. This is true in particular in the case of the spectrum of a mixture of combustion gases obtained through the oxidation of a heavy fuel, such as n-dodecane or a-methylnaphthalene, where a fairly high number of different compounds are present in the whole mixture.

The tabulated spectrum of a-methylnaphthalene is shown in Figure 3.4 where it is compared to the measured spectrum of the a-methylnaphthalene and nitrogen stream coming out from the PFR during the fuel flow rate calibration. A vertical shift has been applied in Figure 3.4 to the tabulated spectrum so that it does not overlap the measured spectrum and they can be compared. The difference in the height of the peaks between the two spectra is due to the different amounts of a-methylnaphthalene analyzed. The figure shows that the fuel molecule did not decompose when exposed to the high temperature of the fuel-nitrogen line – up to 450 °C for this test. Moreover an interpretation of the more important peaks present in the a-methylnaphthalene spectrum is presented:

⁞ Starting from the higher values of wavenumber in the spectrum, first we notice the group of peaks included in the range between $3300\ cm^{-1}$ and $2800\ cm^{-1}$, a

region that is commonly associated with the carbon-hydrogen (C- H) stretching vibrations.

¦ Peak A, around $3070 \, cm^{-1}$, corresponds to the vibration of the aromatic hydrogen atoms and it has been used for the a-methylnaphthalene calibration during the experiments.

¦ Both peaks B and C, in the lower $2800\text{-}3000 \, cm^{-1}$ range, correspond to the carbon-hydrogen stretching of hydrogen atoms attached to the sp^3 hybridized carbon atoms (- CH_3), in this case the methyl absorption peaks.

¦ In the region ranging from approximately $2000 \, cm^{-1}$ to $1700 \, cm^{-1}$, overtones of the mono-substituted a-methylnaphthalene can be seen.

¦ The stretching of the delocalized carbon-carbon double bonds of an aromatic ring can be seen in the range between $1450 \, cm^{-1}$ and $1600 \, cm^{-1}$. All peaks E, F, and G are sharp peaks associated with the aromatic stretch.

¦ Finally, in the lower wavenumber portion of the spectrum, absorption arising from the carbon-hydrogen vibrations of a monosubstituted aromatic can be noticed. Both peaks H and I occur due to these particular vibrations.

Knowledge of the main absorption bands of a particular compound spectrum provides us extremely important information. For example in Figure 3.4, the spectrum of the a-methylnaphthalene flowing into the PFR is compared to the a-methylnaphthalene library spectrum not only to check that the molecule did not pyrolize when exposed to the high temperature of the Nitrogen-Fuel delivery line, but also in order to be sure that no other compounds, such as undesired water vapor or impurities, were present in the

stream. Moreover, since peaks H and I are unique characteristic of aromatic compounds, they have been used to first identify, and then quantify, the a-methylnaphthalene consumption in the oxidation of a binary mixture of n-dodecane and a-methylnaphthalene, as reported in Chapter 5.

The second technique applied to this study is the Non Dispersive Infrared Gas Analysis (NDIR). This method provides online CO and CO_2 measurements from the gas samples continuously extracted from the PFR and delivered to a Siemens Ultramat 22 single-beam gas analyzer. This device operates on the principle that the absorption in the sample chamber increases as the concentration of the gas increases, and the radiation measured by the detector decreases giving an exponential voltage response. This analysis allows mapping the overall reactivity of the hydrocarbons oxidation and it is specifically valid for the low and intermediate temperature regions, which means at temperatures below 900 K. The validity of CO concentration measurements as a reactivity indicator is acceptable mainly because the oxidation reactions dominant in both the low and the intermediate temperature regions produce CO quickly and CO is not converted to CO_2 at a significant rate.

Finally the Gas Chromatography technique, eventually coupled with the Mass Spectroscopy technique, can be applied to quantify the stable intermediate species extracted from the PFR and stored in the heated storage unit. For each GC analysis of samples taken during experiments, species are identified by comparing retention time with those of the standards previously measured. This technique is particularly suitable for the analysis of heavy fuels and should be developed for further analysis of the products and intermediates of reaction.

3.6 FUEL CALIBRATION AND DELIVERY

Calibration and control of the amount of fuel that must be injected into the reactor is a complex process and should be as accurate as possible. After having set the experimental conditions, such as the equivalence ratio or the nitrogen dilution, the corresponding fuel mole fraction (ppm of fuel) is automatically obtained through an Excel spreadsheet based on the following equation:

$$c_{fuel} = \frac{1}{1 + 4.76 \cdot \left[\dfrac{\#C_{atom} + \#H_{atom}/4}{f} \right] \cdot \left[1 + \left[\dfrac{N_{2-dilution}/100}{1 - N_{2-dilution}/100} \right] \right]} \qquad (3.1)$$

The fuel calibration is a process that associates an actual fuel flow rate to the desired ppm of fuel calculated for a particular experiment. A new method for the calibration of the fuel flow rate has been developed specifically for the heavy fuels investigated in this study, which are characterized by a high boiling point. The classical calibration method developed by Koert (1990) does not apply to this class of fuels since they would not completely vaporize inside the heated FTIR cell, causing an over estimation of the actual flow rate. Indeed, if only a portion of the injected fuel vaporizes, then the correlation between the ppm of fuel injected and its absorbance would not be accurate. The classical Koert method consists of a single syringe injection of a known amount of fuel directly into the FTIR cell, which is set at a temperature of 150 ℃ and it is maintained at a sub-atmospheric pressure around 6-7 torr (0.008 atm). For a light compound such n-pentane, whose boiling point at 1 atm is 36 ℃, the vaporization is

almost instantaneous, resulting in an accurate calibration. However, applying this calibration method to the set of heavy fuels investigated here would result in inaccurate calibrations which would not be acceptable.

The application of the classical single injection method to the n-dodecane calibration is shown in Figure 3.5 where the vaporized amount of injected fuel into the FTIR cell (and the corresponding cell pressure increment) is compared to the amount of fuel that ideally should have vaporized. The ideal values are calculated as shown in Appendix B and are based on the ideal hypothesis that the fuel density is constant and its value is that at reference conditions. Due to this hypothesis the ideal values are only approximate, but even if they can not be used for the calibration, they still provide us with useful information to determine the ideal amount of vaporized fuel, and in turn, to determine whether a particular syringe injection is good or not.

As shown in Figure 3.5, the difference between the real and the ideal injection increases as the volume injected increases. When 5 µl of n-dodecane were injected, only about 65% of the fuel vaporized and when the injected volume was increased to 20 µl, only 31% of the fuel vaporized. This problem of fuel vaporization was due mainly to the limits on the maximum temperature of the FTIR cell and to the fact that the injection line was neither heated nor insulated. The temperature for the FTIR is constrained by the melting temperature of the O-rings which seal the cell itself and by the problem of thermally cracking the lens. For these reasons the temperature of the cell has been maintained at 150 ºC. However, due to the too low temperature inside the cell, part of the vaporized fuel condenses on the FTIR lens and along the injection line causing poor absorbance detection.

The calibration curve is obtained injecting different masses of fuel and measuring the pressure increase inside the cell after the fuel has vaporized in order to obtain a measure of the quantity of fuel that has vaporized. The ppm of injected fuel is defined as the ratio between the pressure rise inside the FTIR cell after the fuel injection and the pressure reference of 760 torr. Finally, this value is plotted versus the correspondent absorbance value. As shown in Figure 3.6, the calibration curve thus obtained is far from linear ($R^2 \sim 0.9$) and can not be used to accurately calculate the actual flow rate necessary for an experiment. Moreover, Figure 3.6 shows how two single injection calibrations for n-dodecane measured in two different days, but at the same conditions, differ one from the other, mainly because of the different amount of fuel that vaporized.

Therefore, to solve the problems involved in applying the classical calibration method to the high boiling point fuels, a new double injection calibration method has been developed. This method is based on a two step fuel injection, as described by the following procedures (the operating procedures for this method are listed in Appendix B). First, a known amount of liquid fuel is injected by means of a syringe into a preheated cylinder shown in Figure B.1 and the pressure rise inside this cylinder is measured using a Datametrics barocel pressure sensor. The cylinder containing the vaporized fuel is now refilled with clean nitrogen up to the reference pressure of 760 torr and the mole fraction (ppm) of injected fuel is calculated. Refilling the cylinder allows obtaining a homogenous mixture of fuel and nitrogen uniformly distributed over the whole cylinder volume. Then, the mixture of fuel and nitrogen inside the cylinder is injected into the FTIR cell and the pressure rise is monitored using a second pressure transducer. The FTIR cell is now refilled with clean nitrogen and the exact fuel ppm value is calculated. Finally the gas

sample is ready to be analyzed by the FTIR and a spectrum of the fuel absorbance is generated. Through the application of the "FTIR Calibration Sheet" Excel spreadsheet described in Appendix B, the final plot of the fuel ppm versus the absorbance at a particular wavelength is finally obtained.

The use of a separate cylinder allows obtaining an almost complete vaporization of even the heaviest the fuel. The metal cylinder is heated to a temperature well above the fuel boiling point, temperature which would be too stressful for the FTIR cell. Testing this method with a-methylnaphthalene, n-dodecane, and JP-8, the following correlation between the fuel boiling point and the cylinder temperature has been established:

$$T_{CYLINDER} = T_{FUEL\ BOILING\ POINT} + \sim 30\ °C \qquad\qquad (3.2)$$

The temperature inside the cylinder has been monitored using a type K thermocouple and it has been maintained by means of heating tapes and a double layer of insulation tapes. Table 3.2 briefly summarizes the main difference between the two calibration methods.

Table 3.2 Fuel Calibration Methods Comparison

SINGLE INJECTION METHOD		*DOUBLE INJECTION METHOD*	
$T_{FTIR\ CELL}$	150 °C	$T_{FTIR\ CELL}$ $T_{CYLINDER}$	175 °C $T_{BOILING\ PT} + 30$ °C
$T_{INJECTION\ LINE}$	30 °C	$T_{INJECTION\ LINE}$	175 °C
$V_{FTIR\ CELL}$	600 ml	$V_{FTIR\ CELL}$ $V_{CYLINDER}$	600 ml 500 ml
$P_{FTIR\ CELL}$	5-10 torr	$P_{FTIR\ CELL}$ $P_{CYLINDER}$	5-7 torr 5-7 torr
$t_{INJECTION}$	300 s	$t_{INJECTION\ FTIR\ CELL}$ $t_{INJECTION\ CYLINDER}$	< 5 s < 5 s

The injection time is drastically reduced in the double injection method, reflecting the good suitability of this method for both high and low boiling point fuels. The calibration curves for the single hydrocarbon fuels investigated in this study are presented at the end of this chapter together with their fuel pump calibration curves (Figures 3.7 to 3.18). After the FTIR calibration, it is possible to determine the exact amount (ppm) of fuel that has been delivered to the PFR. Then, we calibrate the flow rate of the pump. This is done by collecting samples from the PFR while running different flow settings on the pump. These samples are analyzed in the FTIR cell as for the first FTIR calibration. Therefore a relationship between the absorbance and the fuel flow rate is obtained. Finally, combining the two calibration curves (fuel mole fraction vs. absorbance and fuel flow rate vs. absorbance) it is possible to determine the correct setting on the pump in order to inject the required quantity of furl into the reactor. For each fuel, several set of

FTIR and Pump calibrations have been performed at different times and have been plotted to show the accuracy and reproducibility of the double injection method. All of the calibration curves have nearly the ideal linear behavior.

In conclusion, due to the strong autoignition behavior of some of the compounds used in this study, the existing methods for fuel delivery were redesigned in order to consistently deliver much lower fuel flow rates. Both the new calibration and delivery methods have greatly increased system repeatability (CO mapping differences less then 5%) and decreased concentration variations during CCD experiments. The modifications have improved reproducibility to the point that, once the calibration curves for a particular fuel have been obtained, they can be reused for further experiments provided that the experimental conditions are the same. However, if some of the experimental conditions, such as the system pressure, are changed, then the Pump calibration curve needs to be remeasured. The FTIR calibration remains valid.

The fuel delivery is now provided via a high pressure ISCO 500D Syringe Pump (see schematic in Figures 3.1 and 3.2), capable of consistently delivering flow rates between 0 to 204 ml/min at a resolution of 0.001 ml/min. The choice of a more expensive piston based syringe pump, versus a more economical HPLC pump (Waters HPLC Pump), was necessitated by the need to maintain accurate flow rates at the lowest settings. Both the HPLC and the Syringe pumps were tested for fluctuation in the amount of fuel delivered over the time, using water. Only the Syringe pump provided the required efficiency and repeatability in the delivery of fuel.

3.7 PFR EXPERIMENTAL METHODOLOGY

Two types of experiments can be performed in the Pressurized Flow Reactor, depending on the type of chemical information that needs to be collected. The first procedure, referred to as Constant Inlet Temperature (CIT) methodology, is particularly suitable for collecting data on the evolution of the intermediate species and final products of combustion. Samples are collected at various locations along the reactor length, each position representing a particular residence time and, in turn, a characteristic reaction time. Therefore, maintaining the reactor at a constant (inlet) temperature, it is possible to follow the evolution of a species as a function of the reaction time providing useful information for establishing and evaluating reaction mechanisms.

The second procedure is both known as Controlled Cool Down (CCD) and as Constant Residence Time (CRT) methodology. A CCD experiment is specifically designed to study the reactivity of a fuel over a wide range of temperatures while keeping the residence time constant. The data collected during a CCD experiment are usually represented in a plot of the CO production as function of the temperature, creating the so called "reactivity map" of the fuel. A typical fuel reactivity map is presented in Figure 3.21 where the start and end of reactivity and the NTC region are identified. As explained in the "Chemical Analysis" section, CO production is an indicator of the overall reactivity of the fuel. Reactivity maps provide useful information on the oxidative behavior of a fuel, including the start and end of reactivity, and the start and width of the NTC region. Moreover they are used to identify the experimental conditions of most interest for a further analysis via a CIT experiment. CCD experiments are also used to deduce the amount of heat released during the reaction, information particularly

interesting for modeling purposes. The method to calculate the heat release is presented by Ramotowski (Ramotowski, 1992). First, the temperature profile (CO formation vs. Temperature) for a CCD is plotted with all the points experiencing reactivity (CO production > 10 ppm) removed. Then, a linear fit is applied to the remaining points, representing an ideal temperature profile for the same CCD experiment conducted without the fuel. Finally the increase in temperature due to heat release during the experiment is obtained subtracting the ideal temperature profile from the real profile.

A CCD experiment is performed by heating the reactor up to the maximum temperature that needs to be investigated, usually well above the low-to-intermediate temperature turnover. Depending on the particular fuel studied and on its oxidative behavior, this temperature usually falls in the range 750 K to 850 K. Once the reactor has reached the maximum temperature selected for the experiment, and it is at nearly isothermal conditions, the reactor heating is discontinued – with the exclusion of the fuel line heater that is required to vaporize the fuel prior to the injection – starting the cool down process for the entire system. The reactor cooling rate is between 2 and 3 °C/min, with the lower value corresponding to the start of NTC, i.e. to the period of maximum reactivity and heat release. While the reactor is cooling, samples are continuously collected and delivered to the NDIR in order to monitor and record the formation of CO and CO_2. During the cooling process, the density of the gases changes as this is a function of the temperature. Therefore the volumetric flow changes and, in order to maintain the residence time constant during the entire experiment, the probe position needs to be continuously adjusted. The probe control and position adjustment are achieved through the computer controlled feedback position system developed by Koert (Koert, 1990).

3.8 STATISTICAL ANALYSIS: CLASSICAL AND EXPLORATORY DATA ANALYSIS

Fundamental in this study is the definition of a method to perform the comparison of the reactivity maps obtained through two or more different CCD experiments. For example, the comparison of the reactivity maps of JP-8 and several mixtures allows identifying the best surrogate fuel, or the comparison of two specifically designed experiments may help to identify the effect of a particular compound on the oxidative behavior of the entire mixture in terms of shifts in location of the NTC, or changes in the shape or in the skewness of the reactivity map. Therefore a new method has been implemented and developed based on a multiple set of quantitative Classical Data Analysis (CDA) techniques.

Classical Data Analysis is among the most popular data analysis techniques together with Exploratory Data Analysis (EDA) and the Bayesian approach. These three approaches are similar in that they all start with a general engineering problem whose solution requires the collection of a set (or more) of data, and all yield an engineering conclusion. The difference is the sequence and focus of the intermediate steps. Thus for classical analysis, the data collection is followed by the imposition of a model (normality, linearity, etc.) and the analysis, estimation, and testing that follows is focused on the parameters of that model. For EDA, the data collection is not followed by a model imposition; rather it is followed immediately by analysis whose goal is to infer what model would be appropriate. Finally for a Bayesian analysis, the analyst attempts to incorporate scientific/engineering knowledge/expertise into the analysis by imposing a data-independent distribution on the parameters of the also-imposed model; the analysis thus consists of formally combining both the prior distribution on the parameters and the

collected data to jointly make inferences and/or do test assumptions about the model parameters (EDA, 2001).

In this study, Classical Data Analysis techniques have been applied together with some Exploratory Data Analysis methods. The statistical analysis tools applied can be grouped into the following three procedures:

1. Quantitative Analysis for Univariate Data (CDA): estimation of statistical significant parameters for a single experiment.

2. Quantitative Analysis for two or more Response Variables (CDA): tests on the measures of dispersion, skewness and location for comparison of two or more experiments.

3. Graphical Analysis for two Response Variables – Quantile-Quantile Plot (EDA): graphical technique for analyzing and comparing two runs of the same experiment.

As a first step in the analysis of every experiment, the resulting reactivity map is analyzed applying the Quantitative Analysis for Univariate Data (procedure #1) in order to compute a summary of characteristic statistical indicators. These parameters can be divided in 3 classes, as summarized in Table 3.3. The mean (μ_1, moment of 1st order), median and midrange of the population are measures of location, since they provide information on the location of the observations. Sample variance (μ_2, moment of 2nd order), standard deviation, range, and quartiles are, on the contrary, measures of the dispersion of the data. Finally the moment of 3rd order is called skewness and it is

representative of the skewness of the distribution, as well as the coefficient of skewness. Of all these statistics, the mean, the variance and the skewness (the first three orders of moments) have been selected to be applied in the comparison of two or more reactivity maps. These three parameters have been coupled with four other observations representative of the overall reactivity behavior of a fuel, specifically the start and end of reactivity and the vertical and horizontal location of the NTC start (procedure #2).

Table 3.3 Quantitative Data Analysis

QUANTITATIVE DATA ANALYSIS		
LOCATION MEASURES	MEAN	μ_1
	MEDIAN	$\xi_{0.50}$
	MIDRANGE	–
DISPERSION MEASURES	SAMPLE VARIANCE	σ^2 (μ_2)
	STANDARD DEVIATION	σ
	UPPER QUARTILE	$\xi_{0.75}$
	LOWER QUARTILE	$\xi_{0.25}$
	RANGE	–
SKEWNESS MEASURES	SKEWNESS	μ_3
	COEFFICIENT OF SKEWNESS	μ_3/σ^3
REACTIVITY MEASURES	START OF REACTIVITY	R1
	END OF REACTIVITY	R2
	START OF NTC (HORIZONTAL LOCATION)	RX
	START OF NTC (VERTICAL LOCATION)	RY

These 7 parameters are aggregated into a single comprehensive parameter, called the Likelihood Index (LI). This index is calculated using the following equation 3.3:

$$LI = \frac{1}{7}\left[\sum_{i=1}^{7}\left(1 - \left|\frac{X_{i,ref} - X_i}{X_{i,ref}}\right|\right)\right] \tag{3.3}$$

where: $X_i = \mu_1$ (mean)   for i = 1

$X_i = \mu_2$ (variance)   for i = 2

$X_i = \mu_3$ (skewness)   for i = 3

$X_i = R_1$ (reactivity start)   for i = 4

$X_i = R_2$ (reactivity end)   for i = 5

$X_i = R_X$ (NTC start, x)   for i = 6

$X_i = R_Y$ (NTC start, y)   for i = 7

Applying equation (3.3) it is possible to calculate LI for different experiments, all compared to the same reference case. This is, for example, the case of candidate JP-8 surrogates that need to be compared with the parent fuel, which is the reference. Due to the definition of LI, it ranges continuously from 0 to 1. LI = 1 represents the reference case, so the reactivity map of a particular fuel or mixture is closer to that of the reference fuel the more its LI approaches unity.

It should be noted that the choice of the three moments as significant statistical parameters representative of a reactivity map was based on the assumption that the data approximately fit a normal distribution. Knowledge of the distribution underlying the

data is indeed required for the choice of the optimal estimators since all the parameters in Table 3.3 are characterized by different levels of noise that are strictly related to the type of underlying distribution. As an example we can notice that scientists and engineers routinely use the mean (average) to estimate the "middle" of a distribution and in this study the mean value of CO production during an experiment has been selected as the estimator of the location of the temperature profile for any particular reactivity map. Thus, the difference between two reactivity maps (at least in terms of location) has been deduced by simply comparing the means of the two populations of data. However the variability and the noisiness of the mean as a location estimator are intrinsically tied to the underlying distribution of the data. For certain distributions the mean is a poor choice. For any given distribution, there exists an optimal choice for the estimator with minimum variability/noisiness. This optimal choice may be, for example, the median, the midrange, the midmean, or the mean itself. The implication of this is to estimate the distribution first, and then – based on the distribution – choose the optimal estimator (EDA, 2001).

However, since every CCD experiment returns an extremely large set of data, the application of the Central Limit Theorem ensures that the distribution of the mean will be normal in any case, and thus the mean production of CO can be used without any risk of yielding a wrong a conclusion even if the real distribution of the data is not normal. Moreover, the skewness parameter (μ_3) has been considered in the data analysis process in order to take into account for the non-normality of the distribution. The non-normality of the distribution has been verified applying the Anderson-Darling (A-D) Test for Normality (Stephens, 1974). This test is used to verify the statistical hypothesis H_0 that a sample of data comes from a specific distribution (normal, Weibull, exponential, etc.).

The A-D test is a modification of the Kolmogorov-Smirnov (K-S) Goodness of Fit Test, a more general non-parametric test, and in our case it provides a more sensitive analysis than the K-S test since it gives more weight to the tails of the distribution. The Anderson-Darling test is defined as follows:

- Statistical Hypotheses:

    H_0: The data follows a specified distribution.

    H_a: The data do not follow the specified distribution.

- Test Statistic: The Anderson-Darling test statistic, A, for $Y_1...Y_i...Y_N$ observations is defined as (F is the cumulative distribution function for the specified distribution):

$$A^2 = -N - \sum_{i=1}^{N} \frac{(2i-1)}{N} \left[\log F(Y_i) + \log(1 - F(Y_{N+1-i})) \right]$$

- Critical Region: The critical values for the Anderson-Darling test are dependent on the specific distribution that is being tested. Tabulated values and formulas have been published (Stephens, 1974) for a few specific distributions (normal, lognormal, exponential, Weibull, logistic, extreme value type 1).

The test is a one-sided test and the hypothesis that the distribution is of a specific form is rejected if the test statistic, A, is greater than the critical value. This test has been applied to the reactivity map of JP-8 (F = 0.3, P = 8 atm, N_2 dilution = 80%, t = 120 ms) using the Dataplot software. The generated output from the test for normality is reported in the following Table 3.4.

Table 3.4 Anderson-Darling Normality Test

A-D 1-SAMPLE NORMALITY TEST		
1. STATISTICS:	NUMBER OF OBSERVATIONS	229.0
	MEAN	249.4
	STANDARD DEVIATION	164.1
	ANDERSON-DARLING TEST STATISTIC VALUE	5.240
2. CRITICAL VALUES:	90.0 % POINT	0.656
	95.0 % POINT	0.787
	97.5 % POINT	0.918
	99.0 % POINT	1.092
3. CONCLUSION (@ THE 5% LEVEL):	THE DATA DO NOT COME FROM A NORMAL DISTRIBUTION.	

Since the returned value for the statistic A is greater than the critical value at the 95.0% point (significance level a = 5 %) the test reject the hypothesis H_0. However it should be noted that the departure from normality is limited, as it can also be noticed in Figure 3.22 where a fuel reactivity map is plotted together with the fitted normal distribution. The distribution approximates very well the temperature profile in the low temperature region, whereas the skewness of the profile in the intermediate temperature region results in the evident departure from normality. Moreover the two reactivity parameters, the start (R1) and end (R2) of reactivity, take into account for the tails behavior of the temperature profile.

A Kolmogorov-Smirnov two Samples Test has also been used to demonstrate that all the collected reactivity maps can be fitted with the same parametric distribution, even

if not normal. Even if this test does not return the value of the parameters of the underlying distribution, it still provides essential information. In fact, since the underlying distribution is the same for every experimental data set (even if with different values of the characterizing parameters), this implies that the three moments can be successfully used to compare different reactivity maps.

Finally, for comparing two runs of the same experiment, the Quantile-Quantile (QQ) Plot method has been applied (procedure #3). This is an effective EDA graphical tool for the analysis of two response variables. Being an EDA technique, the QQ plot postpones the usual assumptions about what kind of model the data follow. It is constructed by plotting the quantiles of one set of data against the corresponding quantiles of the other. If the two distributions were identical, all of the points of the QQ plot would lie exactly on the 45 degree diagonal, whereas departures from this line give us detailed information about how the two distributions differ. This technique is very powerful when comparing two runs of the same experiment, such as in the case of testing the facility reproducibility (see Chapter 4) since it provides a detailed comparison based over the entire range of the distributions instead of based only on a small number of summary statistics (mean, standard deviation, etc.). Moreover, it allows detecting any shift in location, in scale, or a change in symmetry, all from one plot. In particular if the two set of data differ by a shift in location, then the points on the QQ plot would be translated either up or down the 45 degree reference. On the other hand, a shift in scale would result into a change of the slope of the points on the QQ plot.

3.9 CONCLUSIONS

This chapter provided a description of the experimental facilities and analysis techniques used in this study. The pressurized flow reactor facility has been upgraded by the redesign of the line delivering extracted samples to the gas analyzers. Also, due to the physical (boiling point) and chemical (autoignition reactivity) characteristics of some of the diesel compounds investigated in this study, the existing methods for fuel calibration and fuel delivery were redesigned in order to consistently deliver the required flow rates. In combination, these two new methods have greatly increased system repeatability (CO mapping differences less then 5%) and decreased concentration variations during CCD experiments.

A parametric statistical data analysis method to perform the comparison of the reactivity maps obtained through two different CCD experiments has been developed and implemented. This method is based on several statistics and reactivity measures, including the first three moments (mean, variance, and skewness) of the data distributions as measures of location, shape and skewness of each temperature profile as well as measures of reactivity start, end, and peak.

The details of experimental work are discussed in Chapter 4 regarding the oxidation of pure hydrocarbons, in Chapter 5 regarding the oxidation of binary, ternary and larger mixtures, and in Chapter 6 for the synthesis of a chemical surrogate for JP-8.
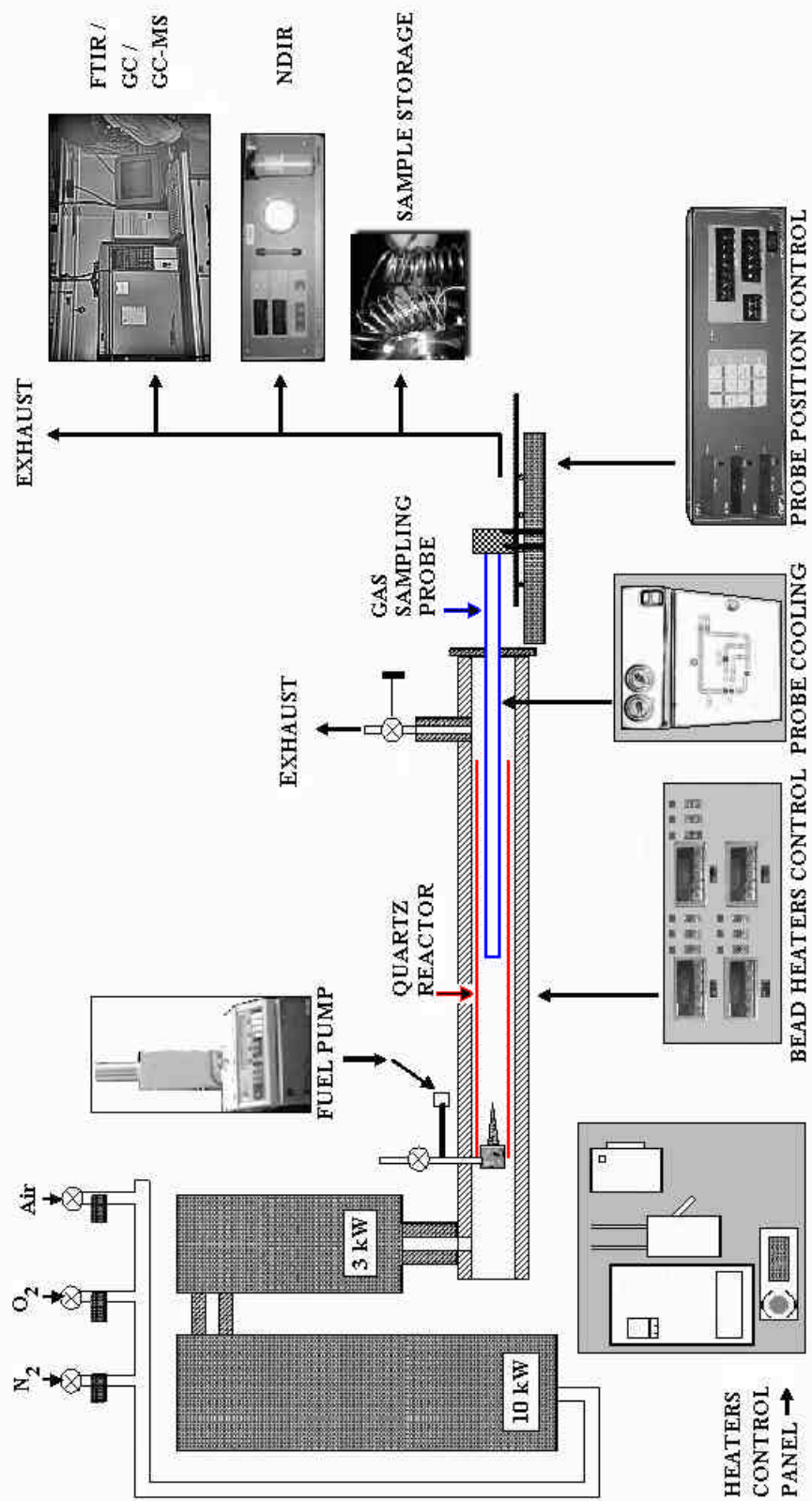
Figure 3.1 PFR Schematic
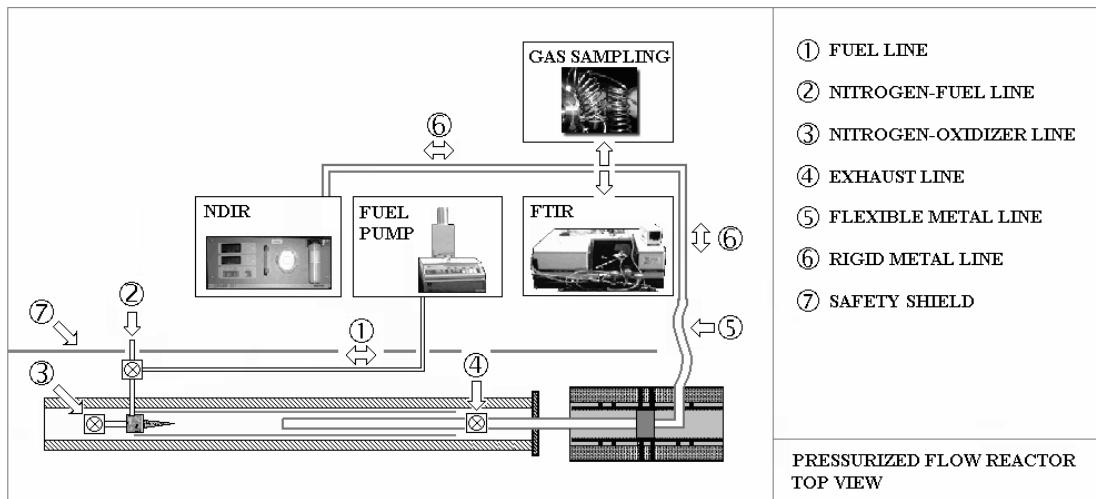
Figure 3.2 PFR Top View
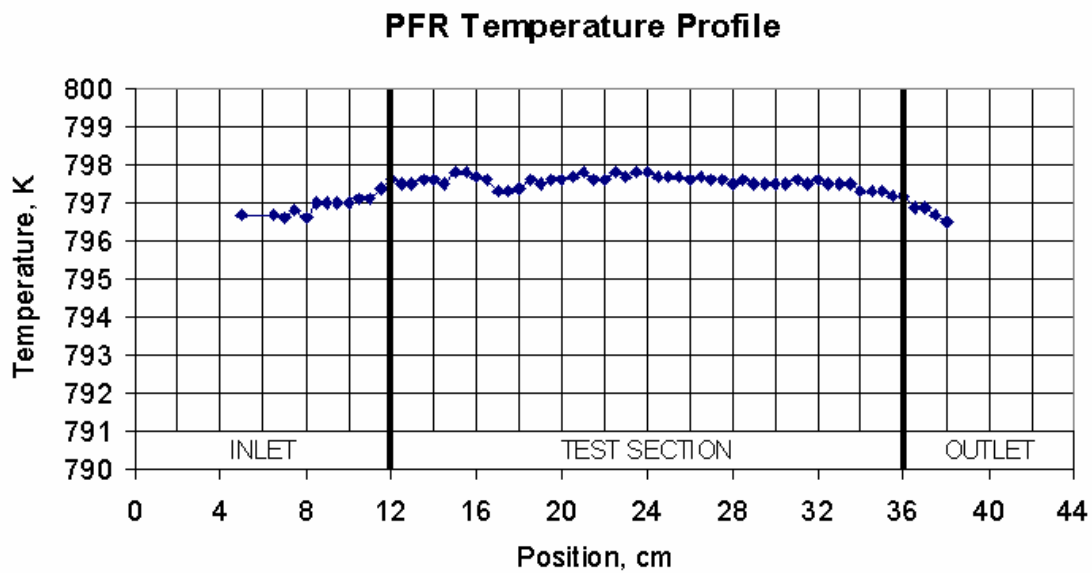
Figure 3.3 PFR Temperature Profile
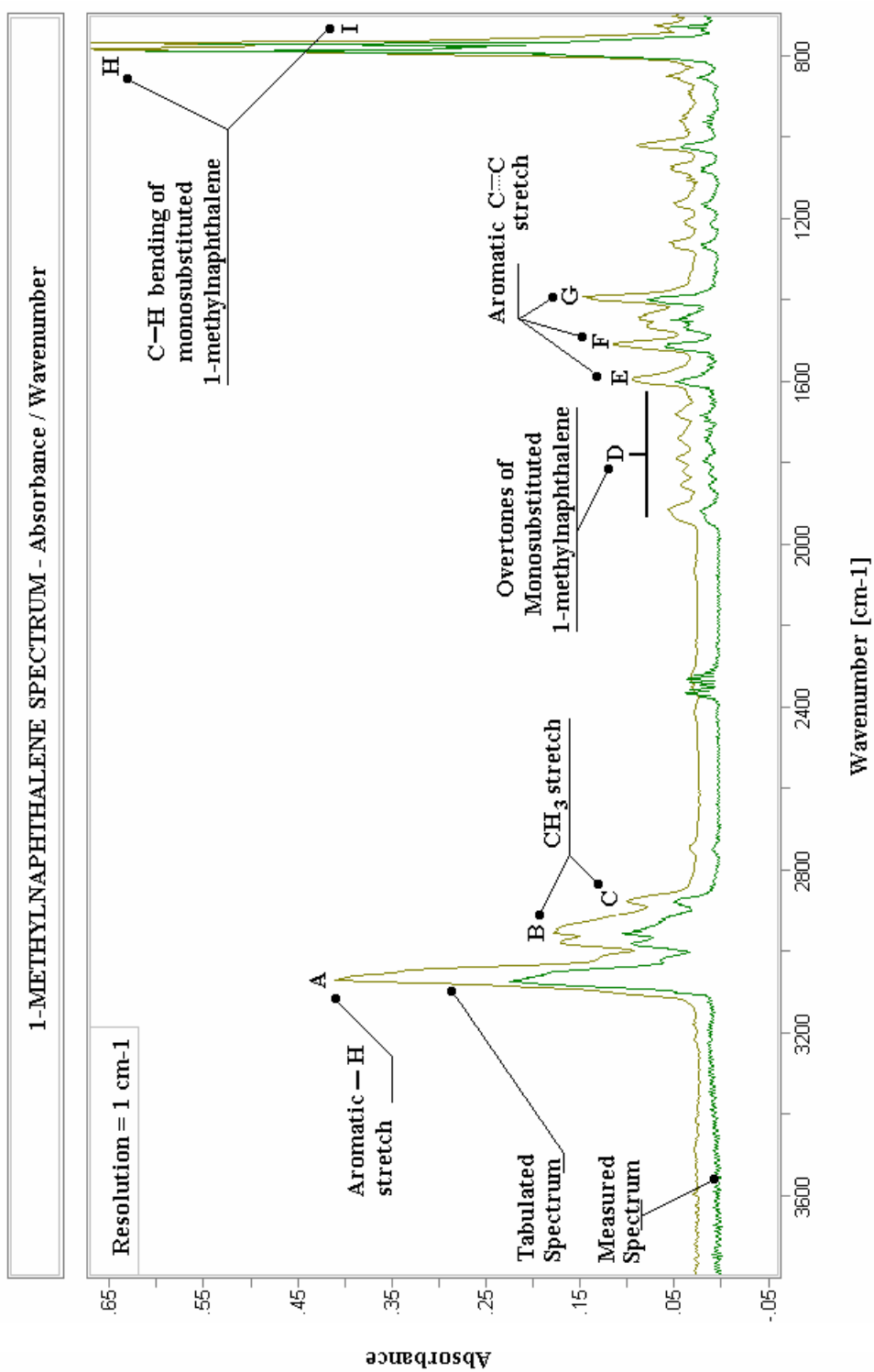
Figure 3.4 a-Methylnaphthalene Spectra Comparison
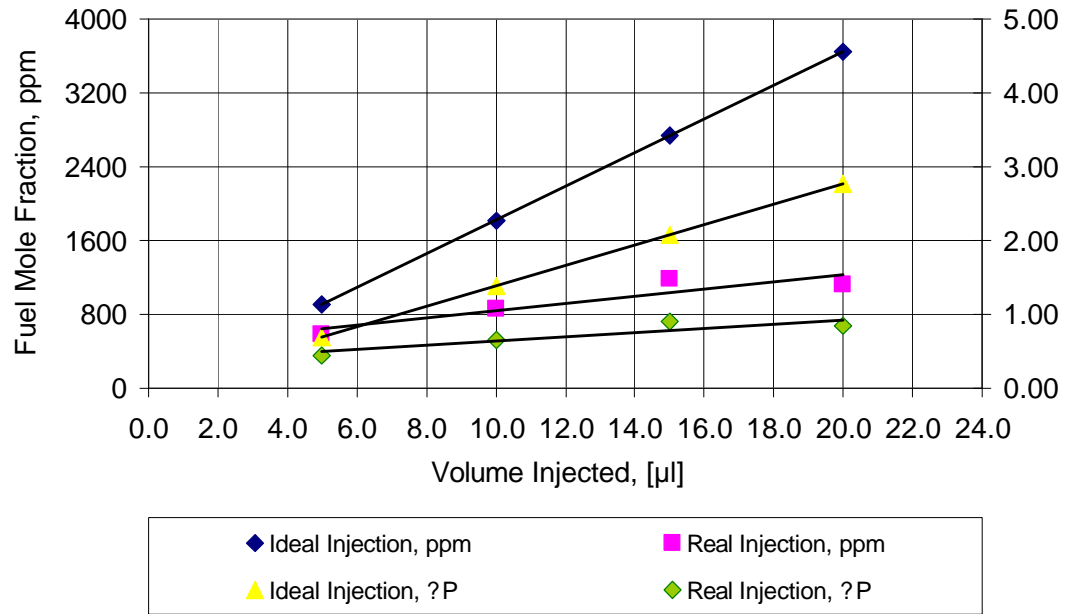
Figure 3.5 Fuel Calibration: Single Injection Method
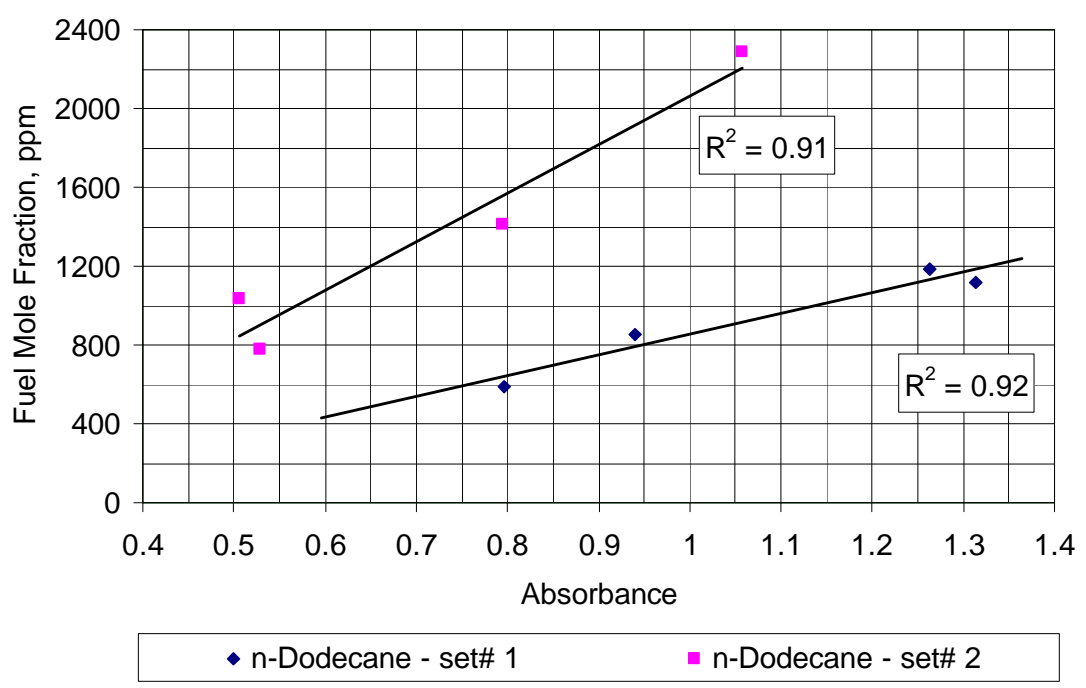
Figure 3.6 Fuel Calibration Curve: Single Injection Method
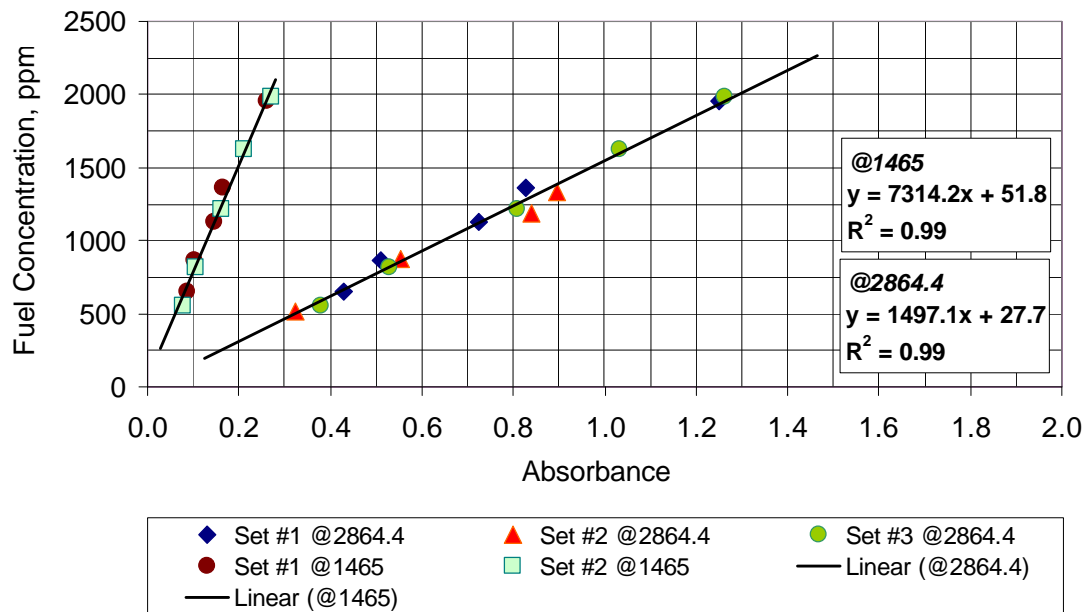
Figure 3.7 Fuel Calibration - FTIR: n-Dodecane
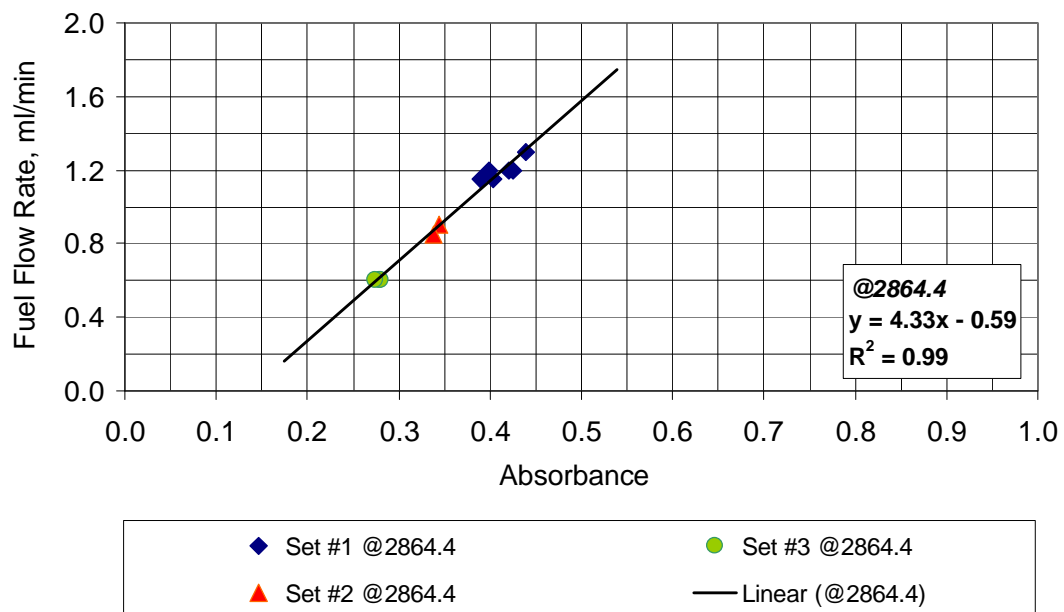
Figure 3.8 Fuel Calibration - PUMP: n-Dodecane
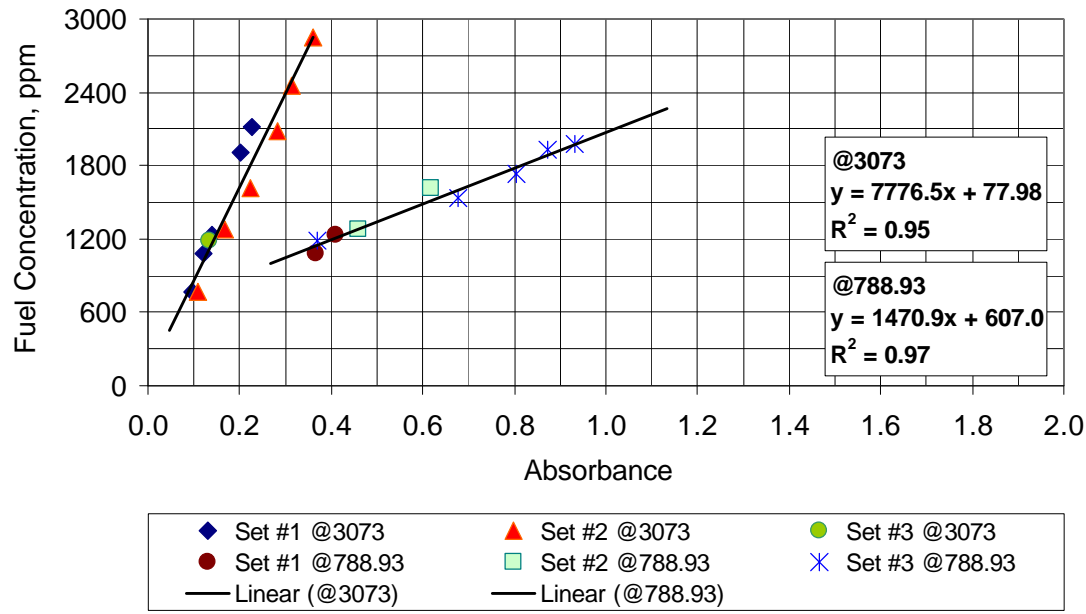
Figure 3.9 Fuel Calibration - FTIR: a-Methylnaphthalene
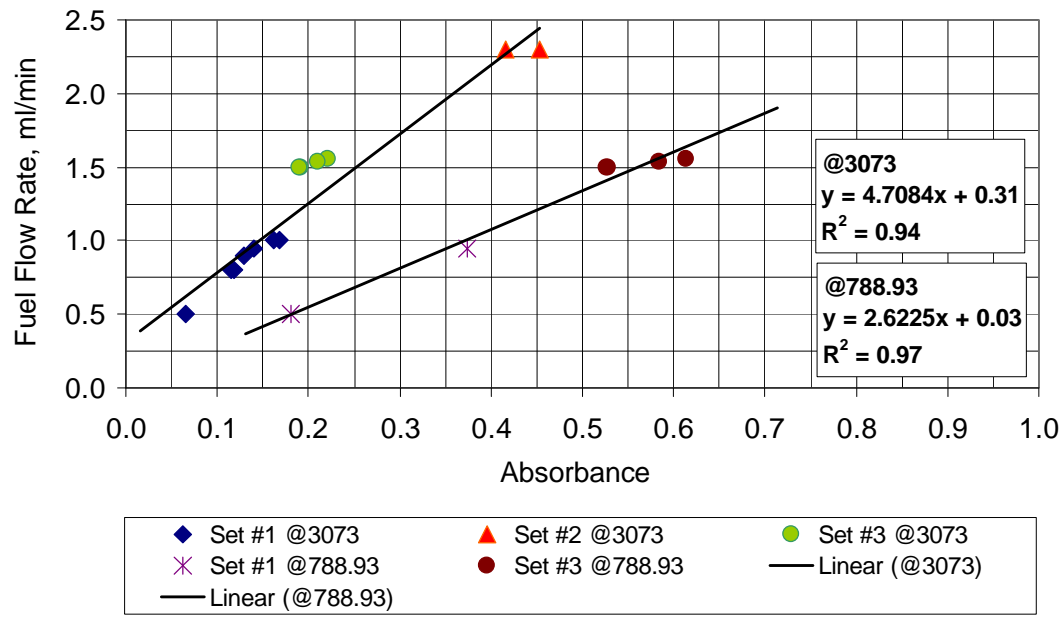
Figure 3.10 Fuel Calibration - PUMP: a-Methylnaphthalene
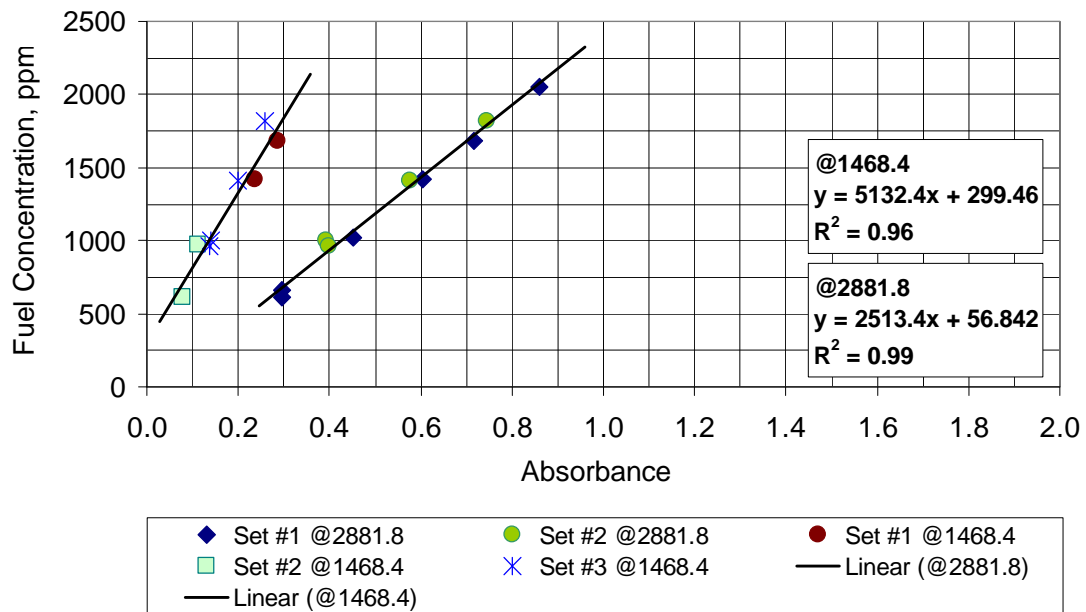
Figure 3.11 Fuel Calibration - FTIR: JP-8
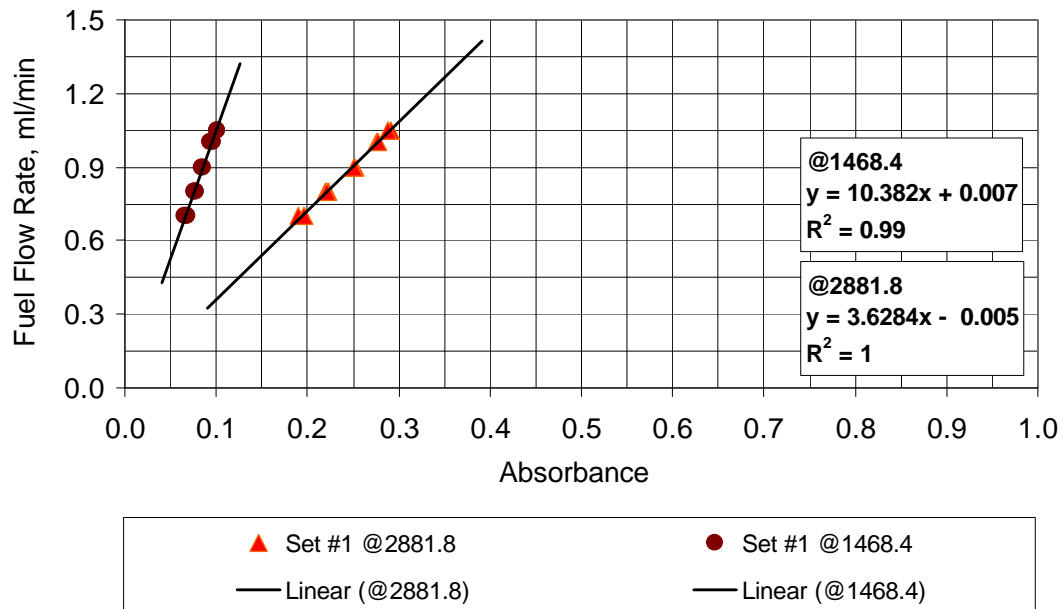
Figure 3.12 Fuel Calibration - PUMP: JP-8

79
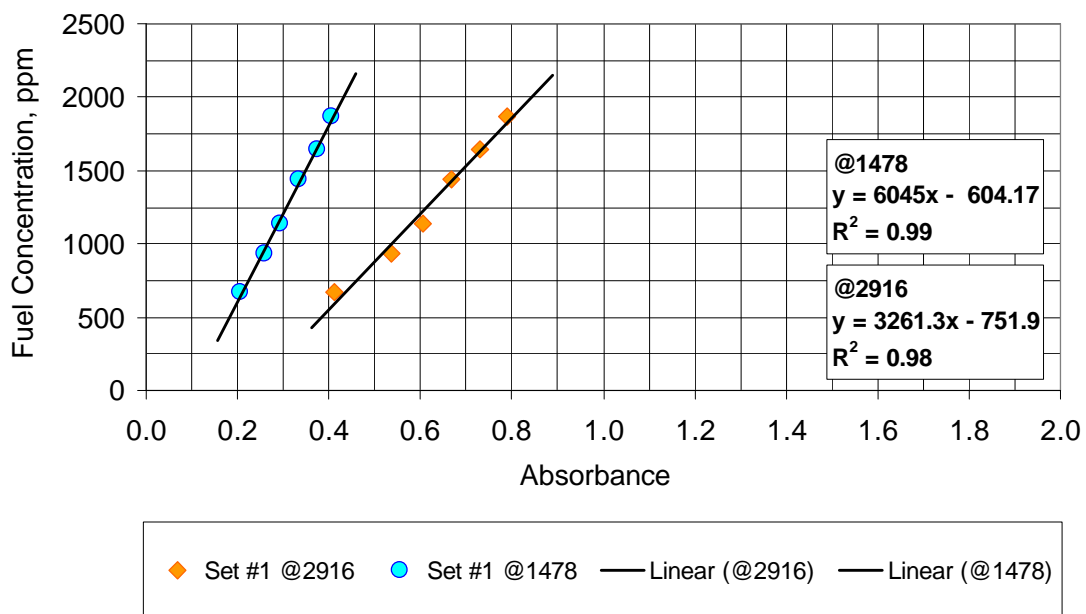
Figure 3.13 Fuel Calibration - FTIR: Isocetane
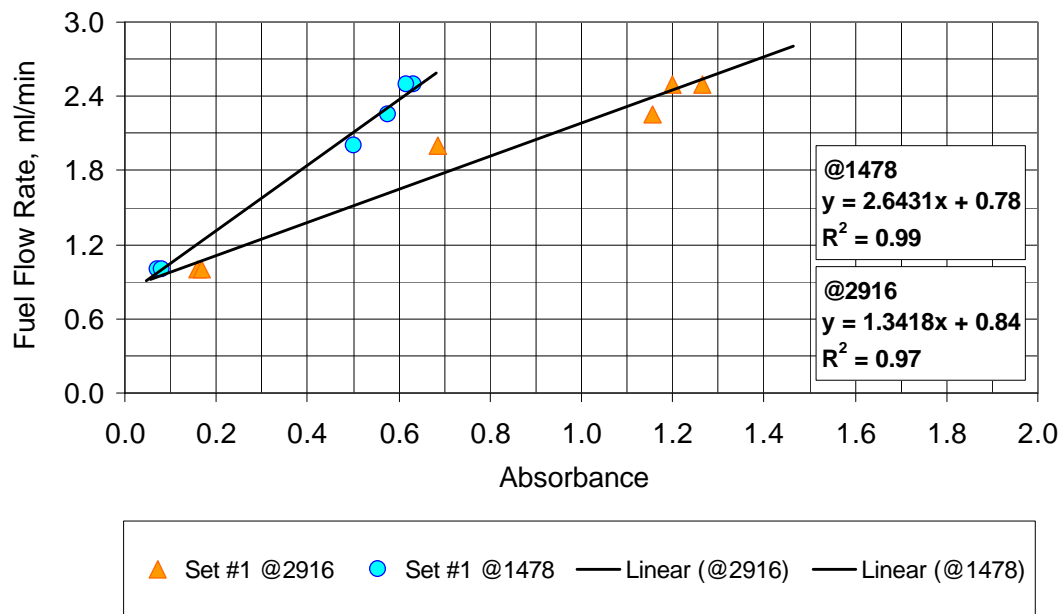
Figure 3.14 Fuel Calibration - PUMP: Isocetane
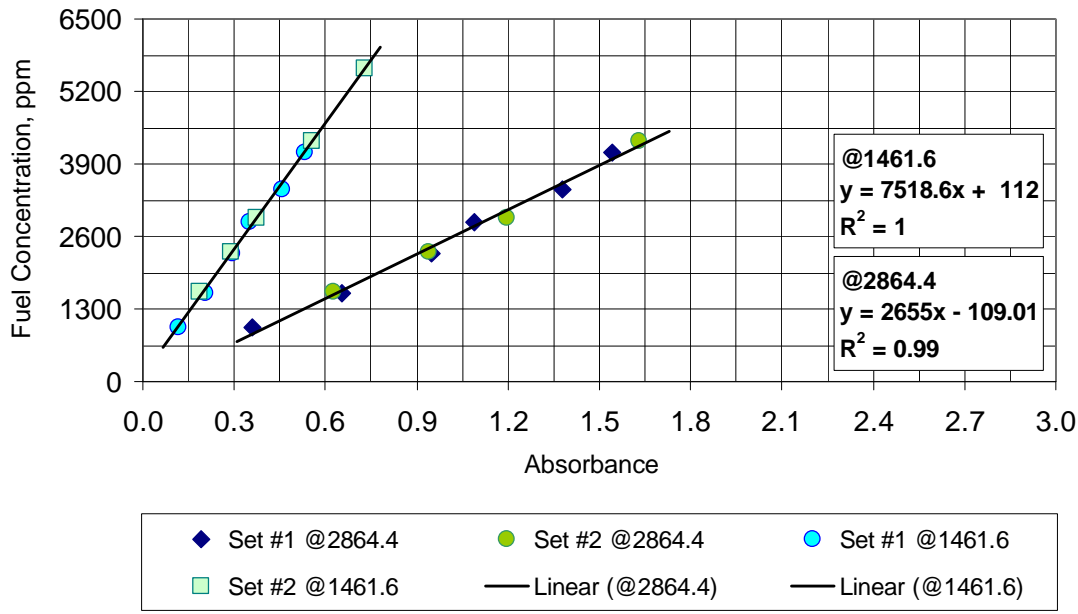
Figure 3.15 Fuel Calibration - FTIR: Methylcyclohexane
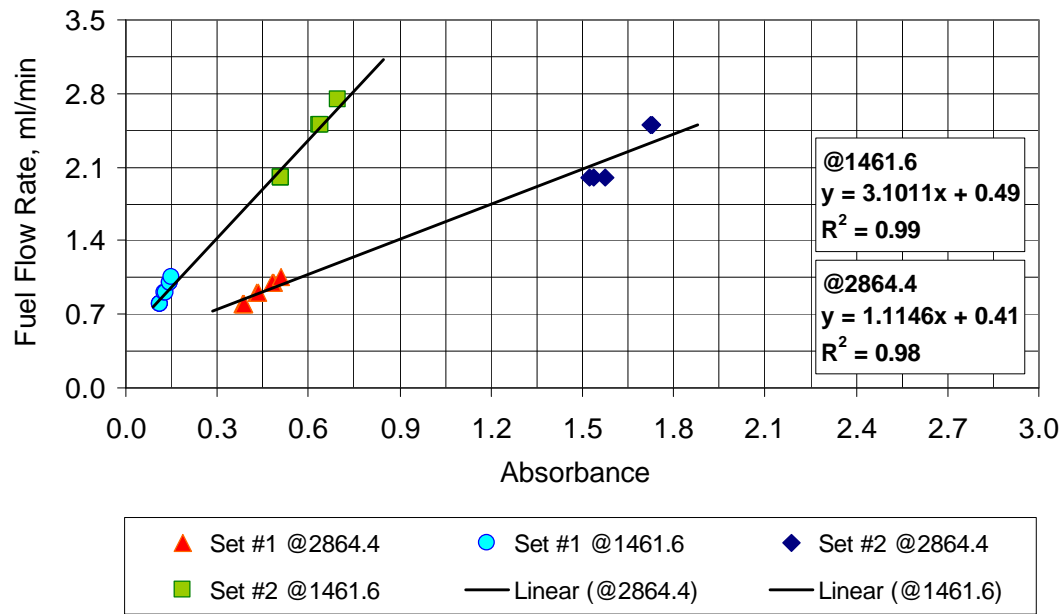
Figure 3.16 Fuel Calibration - PUMP: Methylcyclohexane
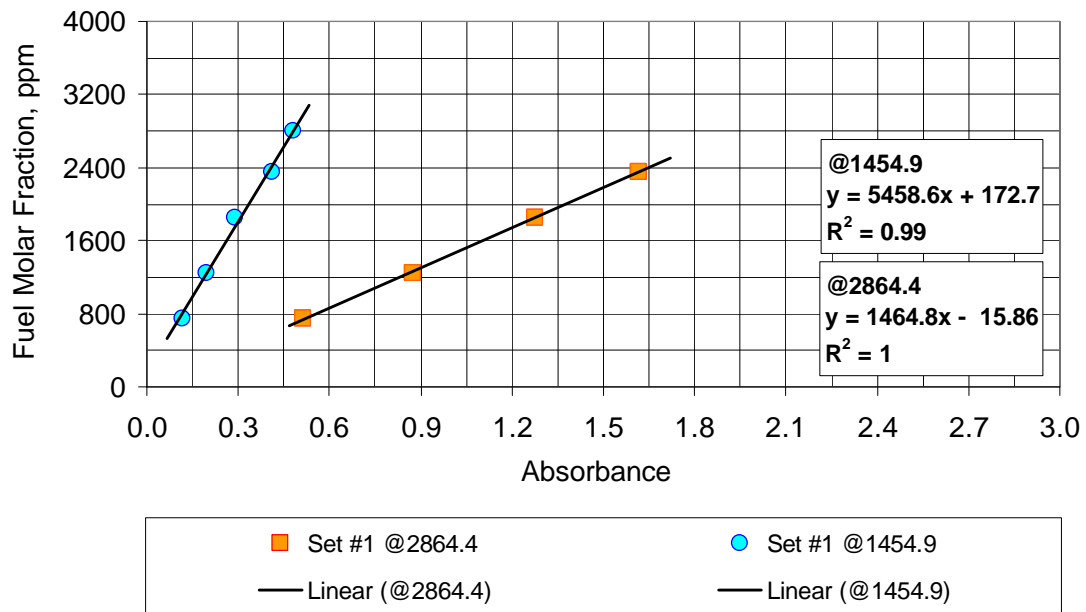
Figure 3.17 Fuel Calibration - FTIR: Decalin
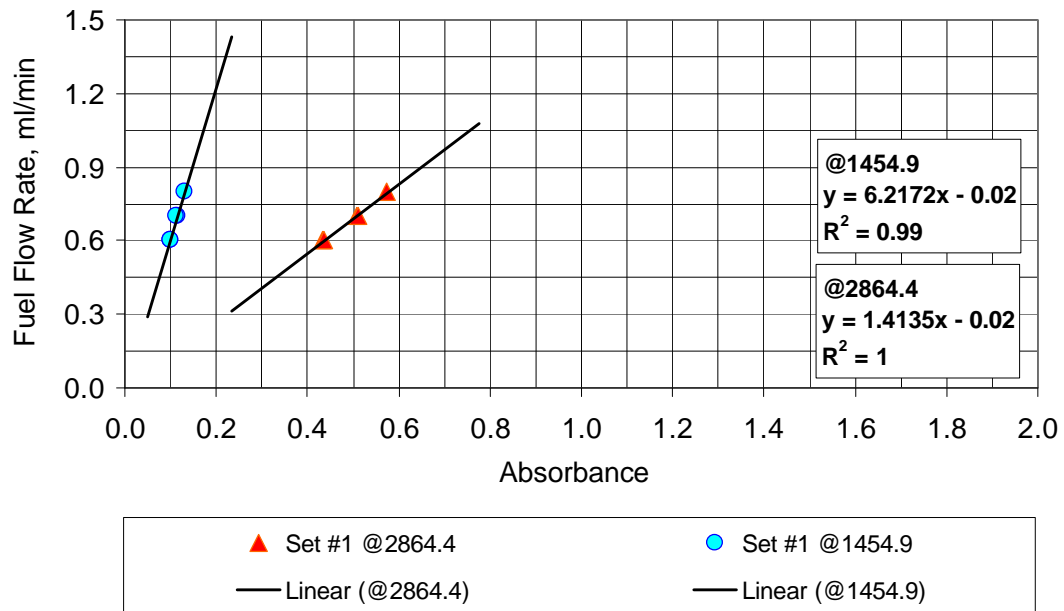
Figure 3.18 Fuel Calibration - PUMP: Decalin
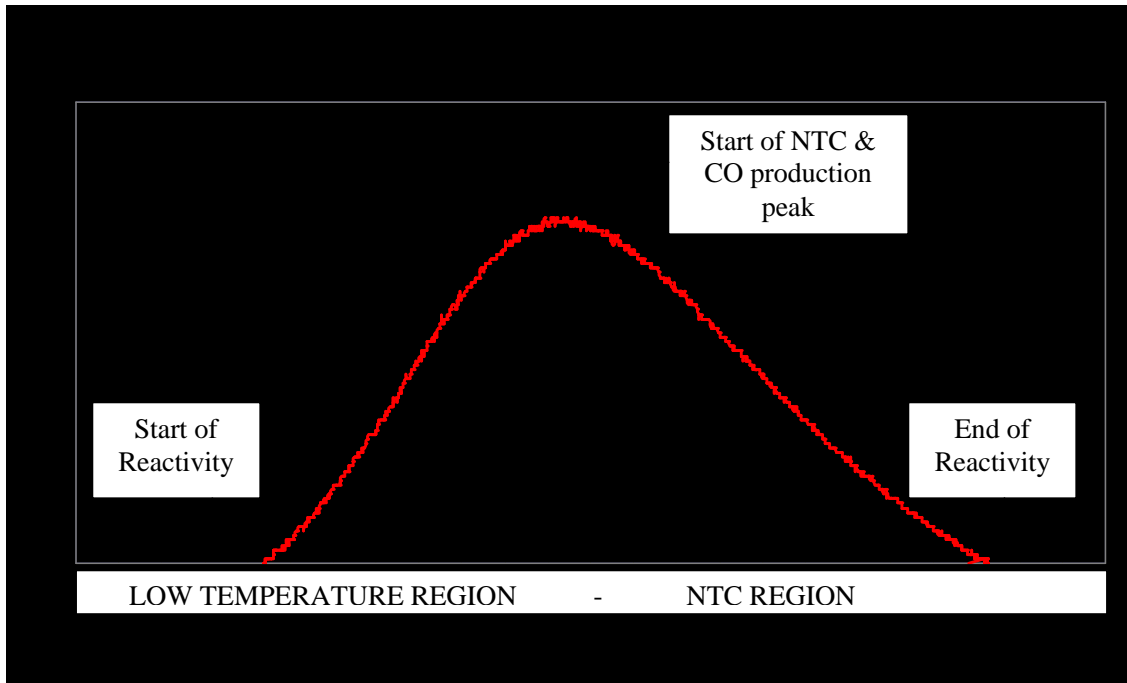
Figure 3.19 Fuel Reactivity Map
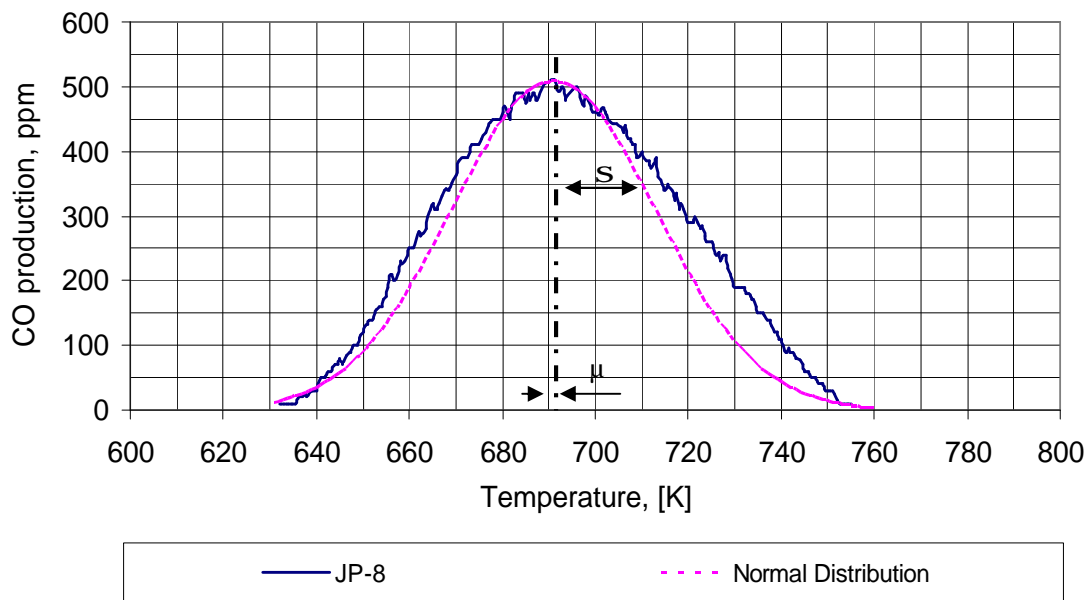
Figure 3.20 Reactivity Map: Normal Fitting

CHAPTER 4 – SINGLE FULL BOILING RANGE FUELS: RESULTS AND DISCUSSION

4.1 INTRODUCTION

This chapter presents the results of an investigation into the oxidation characteristics of the following pure hydrocarbon components of full boiling range fuels: n-dodecane, 2,2,4,4,6,8,8-heptamethylnonane (isocetane), a-methylnaphthalene, decalin, and methylcyclohexane. Experiments were also conducted with n-heptane, to verify the facility reproducibility, as shown in Section 4.2, and to build a linear correlation between the maximum production of carbon monoxide and the Cetane number of a fuel. All these fuels have been selected since they are representative of different classes of compounds which are present in typical diesel and aviation fuels. The experimental conditions – including equivalence ratio (F), pressure (P), nitrogen percent dilution, residence time (t), and fuel flow rate – for the Controlled Cool Down experiments are reported in Table 4.1. Reactivity maps are presented for the various experiments at the end of this Chapter. Nitrogen percent dilution has been calculated based on volumetric flow rates of air (21% oxygen, 79% nitrogen) and nitrogen, using equation 4.1 (Koert, 1990):

$$\% \; Dilution \; = \; \frac{\dot{V}_{N2}}{\dot{V}_{AIR} \; + \; \dot{V}_{N2}} \tag{4.1}$$

The experiments covered a range of temperatures from approximately 600 K up to 800 K at elevated pressures ranging from 8 to 12 atm. Nitrogen dilution varied from 65% to 80%, with 80% necessary for the highly reactive fuels and proving to be the best

experimental condition in order to minimize the amount of heat released. An experimental matrix summarizing all the operating conditions and experimental results is reported in Appendix D. A detailed description of the fuel investigated, including fuel purity grade and supplier, is reported in Appendix C.

Table 4.1 Summary of Experimental Conditions: Single Compound Oxidation

FUEL	F	P [atm]	N_2 DILUTION [%]	t [ms]	FUEL FLOW RATE [ml/min]
N-DODECANE	0.20	8.0	80	120	0.60
	0.25	8.0	80	120	0.85
	0.30	8.0	80	120	1.10
N-HEPTANE	0.4	8.0	85	100	1.48
a-METHYLNAPHTHALENE	0.3	8.0	80	120	0.80
	0.3	8.0	70	175	0.80
	0.5	8.0	80	120	1.50
	0.7	8.0	65	215	2.20
	0.7	12.0	65	250	2.20
ISOCETANE	0.7	8.0	65	180	2.40
METHYLCYCLOHEXANE	0.3	8.0	80	120	1.05
	0.4	8.0	80	120	1.50
	0.6	8.0	70	120	2.00
	0.7	8.0	65	120	2.50
DECALIN	0.3	8.0	80	120	0.80
	0.4	8.0	80	120	1.10

4.2 FACILITY REPRODUCIBILITY: N-HEPTANE OXIDATION

In this section the results of pure n-heptane oxidation are reported. Two CCD experiments were conducted at exactly the same conditions on two different days and measured reactivity maps are compared to verify facility reproducibility. In both cases a clear NTC behavior was identified for this fuel. The experimental conditions for both runs with n-heptane are reported in Table 4.2. Results of quantitative data analysis are listed in Table 4.3, while reactivity maps are shown in Figure 4.1 and Figure 4.2.

A third experiment (not shown in Figure 4.1), was conducted in the temperature range 680 K to 800 K with a n-heptane mole fraction of 800 ppm (P = 8 atm, t = 120 ms) and the CO production peak was measured to be 850 ppm. This information has been used for the development of a correlation between the maximum CO production of a fuel and its Cetane number, as reported in section 4.8.

Table 4.2 Summary of Experimental Conditions: n-Heptane Oxidation

	EXP. NH-1
EQUIVALENCE RATIO	0.4
PRESSURE, [atm]	8.0
N_2 DILUTION, [%]	85
RESIDENCE TIME, [ms]	100
FUEL FLOW RATE, [ml/min]	1.48
FUEL MOLAR FRACTION, [ppm]	1145

Table 4.3 Quantitative Data Analysis: n-Heptane Oxidation

MEASURE	RUN NH-1	RUN NH-2
MEAN, μ_1	483.5	483.9
SAMPLE VARIANCE, μ_2	107,527	110,066
SKEWNESS, μ_3	-0.0344	-0.0559
START OF REACTIVITY, R_1, [K]	636	623
END OF REACTIVITY, R_2, [K]	768	770
START OF NTC, R_X, [K] (HORIZONTAL LOCATION)	705	705
START OF NTC, R_Y , [ppm] (VERTICAL LOCATION)	945	950

As explained in detail in Section 3.6, the introduction of the new fuel delivery system based on a high pressure syringe pump and the application of the new fuel calibration method resulted in considerably improved facility reproducibility. As discussed in this section, the difference in CO production between two runs of the same experiment is now consistently less than 5%.

As shown in Figure 4.1, the reactivity of n-heptane starts at approximately 630 K ± 10 °C and then increases up to 705 K where the CO production reaches its maximum of 950 ppm. This point coincides with the start of the NTC region and identifies the end of a region of increasing reactivity that spans a range of 75 °C ± 10 °C. Further increase in the temperature results into a decrease of CO production until a zero level of reactivity is reached around 770 K ± 5 °C. This point identifies the end of the NTC regime and a region of decreasing reactivity spanning 65 °C ± 5 °C. The two

regions appear to be of slightly different size, as it is also shown by the skewness measure. If temperatures would be increased further, reactivity would again increase signaling the beginning of the intermediate temperature regime. A small temperature rise occurred due to the heat released during the reaction, reaching a peak of $5\,°C \pm 5\,°C$ in coincidence with the maximum reactivity. The small amount of heat released can be related to the extremely high dilution (85%) that has probably masked the heat release effect. The quantitative data analysis conducted on both runs proves that the two temperature profiles are extremely similar. Both the statistical measures and the reactivity measures for the two runs are proof of the facility reproducibility. The main difference between the two reactivity maps appears in the start of reactivity (R_1), and it is reflected in the skewness measure too. In run NH-1 the oxidative process starts approximately at a temperature of 15 °C higher than in the case of run NH-2. This difference may – at least partially – be explained looking at the way the experiments are performed. Fluctuations in the system pressure are observed near the end of an experiment and can explain the observed difference in CO production. As explained in Section 3.7, a CCD experiment is conducted heating the reactor up to the maximum temperature of 800 K and then shutting off the heat sources. Therefore a temperature profile is measured starting from R_2, the point of NTC end, and going towards R_1, the start of reactivity, which is the last point to be measured. In the region close to R_2 the reactor cooling rate is at its maximum and the reactor temperature also drops quickly because of the end of the heat release balancing effect. A quick decrease in reactor temperature is followed by a quick variation in pressure because the gases volumetric flow rates decrease (the gas density is also a function of temperature). Therefore the observed pressure fluctuations can be related to

the slow response of the mass flow controller system to the change in the reactor pressure that is naturally related to the temperature decrease. As suggested in the Recommendations Section 7.3, a computer controlled pressure regulation system would significantly reduce this problem. Finally, it is possible to conclude that, considering all the experiments conducted in this study, R_2 is known with an approximation of $\pm 5\,°C$, whereas R_1 oscillates into a range of about $\pm 10\,°C$.

In Figure 4.2 a quantile-quantile (QQ) plot shows the similarity between temperature profiles for the two runs with n-heptane. In fact, the points in the QQ plot are almost aligned to the 45 degree reference line (see section 3.8). The QQ plot identifies the small difference between the two profiles at the beginning of NTC region. The maximum difference observed is of approximately 5% of the total CO production. This value is lower than in previous studies with this facility and it shows the improvement of the facility reproducibility.

4.3 N-DODECANE OXIDATION

In this section the results of pure n-dodecane oxidation are reported. n-Dodecane is a straight chain alkane composed of 12 atoms joined by single bonds and it has been selected since it is representative of the normal paraffins present in typical diesel and aviation fuels. Moreover, its physical properties, such as density, match those of JP-8 over a wide range of temperatures. Three CCD experiments were conducted at different conditions of equivalence ratio (F = 0.2, 0.25, and 0.3). Reactivity and NTC behavior was clearly observed in all cases. The experimental conditions for all the runs with n-dodecane are reported in Table 4.4. Results of the quantitative data analysis are listed in Table 4.5, while reactivity maps are shown in Figure 4.3.

Table 4.4 Summary of Experimental Conditions: n-Dodecane Oxidation

	EXP. ND-1	EXP. ND-2	EXP. ND-3
EQUIVALENCE RATIO	0.2	0.25	0.3
PRESSURE, [atm]	8.0	8.0	8.0
N_2 DILUTION, [%]	80	80	80
RESIDENCE TIME, [ms]	120	120	120
FUEL FLOW RATE, [ml/min]	0.60	0.85	1.10
FUEL MOLAR FRACTION, [ppm]	454	567	680

Table 4.5 Quantitative Data Analysis: n-Dodecane Oxidation

MEASURE	EXP. ND-1	EXP. ND-2	EXP. ND-3
MEAN, μ_1	397.0	648.4	890.5
SAMPLE VARIANCE, μ_2	57,346.9	164,409	263,870
SKEWNESS, μ_3	-0.05398	0.06371	0.02856
START OF REACTIVITY, R_1, [K]	624	~613	>600
END OF REACTIVITY, R_2, [K]	792	~800	>800
START OF NTC, R_X, [K] (HORIZONTAL LOCATION)	694	693	703
START OF NTC, R_Y, [ppm] (VERTICAL LOCATION)	750	1270	1660

As shown in Figure 4.3, the reactivity of n-dodecane starts and ends at different temperature values, depending on the different experimental conditions. As the fuel molar fraction is increased from Exp. ND-1 to Exp. ND-3, the region of reactivity becomes larger. The points of start and end of reactivity for Exp. ND-1 are respectively about 624 K and 792 K, becoming 613 K and 800 K for Exp. ND-2, and being out of the measured area (< 600 K and > 800 K) for Exp. ND-3. It is particularly interesting to note the correlation between the n-dodecane molar fraction (Table 4.4) and the approximate turnover temperature between the end of NTC region and the start of the intermediate regime (R_2, in Table 4.5). Increasing the fuel molar fraction results in a shift of R_2 towards higher temperatures. This information is interesting at the light of the role that n-dodecane plays in the JP-8 surrogate mixture (see Chapter 6). In fact, since all the other fuels present in the surrogate mixture are less reactive than n-dodecane, it is n-dodecane

itself that drives the start and end of the entire mixture reactivity, creating a radical pool large enough to initiate the oxidation of the other compounds. Therefore, once the points R_1 and R_2 from the JP-8 reactivity map are known ($\pm$ 10 °C), it is possible to approximately predict the amount of n-dodecane that is required in the surrogate to initiate and finish the oxidation at the correct temperature values. Considering that at the same conditions of Exp. ND-3 the value of R_2 for JP-8 is about 770 K (see Section 6.3), approximately 30% of n-dodecane is required. Of course, this prediction is only valid when looking at R_1 and R_2, while the overall CO production of a mixture can not be predicted from the n-dodecane temperature profile only, since the oxidative behavior of the mixture – whether synergistic or antagonistic – is unknown a priori.

CO production reaches a peak at approximately 695 K for Exp. ND-1, 695 K for Exp. ND-2, and 705 K for Exp. ND-3. The shift to the higher temperatures of the reactivity map for the peak position of Exp. ND-3 is not expected. In theory when the fuel molar concentration is increased, the start of NTC should shift to the left. The anomalous shift in Exp. ND-3 is probably related to the larger heat release from this mixture that increases the true reaction temperature. The effect of heat release on reactor temperature rise has been approximately calculated following Ramotowski (Ramotowski, 1992) and it is estimated to be, at the NTC start, 5 °C for Exp. ND-1, 10 °C for Exp. ND-2, and 20 °C for Exp. ND-3. Finally, the quantitative analysis conducted on the three data set shows that the three reactivity maps are similar, with a linear change in the location and shape of the temperature profiles depending mainly on the fuel molar fraction.

4.4 DECALIN OXIDATION

In this section the results of the oxidation of pure decalin (mixture of *cis* and *trans* decahydronaphthalene, see Appendix C) are reported. Decalin is a bicyclical naphthenic compound and it is a typical component of jet fuels since it has desirable gravimetric and volumetric energy densities and good combustion performance (Maurice et al., 2001). Moreover, it has a boiling point that falls approximately in the middle of the kerosene-type jet fuel boiling range and its ignition behavior, measured by the Cetane number, is comparable to that of JP-8. Two CCD experiments were conducted at different conditions of equivalence ratio (F = 0.3, and 0.4). Reactivity and NTC behavior were clearly observed in all cases. The experimental conditions for all the runs with decalin are summarized in Table 4.6. Results of the quantitative data analysis are listed in Table 4.7, while reactivity maps are shown in Figure 4.4.

Table 4.6 Summary of Experimental Conditions: Decalin Oxidation

	EXP. DC-1	*EXP. DC-2*
EQUIVALENCE RATIO	0.3	0.4
PRESSURE, [atm]	8.0	8.0
N_2 DILUTION, [%]	80	80
RESIDENCE TIME, [ms]	120	120
FUEL FLOW RATE, [ml/min]	0.80	1.10
FUEL MOLAR FRACTION, [ppm]	868	1157

Table 4.7 Quantitative Data Analysis: Decalin Oxidation

MEASURE	EXP. DC-1	EXP. DC-2
MEAN, μ_1	334.6	486.9
SAMPLE VARIANCE, μ_2	29,089	78,093
SKEWNESS, μ_3	-0.45328	-0.38219
START OF REACTIVITY, R_1, [K]	656	651
END OF REACTIVITY, R_2, [K]	724	726
START OF NTC, R_x, [K] (HORIZONTAL LOCATION)	696	700
START OF NTC, R_Y, [ppm] (VERTICAL LOCATION)	560	850

As shown in Figure 4.4, the reactivity region for decalin is very narrow, for example when compared to that of a fuel with similar CN, such as n-heptane. Reactivity starts and ends at different temperature values, depending on the different experimental conditions, but these differences are small (approximately 5 °C), compared to the n-dodecane values. As the fuel molar fraction is increased from Exp. DC-1 to Exp. DC-2, the extent of CO production becomes larger, but R_1 and R_2 change just slightly. In fact the points of start and end of reactivity for Exp. DC-1 are respectively about 656 K and 724 K, while for Exp. DC-2 they are about 651 K and 726 K. The narrow extent of the reactivity region (from R_1 to R_2) for decalin (and for methylcyclohexane too, as reported in Section 4.6) can explain the narrow temperature profile observed for JP-8 since cycloalkanes represents up to the 20% of the JP-8 volumetric composition. Even though decalin proved to react over only a small temperature region, once the reaction is

initiated, the CO production rapidly increases. Considering the quantitative analysis, the high value of the skewness measure reflects the huge amount of heat that is released during the reaction. Moreover, considering the region near the end of R_2 – which actually is the start of the CCD experiment – the heat released is the cause of the unexpected inverse concavity of the temperature profile and the temperature rise has been calculated to be approximately 5 °C ± 5 °C for Exp. DC-1 and 8 °C ± 5 °C for Exp. DC-2. However, the maximum heat release occurred in coincidence with the start of NTC and maximum of CO production and it has been calculated to be 17 °C ± 10 °C for Exp. DC-1 and 23 °C ± 10 °C for Exp. DC-2. The CO production almost linearly increases with the fuel molar fraction and the peak of maximum CO production occurs for both experiments at about 700 K. Fluctuations in the system pressure and CO production are observed in particular for Exp. DC-2 during the period of maximum reactivity and are reflected in the reactivity map shown in Figure 4.4.

4.5 a-METHYLNAPHTHALENE OXIDATION

In this section the results of the oxidation of pure a-methylnaphthalene are reported. This is a bicyclical compound of the aromatic class and it was the original low reference point for the Cetane scale (CN = 0). Due to its high density, a-methylnaphthalene has a high energy content per unit volume, a requirement for aviation fuels. However a-methylnaphthalene is also characterized by a poor combustion quality and low-temperature flow properties, even if the contents of the naphthalene-type aromatics is limited to 3% for jet fuels. This compound has been chosen as a JP-8 surrogate component candidate since it has been studied extensively and good kinetic

models already exist. Five CCD experiments were conducted at different conditions of equivalence ratio, pressure and nitrogen dilution, as reported in Table 4.8. Reactivity was not observed in any case, even at the drastic conditions of Exp. MN-5, because of the high stability of a-methylnaphthalene double benzenic ring. In Exp. MN-5, the reactor pressure was raised to 12 atm, in order to provide conditions favorable for the start of reactivity. In fact, considering experiments MN-4 and MN-5, the pressure rise from 8 atm to 12 atm is reflected as a 50% increase in the fuel molar flow rate, from 0.4629 mol/m^3 to 0.6943 mol/m^3. However, even at these conditions the fuel did not ignite. Therefore higher temperatures and pressures are needed to, first, break the a-methylnaphthalene molecule by pyrolysis and then start the oxidative process. The nitrogen dilution was lowered from 80% in experiments MN-1 and MN-3 to the minimum limit of 65% in experiments MN-4 and MN-5. Lower percentages of nitrogen dilution could not be achieved in the reactor without the risk of thermally stressing the reactor itself and without creating mixing problems in the nozzle.

Table 4.8 Summary of Experimental Conditions: a-Methylnaphthalene Oxidation

	EXP. MN-1	EXP. MN-2	EXP. MN-3	EXP. MN-4	EXP. MN-5
EQUIVALENCE RATIO	0.3	0.3	0.5	0.7	0.7
PRESSURE, [atm]	8.0	8.0	8.0	8.0	12.0
N$_2$ DILUTION, [%]	80	70	80	65	65
RESIDENCE TIME, [ms]	120	175	120	215	250
FUEL FLOW RATE, [ml/min]	0.8	0.8	1.5	2.2	2.2
FUEL MOLAR FRACTION, [ppm]	932	1398	1553	3798	3798

4.6 METHYLCYCLOHEXANE OXIDATION

In this section results of pure methylcyclohexane oxidation are reported. This is a monocyclic compound of the naphthenic class and it is a typical component of aviation fuels and their surrogates. For example, it is a major component of JP-9, a specialty fuel that has been developed for demanding applications such as aircraft-launched missiles. In fact, being a hydrocarbon of the naphthenic class, methylcyclohexane is characterized by high volumetric energy content, clean burning, and good low-temperature performance. Four CCD experiments were conducted at different conditions of equivalence ratio and nitrogen dilution (see Table 4.9). Methylcyclohexane did not oxidize at the leanest conditions (equivalence ratio $F = 0.30$, N_2 dilution $= 80\%$, Exp. MC-1, and $F = 0.40$, N_2 dilution $= 80\%$, Exp. MC-2) while it was explosive at the less lean conditions ($F = 0.60$, N_2 dilution $= 70\%$, Exp. MC-3, and $F = 0.70$, N_2 dilution $= 65\%$, Exp. MC-4). At the experimental conditions of Exp. MC-1 and Exp. MC-2, methylcyclohexane resisted ignition over the temperature range tested (660 K to 800 K). At the experimental conditions of Exp. MC-3 and Exp. MC-4, methylcyclohexane ignited when the reactor temperature decreased from 800 K to 720 K and 750 K, respectively, but its oxidation was unstable and both experiments were halted when a CO production of approximately 2000 ppm was measured at slightly lower temperatures. The magnitude of the heat release was apparent in that before the reactivity started the reactor was cooling at a 3 °C/min rate while after ignition the reactor "reheated" at 2 °C/min. In conclusion, controlled oxidation of methylcyclohexane was not achievable in our system due a very narrow band of conditions over which the reaction could be stabilized. However, it should be noted that the end of reaction temperature in Exp. MC-3 ($R_2 = 720$ K) and

MC-4 (R_2 = 750 K) is very low compared to that of n-dodecane ($R_2 \sim$ 790 K), but similar to decalin ($R_2 \sim$ 725 K). Thus, an oxidative behavior characterized by a very narrow temperature profile and high reactivity seems to occur for methylcyclohexane. As shown in the following chapters, this characteristic can explain the oxidative behavior of a very complex mixture such as JP-8, which contains up to 20% (v/v) of naphthenic class compounds.

Table 4.9 Summary of Experimental Conditions: Methylcyclohexane Oxidation

	EXP. MC-1	*EXP. MC-2*	*EXP. MC-3*	*EXP. MC-4*
EQUIVALENCE RATIO	0.3	0.4	0.6	0.7
PRESSURE, [atm]	8.0	8.0	8.0	8.0
N_2 DILUTION, [%]	80	80	70	65
RESIDENCE TIME, [ms]	120	120	120	120
FUEL FLOW RATE, [ml/min]	1.05	1.50	2.00	2.50
FUEL MOLAR FRACTION, [ppm]	1199	1598	3588	4878

4.7 ISOCETANE OXIDATION

In this section the results of the oxidation of pure 2,2,4,6,6,8,8-heptamethylnonane (isocetane) are reported. Isocetane is a branched alkane and it is the reference point for the low end of the Cetane scale (CN = 15). For this reason this compound has been chosen in this study to represent the iso-paraffinic class of hydrocarbons in the development of JP-8 surrogate. Due to its high cost (see Appendix C), only one controlled cool down experiments was conducted. The experimental conditions in the reactor were chosen to favor reactivity and are listed in Table 4.10. The nitrogen dilution was set at its minimum value (65%) and a high concentration of oxygen was assured by the equivalence ratio of 0.7. However, reactivity was not observed over the range of temperatures tested (600 K to 800 K) due to the high resistance of isocetane to ignition, which is also reflected in its low Cetane number.

Table 4.10 Summary of Experimental Conditions: Isocetane Oxidation

	EXP. IC-1
EQUIVALENCE RATIO	0.7
PRESSURE, [atm]	8.0
N_2 DILUTION, [%]	65
RESIDENCE TIME, [ms]	180
FUEL FLOW RATE, [ml/min]	2.40
FUEL MOLAR FRACTION, [ppm]	2906

4.8 CETANE NUMBER – CO PEAK CORRELATION DEVELOPMENT

Following Wilk (Wilk et al., 1989), the results from the experimental oxidation of pure decalin (CN = 48), n-heptane (CN = 56), and n-dodecane (CN = 88) have been used to develop a linear correlation between fuel Cetane numbers and maximum production of CO. This correlation is similar to that developed by Wilk between the fuel Octane number and the maximum CO production, and is shown in Figure 4.5. The measured CO peaks were 560 ppm for decalin, 850 ppm for n-heptane, and 2200 ppm for n-dodecane. For decalin and n-heptane these are measured values, for n-dodecane the value was linearly extrapolated from the results of the 3 CCD experiments described in Section 4.3. This is due to the fact that to be compared all the experiments need to be performed at the same conditions of pressure, residence time, and fuel concentration. The correlation has been developed for $P = 8$ atm, $t = 120$ ms, and fuel mole fraction of approximately 800 ppm $\pm$ 75 ppm. Therefore, since for n-dodecane the experiments were conducted with 454 ppm, 567 ppm, and 680 ppm, a CO peak value for n-dodecane at 800 ppm had to be calculated. For 800 ppm of n-dodecane molar fraction, the corresponding CO peak has been determined to be 2200 ppm. It should be noted that the relation between the fuel molar fraction and the maximum CO production is linear ($R^2 = 0.99$) for the three experiments with n-dodecane, so a small error is expected from the mathematical extrapolation.

As shown in Figure 4.5, the correlation between Cetane number and CO peak is linear ($R^2 = 0.99$) and it can be applied for different purposes. For example, in Chapter 5 it is applied to verify the validity of linear blending assumption for the different mixtures developed and to extrapolate the blending Cetane numbers. Moreover the intersection

between the linear interpolation and the horizontal axis provides a prediction on whether the oxidation of a specific fuel can be achieved at those particular experimental conditions. Fuels with a Cetane number lower than 35 (a-methylnaphthalene (0), isocetane (15), and methylcyclohexane (20)) are predicted – and verified – not to ignite.

4.9 CONCLUSIONS

In an effort to expand kinetic and mechanistic information for larger hydrocarbon oxidation, fifteen controlled cool down experiments were conducted for five pure fuels to create a database regarding the ignition behavior of typical components of full boiling range fuels. Strong NTC behavior was observed for the most reactive compounds, specifically n-dodecane and decalin. Even though NTC behavior is expected for isocetane and methylcyclohexane, at the lean conditions tested reactivity was not observed. a-Methylnaphthalene, a bicyclical compound which is extremely resistant to ignition, could not be oxidized at the various conditions tested. The oxidative behavior of these three less reactive compounds will be reported in Chapter 5 based on experiments with binary blends with n-dodecane. Comparing the reactivity maps of n-dodecane and decalin, decalin reacted over a very narrow temperature range, approximately between 725 K and 655 K, compared to the corresponding values for n-dodecane, 800 K and 600 K. The characteristic of reacting over a narrow temperature range shown by decalin was also observed in the oxidation of methylcyclohexane, another naphthenic hydrocarbon. As shown in the following chapters, this characteristic can explain the oxidative behavior of a very complex mixture such as JP-8, which contains up to 20% by volume of naphthenic compounds.

N-heptane was oxidized to verify the facility reproducibility and because its ignition behavior, measured in terms of Cetane number, is intermediate between the high reactive n-dodecane and the low reactive isocetane, methylcyclohexane and a-methylnaphthalene. Two runs were conducted on different days, but at the same conditions. Both qualitative and quantitative analyses of measured reactivity maps showed the high degree of facility reproducibility achieved by upgrading the fuel calibration and fuel delivery systems.

A linear correlation between the Cetane number and the fuel molar fraction has been developed based on data from n-heptane, n-dodecane, and decalin oxidation. This correlation will be used to verify the validity of linear blending assumption for the different mixtures analyzed in Chapter 5 and to extrapolate the blending Cetane numbers for the JP-8 surrogate components.

Reactivity Map: n-Heptane
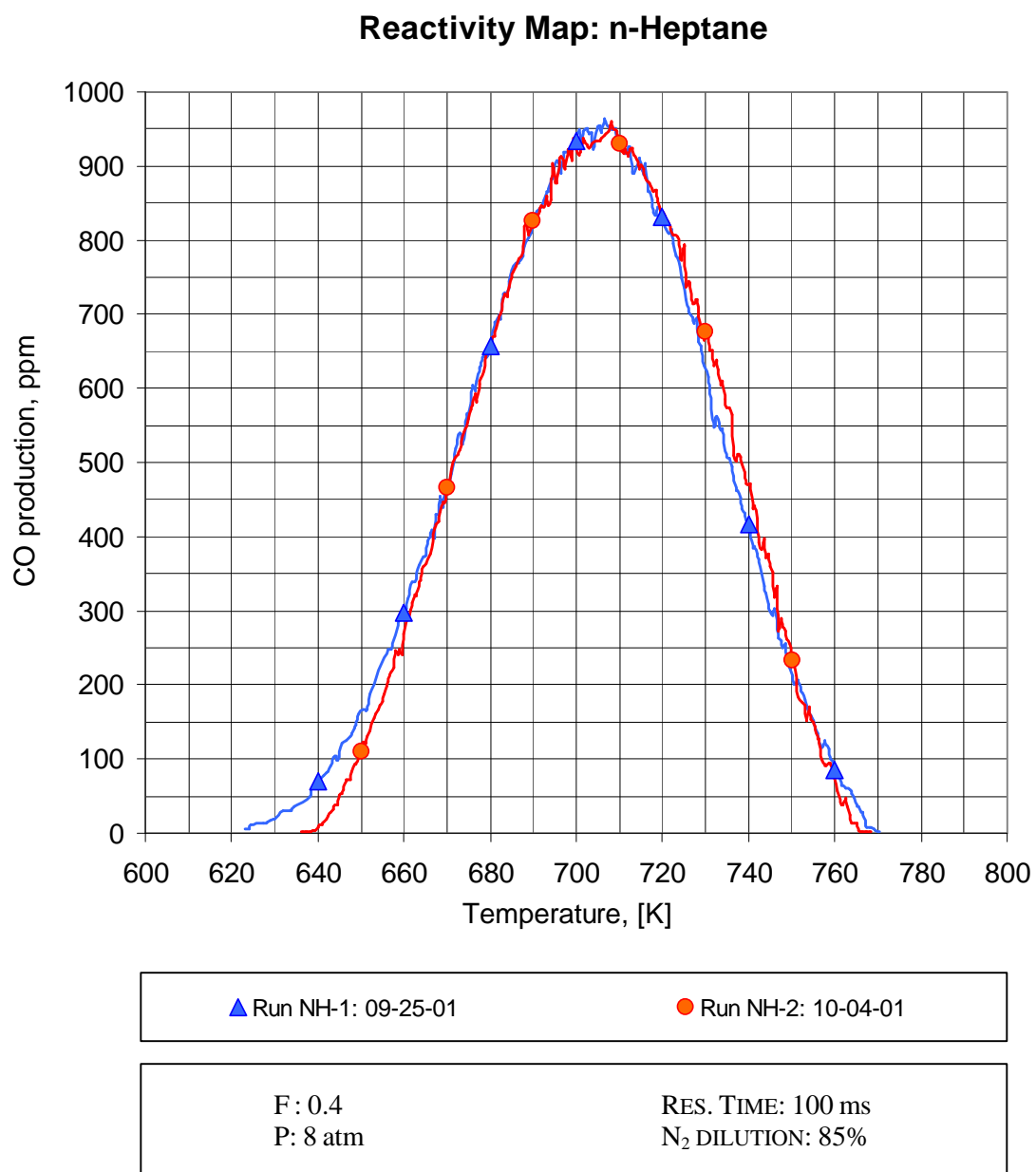
Figure 4.1 Facility Reproducibility: n-Heptane Reactivity Map
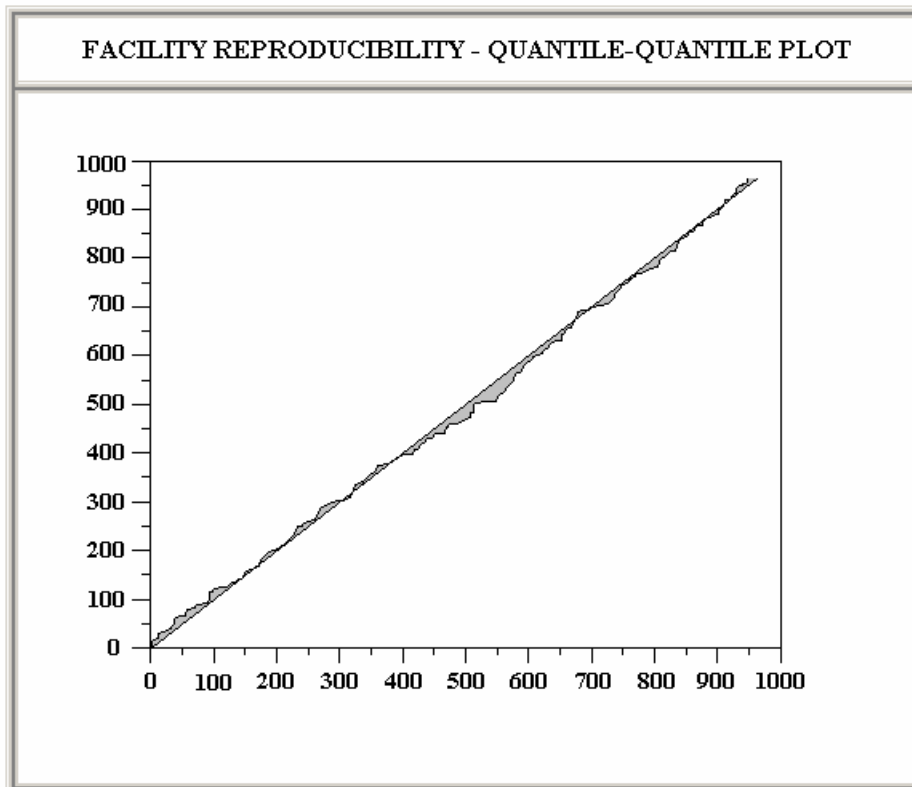
Figure 4.2 Facility Reproducibility: Quantile-Quantile Plot
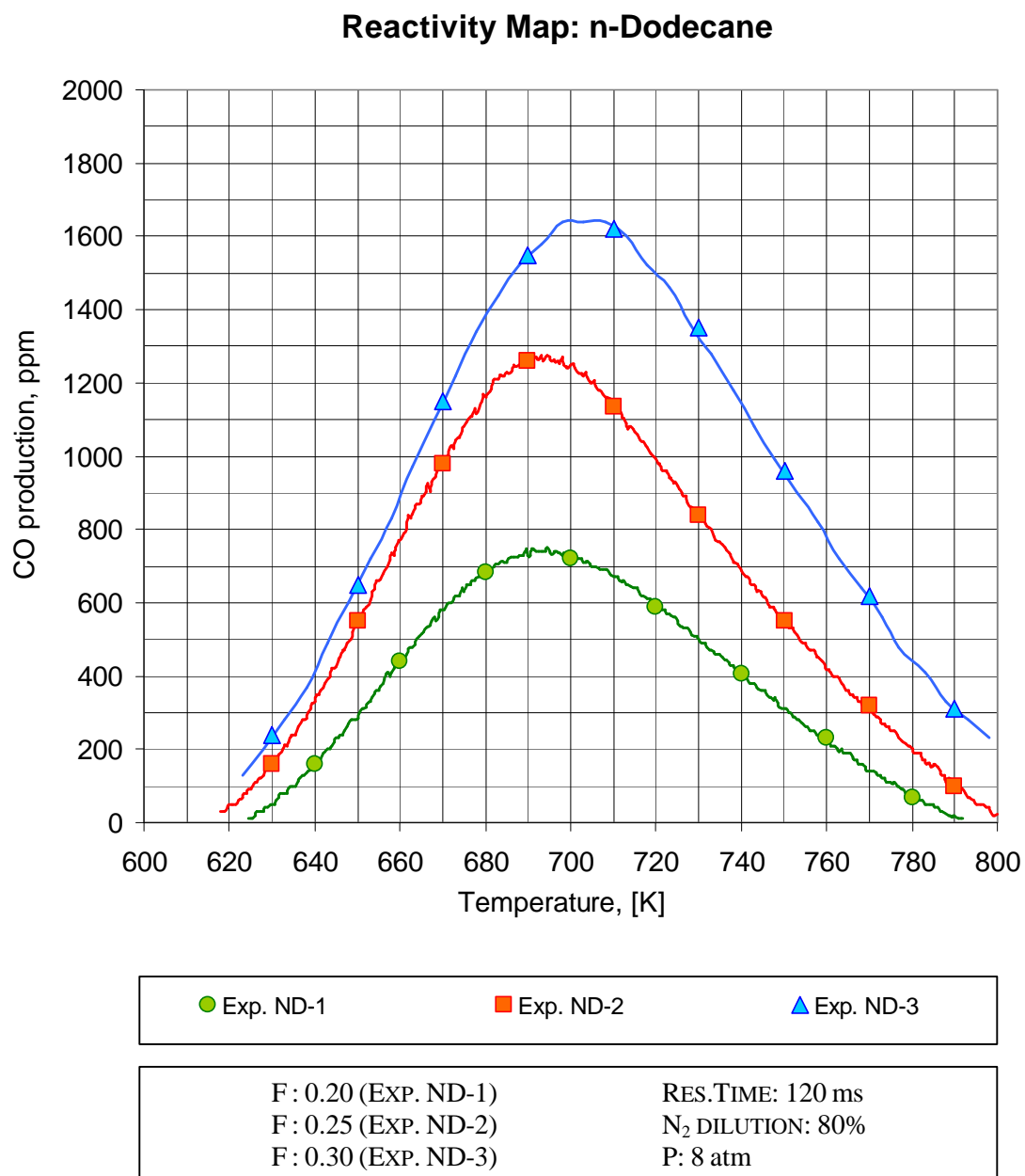
Figure 4.3 Reactivity Map: n-Dodecane

Reactivity Map: Decalin
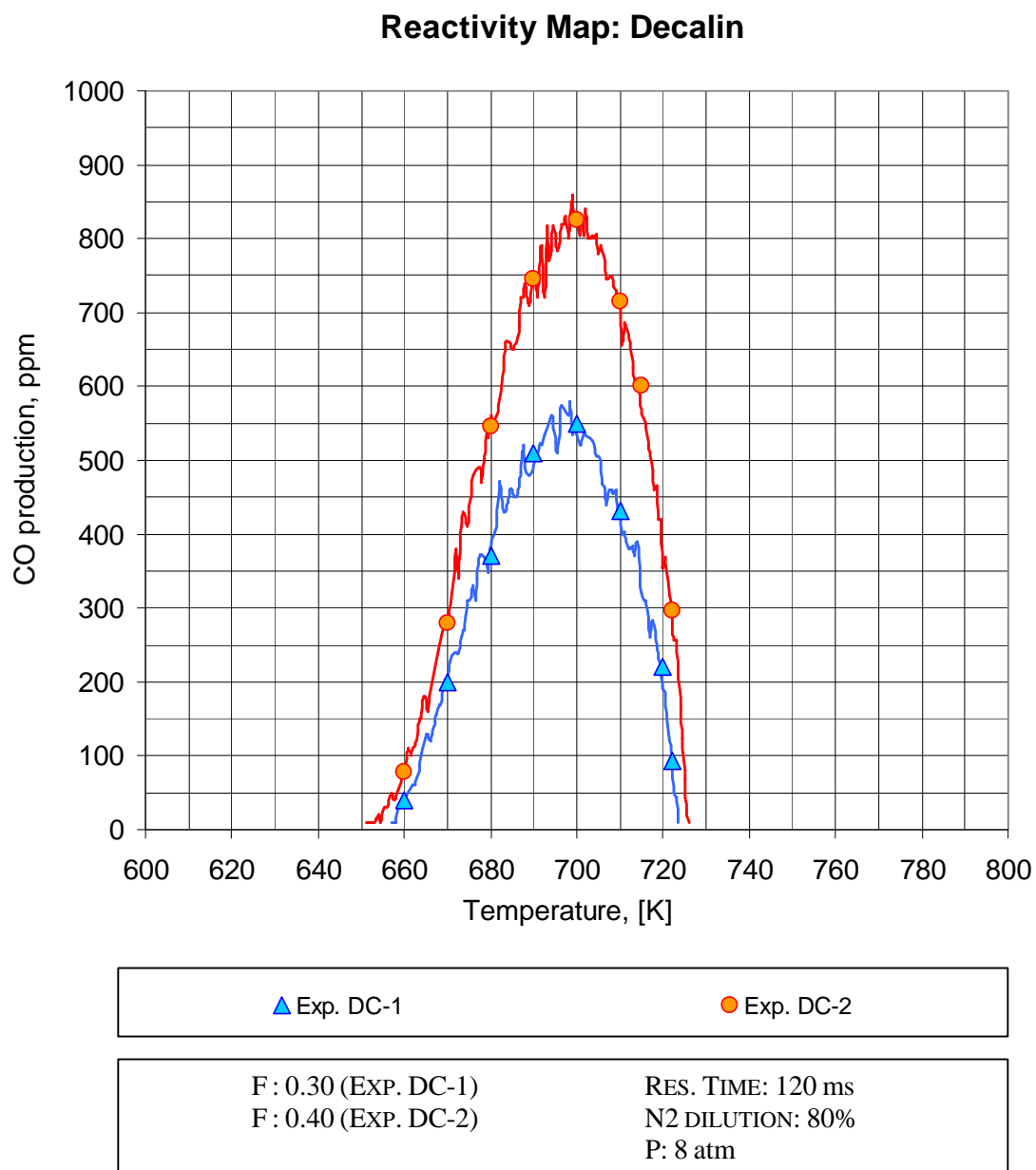
Figure 4.4 Reactivity Map: Decalin

Cetane Number - CO Peak Correlation
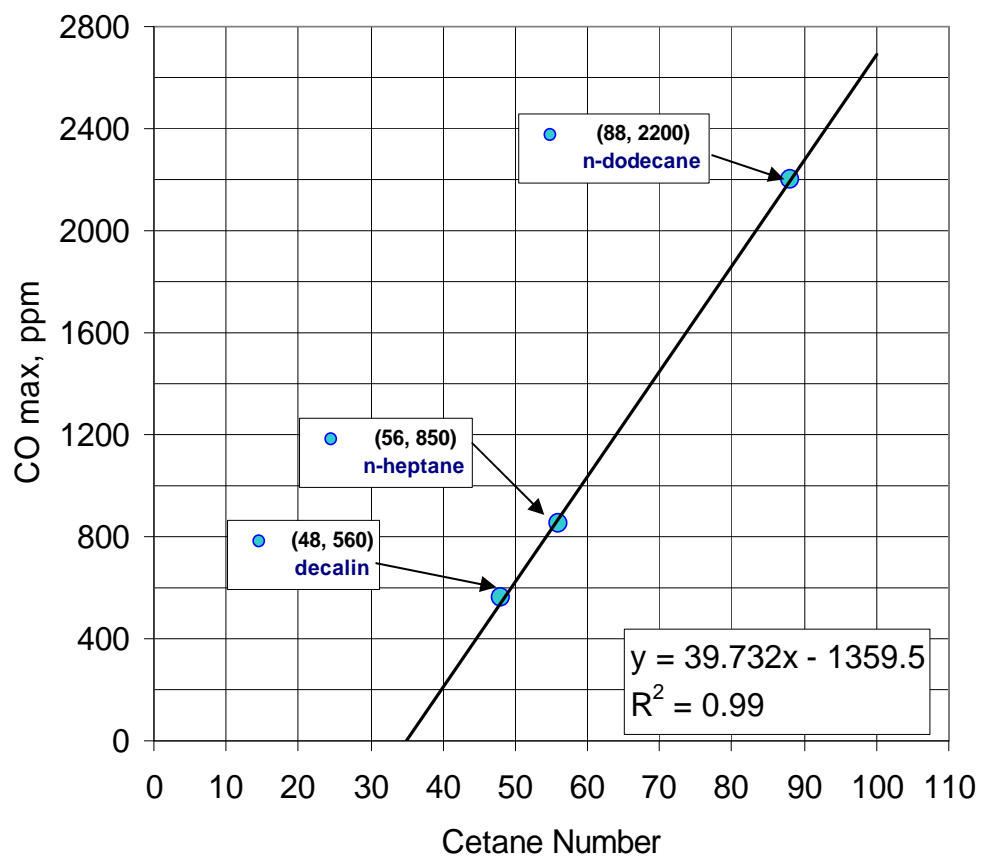
Figure 4.5 Cetane Number – CO Peak Correlation

CHAPTER 5 – MULTICOMPONENT MIXTURES: RESULTS AND DISCUSSION

5.1 INTRODUCTION

This chapter presents the results of an investigation into the oxidation characteristics of several binary, ternary and larger mixtures of full boiling range fuels. Three binary blends were designed with the same base fuel, n-dodecane, while the other compounds were a-methylnaphthalene, methylcyclohexane and isocetane. Since reactivity for these three pure compounds could not be observed (see Chapter 4), their oxidative behavior was indirectly investigated blending them with n-dodecane. Since n-dodecane proved to be a very reactive compound, it has been used to create a radical pool large enough to react with the other fuels. Initially these mixtures were designed with the same Cetane number of 45, which is close to that of JP-8. Reactivity was observed for all the binary mixture tested.

The antagonistic and synergistic behavior of more complex mixtures was investigated by blending up to five components per mixture. Using n-dodecane and isocetane as base fuels, two ternary mixtures were designed to test the effect of two aromatic compounds, a-methylnaphthalene and hexylbenzene, on NTC behavior. In two blends with alkanes and aromatics, the effect of different naphthenic compound addition has been investigated. Blending Cetane numbers were determined using the linear correlation between the maximum CO production and the fuel Cetane Number. This correlation was developed and tested using the data obtained from the oxidation of pure hydrocarbons, as reported in Section 4.8. In conclusion, three binary, two ternary, and two larger mixtures were designed with a CN of approximately 45. Their oxidative

behavior was investigated measuring their reactivity profile during a set of controlled cool down experiments. Most of the experiments were conducted at the same conditions, specifically residence time of 120 ms, pressure of 8 atm, and equivalence ratio of 0.3. A summary of the composition of the different mixtures studied is presented in Table 5.1, while the experimental conditions for each case are reported in their corresponding section and in the complete experimental matrix in Appendix D. Finally, a detailed description and analysis of each experiment is presented in the following sections of this Chapter.

Table 5.1 Summary of Mixtures' Composition, Vol. %

MIX. #	N-DODECANE	ISO-CETANE	METHYL-CYCLOHEXANE	DECALIN	a-METHYL-NAPHTHALENE	HEXYL-BENZENE
M1	40	60	–	–	–	–
M2	37	–	63	–	–	–
M3	51	–	–	–	49	–
M4	44	41	–	–	15	–
M5	39	46	–	–	–	15
M6	32	30	20	–	18	–
M7	32	30	15	5	18	–
M8	43	27	15	0	15	–
M9	41	29	10	5	15	–

5.2 BINARY MIXTURE OXIDATION: 40% N-DODECANE, 60% ISOCETANE

In this section the results of the oxidation of a binary mixture (mixture M1) containing 40% of n-dodecane and 60% of 2,2,4,4,6,8,8-heptamethylnonane (isocetane) are reported. This blend has been designed to indirectly investigate the oxidative behavior of isocetane since this compound demonstrated resistance to oxidation (see Section 4.7) when tested in pure form at the same lean conditions. Two CCD experiments were conducted at different conditions of nitrogen dilution (70%, and 80%), while the other parameters were kept constant. Reactivity was clearly observed in both cases. Moreover, monitoring fuel consumption, the oxidative behavior of isocetane was observed. Experimental conditions for both runs with mixture M1 are summarized in Table 5.2. Results of the quantitative data analysis are listed in Table 5.3, while reactivity maps are shown in Figure 5.1 (Exp. M1-1 and Fuel Consumption) and Figure 5.2 (Exp. M1-2).

Table 5.2 Summary of Experimental Conditions: Mixture M1

	EXP. M1-1	*EXP. M1-2*
EQUIVALENCE RATIO	0.3	0.3
PRESSURE, [atm]	8.0	8.0
N_2 DILUTION, [%]	70	80
RESIDENCE TIME, [ms]	120	120
FUEL FLOW RATE, [ml/min]	1.0	1.0
FUEL MOLAR fraction, [ppm]	870	580

Table 5.3 Quantitative Data Analysis: Mixture M1

MEASURE	EXP. M1-1	EXP. M1-2
MEAN, μ_1	495.7	234.3
SAMPLE VARIANCE, μ_2	119,396	21,941
SKEWNESS, μ_3	0.1874	0.0322
START OF REACTIVITY, R_1, [K]	603	628
END OF REACTIVITY, R_2, [K]	798	767
START OF NTC, R_x, [K] (HORIZONTAL LOCATION)	697	694
START OF NTC, R_Y, [ppm] (VERTICAL LOCATION)	1050	460

Using linear blending rules this mixture of n-dodecane and isocetane has an overall CN of 45. The results for R_y from the quantitative analysis shown in Table 5.3 can be interpolated to obtain the R_y value (~ 900 ppm) for an experiment with 800 ppm of fuel molar fraction. This value is far from what expected using the CN – CO peak correlation (see Figure 5.8). Therefore the linear blending assumption can not be considered valid for this binary mixture. As it can be inferred from the value of R_y for both experiments, the interaction between the two fuels resulted in an antagonistic effect, that is the mixture was more reactive than a linear blend of the two components. In fact, simply considering the richer experimental conditions of Exp. M1-1, pure isocetane would not even react at these conditions, while 350 ppm of n-dodecane (i.e., 40% of the fuel molar fraction for Exp. M1-1) would produce a maximum CO of approximately only 315 ppm (from the interpolation of pure n-dodecane experimental results shown in

Section 4.3). In order to take into account the non-linearity shown by this mixture, the Cetane number – CO peak correlation has been applied to estimate a blending Cetane number for isocetane of 33. More details on the calculation of blending CN are provided in Section 5.7.

Comparing results from Exp. M1-1 and Exp. M1-2, it can be noticed that the temperature interval of reactivity, that is the difference between R_1 and R_2 becomes larger when the nitrogen dilution is reduced from 80% to 70%. In fact, the difference between the two runs is 25 °C for R_1, and 30 °C for R_2. The amount of heat released was minimized for Exp. M1-2, where no temperature rise was observed during the experiment, while a maximum 10 °C $\pm$ 5 °C temperature rise occurred at the start of the NTC regime in Exp. M1-1.

Reactivity of isocetane was monitored over the temperature range 600 K to 800 K collecting gas samples from the reactor and analyzing them online with the FTIR during Exp. M1-1. Samples were collected approximately every 20 °C during the CCD. Isocetane was identified using the wavenumber 2916 absorption peak and n-dodecane was identified by wavenumber 2864.4. Considering the absorption levels for the unreacted mixture as unity, any difference in the peak absorption for each sample was converted into fuel consumption. Fuel consumption for both n-dodecane and isocetane is reported in Figure 5.1. A clear NTC behavior was noted for both compounds in mixture M1. Fuel consumption for n-dodecane could not be measured with certainty in the region near the start of NTC, that is at the maximum of reactivity (dotted line in Figure 5.1), because several intermediates of the oxidation also absorb at 2864.4 cm^{-1}. The dotted line in Figure 5.1 refers to the values for the absorption measured at exactly the wavenumber

2864.4, even if a peak could not be clearly identified at that position, and therefore it can be considered as indicative of the minimum values of n-dodecane fuel consumption. In conclusion, the results from mixture M1 showed that isocetane participates in the overall mixture reactivity, even if it at the same experimental conditions, pure isocetane was unreactive. Moreover, the interactions between the n-paraffin and the iso-paraffin were antagonistic with respect to Cetane number and the mixture was more reactive than simple linear blending of the individual compounds.

5.3 BINARY MIXTURE OXIDATION: 37% N-DODECANE, 63% METHYLCYCLOHEXANE

In this section results from the oxidation of binary mixture M2 containing 37% of n-dodecane and 63% of methylcyclohexane are reported. This blend was used to indirectly investigate the oxidation behavior of methylcyclohexane (see Section 4.6). Two CCD experiments were conducted at different levels of nitrogen dilution (70%, and 80%), while holding the other parameters constant. Reactivity was clearly observed in both cases. Experimental conditions for both runs with mixture M2 are summarized in Table 5.4. Results of quantitative data analysis are listed in Table 5.5, while reactivity maps are shown in Figure 5.3.

Table 5.4 Summary of Experimental Conditions: Mixture M2

	EXP. M2-1	EXP. M2-2
EQUIVALENCE RATIO	0.3	0.3
PRESSURE, [atm]	8.0	8.0
N_2 DILUTION, [%]	70	80
RESIDENCE TIME, [ms]	120	120
FUEL FLOW RATE, [ml/min]	1.05	1.05
FUEL MOLAR FRACTION, [ppm]	1516	1011

Table 5.5 Quantitative Data Analysis: Mixture M2

MEASURE	EXP. M2-1	EXP. M2-2
MEAN, μ_1	970.7	599.6
SAMPLE VARIANCE, μ_2	662,062	159,212
SKEWNESS, μ_3	0.2076	-0.0915
START OF REACTIVITY, R_1, [K]	630	641
END OF REACTIVITY, R_2, [K]	771	754
START OF NTC, R_X, [K] (HORIZONTAL LOCATION)	706	700
START OF NTC, R_Y, [ppm] (VERTICAL LOCATION)	2200	1150

According to linear blending rules, this blend has an overall CN of 45. On the basis of a fuel molar fraction of approximately 800 ppm, the maximum CO production for mixture M2 is estimated to be 860 ppm. As shown in Figure 5.8, 860 ppm is far off from what is expected for a 45 CN mixture, thus the linear blending assumption is not valid in this case. In order to account for the non-linearity shown by this mixture, the Cetane number – CO peak correlation has been applied to estimate a blending Cetane number for methylcyclohexane of 33. More details on the calculation of blending CN are provided in Section 5.7.

As can be inferred from the value of R_y, for both experiments the interaction between the two fuels resulted in an antagonistic effect, that is the mixture was more reactive than expected for a linear blend of the two components. In fact, simply considering the richer experimental conditions of Exp. M2-1, pure methylcyclohexane

would not even react, while 560 ppm of n-dodecane (i.e., 37% of the fuel molar fraction for Exp. M2-1) would produce a maximum CO of approximately 1270 ppm (Exp. ND-2 in Section 4.3). Moreover, comparing Exp. M2-1 with Exp. ND-2 we notice that mixture M2 reacts over a narrower temperature range, approximately from $630\,K \pm 10\,°C$ to $771\,K \pm 5\,°C$ instead of from $613\,K$ to $800\,K$ for ND. However, once the reaction is initiated, in both Exp. M2-1 and Exp. M2-2 for mixture M2, the production of CO rapidly increases and fluctuates, a behavior already seen for pure methylcyclohexane (see Section 4.6). A huge amount of heat was released during these experiments. For Exp. M2-1, heat released caused a maximum temperature rise of $30\,°C \pm 10\,°C$ at the start of NTC, while for Exp. M2-2 the maximum temperature rise has been estimated in $20\,°C \pm 5\,°C$. The difference between the heat released during the two experiments together with the facility reproducibility tolerances explain the unexpected result of R_x being higher for Exp. M2-1 than for Exp. M2-2 (see the quantitative data analysis, Table 5.5).

In conclusion, the oxidation of mixture M2 showed that methylcyclohexane participates in the overall mixture reactivity, even if it at the same experimental conditions pure methylcyclohexane was unreactive. Moreover, the interaction between the n-paraffin and the cycloalkane produced a mixture that was more reactive than the individual compounds.

5.4 BINARY MIXTURE OXIDATION: 51% N-DODECANE, 49% a-METHYLNAPHTHALENE

In this Section the results from the oxidation of binary mixture M3 containing 51% of n-dodecane and 49% of a-methylnaphthalene are reported. This blend was used to indirectly investigate the oxidation behavior of a-methylnaphthalene since by itself this compound was extremely resistant to ignition (see Section 4.5). Two CCD experiments were conducted at different nitrogen dilutions (70%, and 80%), while the other parameters were kept constant. Reactivity was clearly observed in both cases. Moreover, monitoring fuel consumption, the oxidative behavior of a-methylnaphthalene was observed. Experimental conditions for both runs with mixture M3 are summarized in Table 5.6. Results of quantitative data analysis are listed in Table 5.7, while reactivity maps are shown in Figure 5.4 (Exp. M3-1 and Fuel Consumption) and Figure 5.5 (Exp. M3-2).

Table 5.6 Summary of Experimental Conditions: Mixture M3

	EXP. M3-1	EXP. M3-2
EQUIVALENCE RATIO	0.3	0.3
PRESSURE, [atm]	8.0	8.0
N_2 DILUTION, [%]	70	80
RESIDENCE TIME, [ms]	120	120
FUEL FLOW RATE, [ml/min]	0.90	0.9
FUEL MOLAR FRACTION, [ppm]	1220	814

Table 5.7 Quantitative Data Analysis: Mixture M3

MEASURE	EXP. M3-1	EXP. M3-2
MEAN, μ_1	554.3	262.4
SAMPLE VARIANCE, μ_2	102,864	22,402
SKEWNESS, μ_3	-0.059	-0.1690
START OF REACTIVITY, R_1, [K]	627	642
END OF REACTIVITY, R_2, [K]	> 800	780
START OF NTC, R_X, [K] (HORIZONTAL LOCATION)	700	696
START OF NTC, R_Y, [ppm] (VERTICAL LOCATION)	1030	480

According to linear blending rules, this blend has an overall CN of 45. The quantitative analysis shown in Table 5.7 reports a value for R_y of 480 that is close to what expected using the CN – CO peak correlation (see Figure 5.8). Therefore the linear blending assumption can be considered valid for this binary mixture. Moreover this is an indirect confirmation that the aromatic component did not act as an inert dilutant in the mixture, since otherwise reactivity would have been higher. In fact, comparing the CO production for Exp. M3-2 (R_y = 1030, n-dodecane molar fraction = 630 ppm) with that of pure n-dodecane (Exp. ND-3, R_y = 1660, n-dodecane molar fraction = 680 ppm), it is clear that the addition of the aromatic component reduced the reactivity over that of pure n-dodecane. Moreover, reactivity of a-methylnaphthalene has been directly monitored over the temperature range 620 K to 800 K, collecting gas samples from the reactor and analyzing them online with the FTIR during Exp. M3-1. Samples were collected

approximately every 10 °C during the CCD. Considering the spectrum of the collected gas, a-methylnaphthalene was identified using the characteristic absorption peaks that arise in the lower wavenumber portion of the spectrum at wavenumber 788.93. n-Dodecane was identified by its peak at wavenumber 2864.4. Considering the absorption levels for the unreacted mixture as unity, any difference in the peak absorption for each sample can be converted into fuel consumption. Fuel consumption for both n-dodecane and a-methylnaphthalene is reported in Figure 5.3. The data show that while the n-dodecane fuel consumption exhibits a clear NTC behavior, the a-methylnaphthalene is consumed during the experiment in an almost constant percentage. A weak NTC behavior is observed for a-methylnaphthalene in mixture M3, as is expected from an aromatic compound. Fuel consumption for n-dodecane could not be successfully measured in the region near the start of NTC, that is at the maximum of reactivity (dotted line in Figure 5.4), because several intermediates of the oxidation also absorb at 2864.4 cm^{-1}. The dotted line in Figure 5.4 refers to the values for the absorption measured at exactly the wavenumber 2864.4, even if a peak could not be clearly identified at that position, and therefore it can be considered as indicative of the minimum values of n-dodecane fuel consumption. In conclusion, the oxidation of mixture M3 showed that a-methylnaphthalene participates in the overall mixture reactivity, even if it at the same experimental conditions, pure a-methylnaphthalene was unreactive. The decrease in CO production for mixture M3 with respect to pure n-dodecane, shows that the interaction between the aromatic and the alkane components of the mixture produces an inhibiting effect.

5.5 TERNARY MIXTURE OXIDATION: THE AROMATIC COMPONENT EFFECT

In this section the results of the oxidation of two ternary mixtures, mixture M4 and mixture M5 (see Table 5.1) are reported. These mixtures were designed to investigate the effect of different aromatic components in the oxidative behavior of a blend of paraffins. Specifically, mixture M4 is constituted of 44% n-dodecane, 41% isocetane, and 15% a-methylnaphthalene, while mixture M5 is a blend of 39% n-dodecane, 46% isocetane, and 15% hexylbenzene. Two CCD experiments were conducted at exactly the same conditions and the summary of experimental conditions is reported in Table 5.8. Results of quantitative data analysis are listed in Table 5.9, while reactivity maps are shown in Figure 5.6.

Table 5.8 Summary of Experimental Conditions: Mixtures M4 and M5

	EXP. M4-1	*EXP. M5-1*
EQUIVALENCE RATIO	0.3	0.3
PRESSURE, [atm]	8.0	8.0
N_2 DILUTION, [%]	80	80
RESIDENCE TIME, [ms]	120	120
FUEL FLOW RATE, [ml/min]	1.0	1.0
FUEL MOLAR fraction, [ppm]	652	614

Table 5.9 Quantitative Data Analysis: Mixtures M4 and M5

MEASURE	EXP. M4-1	EXP. M5-1
MEAN, μ_1	305.6	288.74
SAMPLE VARIANCE, μ_2	40,550	36,251
SKEWNESS, μ_3	0.1056	0.1086
START OF REACTIVITY, R_1, [K]	626	621
END OF REACTIVITY, R_2, [K]	783	779
START OF NTC, R_X, [K] (HORIZONTAL LOCATION)	694	694
START OF NTC, R_Y, [ppm] (VERTICAL LOCATION)	600	570

As before, the mixture composition was selected based on linear blending and a set point of 45 for Cetane number. Moreover, the 15% aromatic content is close to the average volumetric aromatic content in JP-8 of 18.2%.

Hexylbenzene is a monocyclic alkyl aromatic with a 6 carbon atom side chain. This compound may be used in the development of the JP-8 surrogate in lieu of a-methylnaphthalene to represent the aromatic class. In fact, even if in the real fuel the total volumetric amount of aromatics is on average 18% (and maximum 25%), the military specifications require that only 3% of the aromatics can be of the naphthalene-type. On the contrary alkyl benzenes are the major aromatic components.

From the distribution of the alkyl benzenes in Jet A reported by Edwards (Edwards, 2001), it appears that the most appropriate component to represent this class should have between 8 and 12 carbon atoms. Thus, restricting the focus on the alkyl

benzenes with a straight carbon chain (not branched, to minimize the fuel cost), potential compounds range from ethylbenzene (C8) to hexylbenzene (C12). In this study, the choice of the alkylbenzenic compound was based on two factors. First, between the potential alkylbenzenes, hexylbenzene has a H/C ratio ($H/C_{hexylbenzene}$ = 1.5, $H/C_{ethylbenzene}$ = 1.25) closer to the value published for JP-8 (H/C_{JP8} = 1.9). Second, the Cetane number is known only for hexylbenzene. On the other hand, ethylbenzene would represent a better choice when considering the fuel cost.

However, as shown by results from oxidation of these mixtures (Figure 5.6), no significant difference is observed between the two reactivity profiles. Following the techniques outlined in Section 3.8, a Likelihood Index (LI) of 0.97 for the two reactivity maps was determined, proving that there is no substantial difference between their results. Moreover, in both cases, the addition of the aromatic component inhibited the overall mixture reactivity, as can be inferred by the values of R_y.

Therefore, considering that the fuel cost is an important parameter in the selection of a surrogate, a-methylnaphthalene can be considered a better choice than hexylbenzene. However, while the analysis of the reactivity maps did not show any significant difference between these two aromatics, their underlying chemistry may be different and should receive further attention.

5.6 LARGE MIXTURE OXIDATION: THE NAPHTHENIC COMPONENT EFFECT

In this section the results of the oxidation of mixture M6 and mixture M7 (see Table 5.1) are reported. These two mixtures were designed to investigate the effect of the naphthenic component in a blend of paraffins and aromatics. Mixture M6 constitutes of 32% n-dodecane, 30% isocetane, 18% a-methylnaphthalene, and 20% methylcyclohexane and mixture M7 is a blend of 32% n-dodecane, 30% isocetane, 18% a-methylnaphthalene, 15% methylcyclohexane, and 5% decalin. Two CCD experiments were conducted at exactly the same conditions and the summary of experimental conditions is reported in Table 5.10. Results of quantitative data analysis are listed in Table 5.11, while reactivity maps are shown in Figure 5.7.

Table 5.10 Summary of Experimental Conditions: Mixtures M6 and M7

	EXP. M6-1	*EXP. M7-1*
EQUIVALENCE RATIO	0.3	0.3
PRESSURE, [atm]	8.0	8.0
N_2 DILUTION, [%]	80	80
RESIDENCE TIME, [ms]	120	120
FUEL FLOW RATE, [ml/min]	1.0	1.0
FUEL MOLAR fraction, [ppm]	780	767

Table 5.11 Quantitative Data Analysis: Mixtures M6 and M7

MEASURE	EXP. M6-1	EXP. M7-1
MEAN, μ_1	253	273
SAMPLE VARIANCE, μ_2	30,160	33,662
SKEWNESS, μ_3	0.087	0.0419
START OF REACTIVITY, R_1, [K]	640	635
END OF REACTIVITY, R_2, [K]	767	765
START OF NTC, R_X, [K] (HORIZONTAL LOCATION)	700	695
START OF NTC, R_Y, [ppm] (VERTICAL LOCATION)	520	550

Naphthenes represent a large portion (~ 20%) of JP-8 and approximately 2/3 of this portion are monocyclic components; the rest are primarily two or three ring compounds. Therefore the monocyclic methylcyclohexane of M6 has been replaced in M7 by a blend of methylcyclohexane and decalin (bicyclic) to see if a better match with JP-8 reactivity could be obtained. Since the two mixtures have similar fuel molar fraction and the CCD experiments were conducted at the same conditions, the resulting reactivity maps can be compared directly. From Figure 5.7, the major effect of decalin addition appears to be a small shift of the temperature profile to lower temperatures. In particular the start of the NTC regime shifts from approximately 700 K for mixture M6 to 695 K in mixture M7, while at the same experimental conditions (see results from Chapter 6) the NTC regime for JP-8 starts at approximately 692 K. Moreover, smoother oxidation behavior was noted for M7 relative to M6 during the CCD experiments. Therefore,

considering the shift in temperature profile and that methylcyclohexane was too reactive when added to n-dodecane (see Section 5.3), the addition of decalin to mixture M6 is beneficial. The shift in temperature profile is the only apparent difference between M6 and M7. The difference in the two means is due to the slightly lower reactivity of mixture M6 compared to mixture M7. This difference is very small (30 ppm of CO at the maximum production) and can be attributed to experimental reproducibility. Finally, considering the linear blending assumption, mixture M6 has a Cetane number of 37, while mixture M7 is characterized by a Cetane number of 38. However, considering the Cetane number – CO peak correlation (Figure 4.5), a mixture with those values of CN should produce at the maximum of reactivity approximately 200 ppm of CO. Since R_y is well above this number for both mixtures, the linear blending assumption is not valid.

5.7 CETANE NUMBER – CO PEAK CORRELATION APPLICATION

In Chapter 4 a correlation between the Cetane number and the maximum CO production was developed based on the oxidation of three pure hydrocarbons at fixed experimental conditions. This correlation, shown in Figure 4.5, has been used to verify whether the linear blending assumption was valid for each of the mixtures reported in Chapter 5. The concept of linear blending has been discussed in Section 1.5 and it is very important in the definition of a chemical surrogate since it allows predicting the ignition behavior of a complex mixture a priori. Unfortunately, the validity of the linear blending assumption usually decreases as the mixture complexity increases and it is negatively – and unpredictably – affected by certain hydrocarbons. For example, as shown by the experimental results reported in this Chapter, both isocetane and methylcyclohexane

behaved in a highly non-linear fashion when blended with pure n-dodecane. In Figure 5.8 the Cetane number – CO peak correlation is reproduced together with the points relative to the 7 mixtures tested (see Table 5.1). For mixtures M3, M4 and M5 (mixture M5 is not shown in Figure 5.8) the linear blending approximation appears to be valid; however for the two binary mixtures, M1 and M2, as well as for the larger mixtures, M6 and M7, this is not the case. The CO correlation has been applied to derive the actual CN for these mixtures. Once these values are known, it is possible to calculate the theoretically optimal blending CNs for the different hydrocarbons solving a linear system based on several equations similar to equation 1.1. In order to do this, a matrix containing the hydrocarbon volumetric content for all the mixtures except mixture M5 (the blending CN for hexylbenzene was not of interest) has been designed. Two other mixtures (M8 and M9) where added to the matrix to improve the successive optimization process. The final matrix **A** and the coefficient vector b are shown in the following expressions 5.1 and 5.2:

$$A = \begin{bmatrix} 40 & 60 & 0 & 0 & 0 \\ 37 & 0 & 63 & 0 & 0 \\ 51 & 0 & 0 & 0 & 49 \\ 44 & 41 & 0 & 0 & 15 \\ 32 & 30 & 20 & 0 & 18 \\ 32 & 30 & 15 & 5 & 18 \\ 43 & 27 & 15 & 0 & 15 \\ 41 & 29 & 10 & 5 & 15 \end{bmatrix} \quad (5.1) \qquad b = \begin{bmatrix} 57 \\ 56 \\ 45 \\ 52 \\ 46 \\ 46 \\ 53 \\ 53 \end{bmatrix} \quad (5.2)$$

In matrix A, every column represents the volumetric content of a particular hydrocarbon in a mixture, specifically from left to right, n-dodecane, isocetane, methylcyclohexane, decalin, and a-methylnaphthalene. Every row represents the composition of a specific mixture. The mixtures are listed in matrix A in exactly the same order they are listed in Table 5.1. The reactivity maps for mixtures M8 and M9 are not shown, even though their maximum CO production value has been determined and it is reported in vector $\underline{b}$.

Since $\underline{A}$ is a 5 x 8 matrix and $\underline{b}$ is a 1 x 8 column vector, the $\underline{CN}_{blending}$ column vector is 1 x 5 and the overall system ($\underline{CN}_{blending} = \underline{A} \cdot \underline{b}$) is over-determined. Therefore the exact solution to this system does not exist, but the optimal solution can be calculated in terms of a least mean square approximation. The optimal $CN_{blending}$ values calculated using Matlab® are reported in Table 5.12, together with the CN values for the corresponding fuel.

Table 5.12 Optimal Blending Cetane Numbers

FUEL	*BLENDING CN*	*CETANE NUMBER*
N-DODECANE	90	88
ISOCETANE	33	15
METHYLCYCLOHEXANE	36	20
DECALIN	50	48
a-METHYLNAPHTHALENE	0	0

Literature values for Blending CNs are rare and are not tabulated for these five hydrocarbons (Rose and Cooper, 1955). However, the calculated optimal blending CNs values are within the typical range for Blending CNs. Moreover, it should be noticed that the blending Cetane Numbers calculated are the result of an optimization process that depends strictly on the way they were derived (i.e., the specific experimental conditions of the Cetane Number – CO peak correlation). However, they still are extremely important in the synthesis of a JP-8 surrogate, allowing accurate a priori predictions of surrogate's ignition behavior as reported in Chapter 6.

5.8 CONCLUSIONS

The oxidative behavior of several binary, ternary, and larger mixtures has been extensively investigated. The antagonistic and synergistic behavior of such complex mixtures has been outlined by direct comparison of their relative reactivity maps. The main results reported in this Chapter are summarized as follows.

1) The oxidation of methylcyclohexane, isocetane, and a-methylnaphthalene has been indirectly observed by blending each of these hydrocarbons with pure n-dodecane. The presence of n-dodecane accounted for the development of a radical pool large enough to initiate the oxidation of the other fuel, which would otherwise be unreactive at the tested conditions. Strong NTC behavior was observed for both fuels in the isocetane/n-dodecane mixture M1 and for the methylcyclohexane/n-dodecane mixture M2, while a-methylnaphthalene revealed a weak NTC behavior in the a-methylnaphthalene/n-dodecane mixture M3.

2) The effect of the aromatic components has been studied. No significant differences were observed between the two aromatics tested, a-methylnaphthalene and hexylbenzene. Therefore, the less expensive naphthalene was selected to represent the aromatics in the JP-8 surrogate.

3) The effect of the naphthenic components has been studied. Both the naphthenes tested showed peculiar characteristics. Methylcyclohexane was extremely reactive when mixed with n-dodecane, while the addition of decalin to the mixture resulted in a small shift of the temperature profile towards lower temperatures. This produces a better match with the JP-8 reactivity maps. Therefore both naphthenes will be included in the final JP-8 surrogate, as described in Chapter 6.

4) Finally, the Cetane number – CO peak correlation developed on the basis of the oxidation of pure n-dodecane, n-heptane, and decalin, has been used to verify whether the oxidative behavior of the studied mixtures could have been successfully predicted on the basis of the linear blending assumption. Since this assumption was shown not to be valid for complex mixtures, optimal blending Cetane numbers have been mathematically derived for the five hydrocarbons that will constitute the JP-8 surrogate.
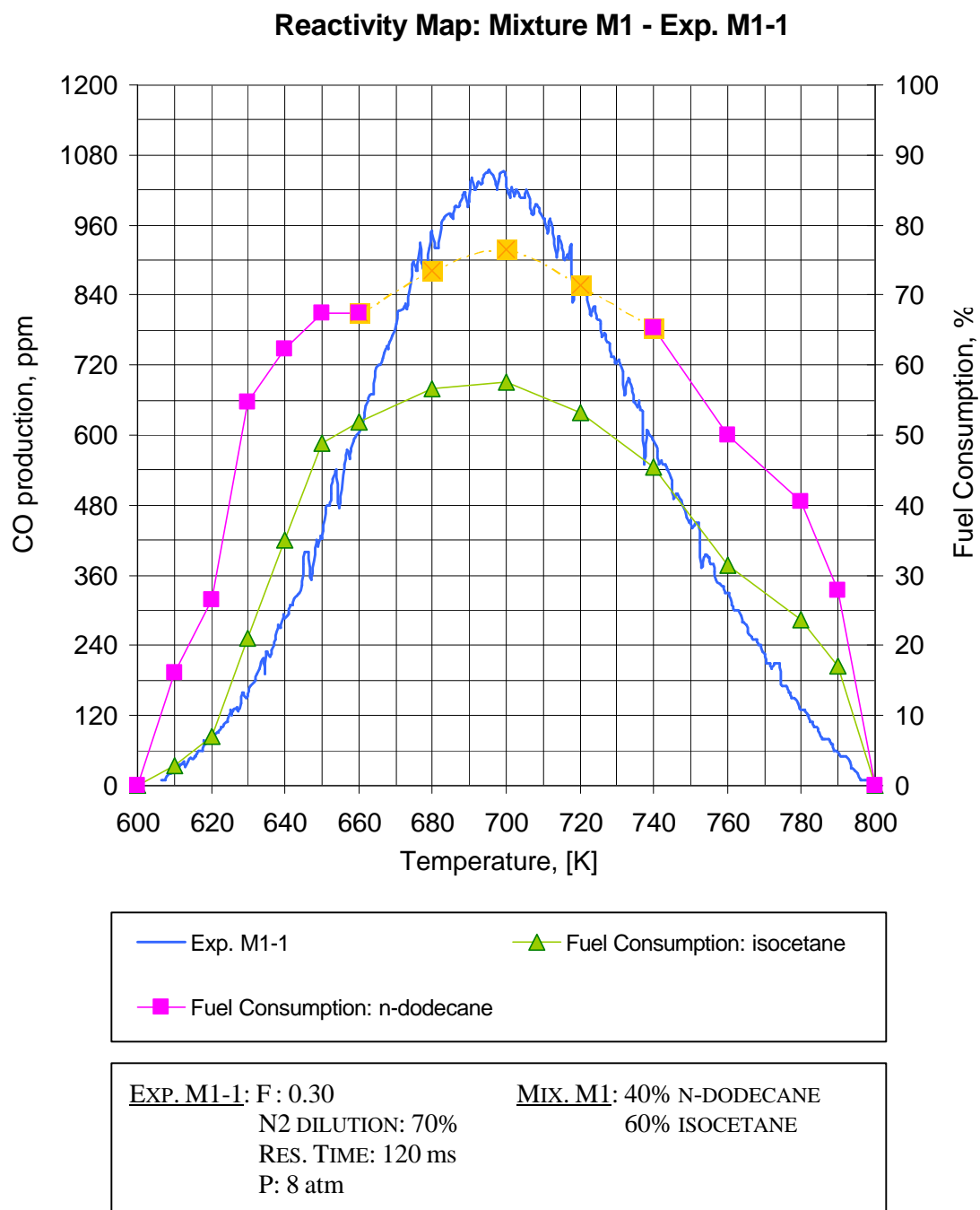
Figure 5.1 Reactivity Map and Fuel Consumption: Mixture M1, Exp. M1-1

Reactivity Map: Mixture M1 - Exp. M1-2

Exp. M1-2: F : 0.30
        N2 DILUTION: 80%
        RES. TIME: 120 ms
        P: 8 atm

MIX. M1: 40% N-DODECANE
         60% ISOCETANE
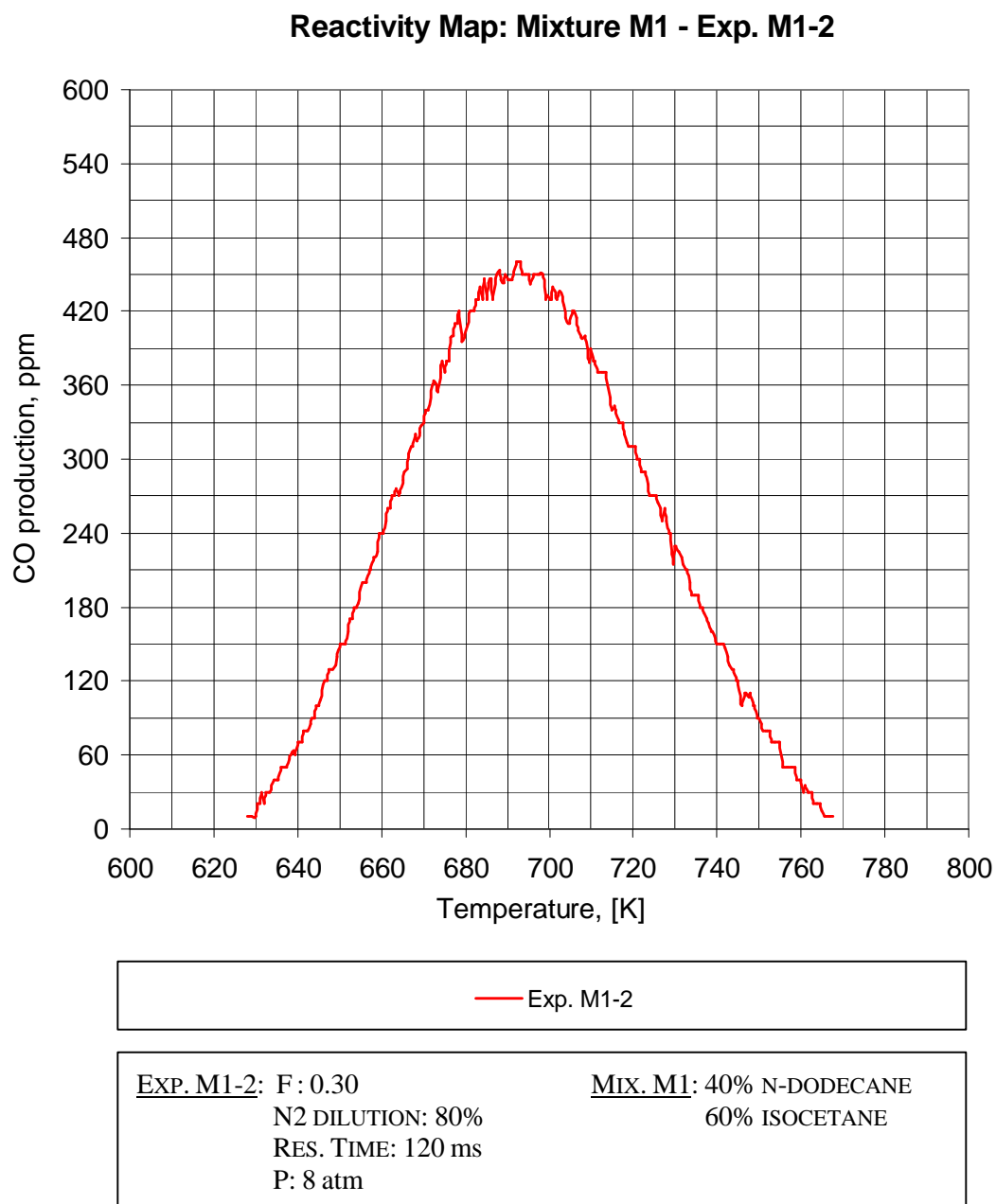
Figure 5.2 Reactivity Map: Mixture M1, Exp. M1-2
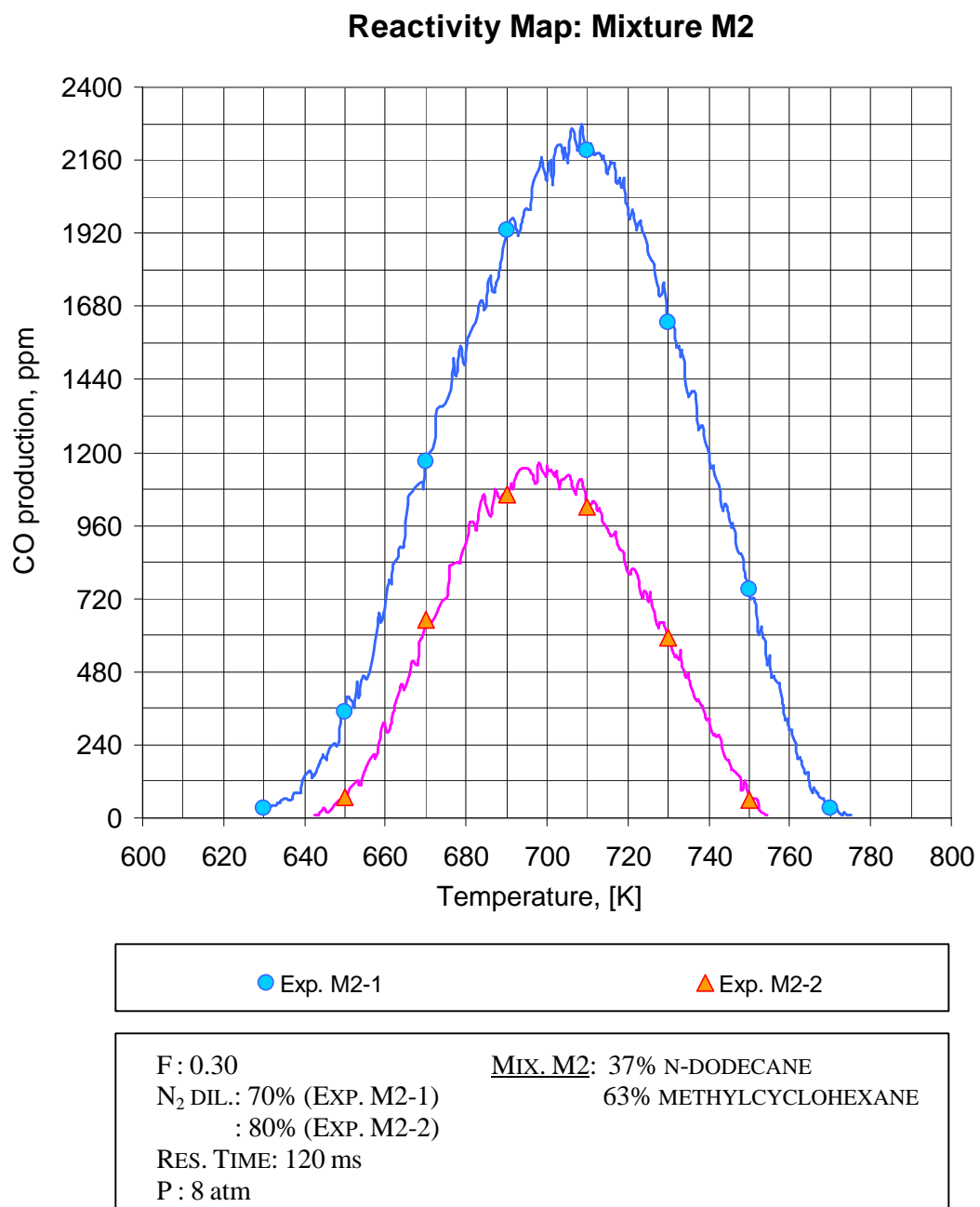
Figure 5.3 Reactivity Map: Mixture M2
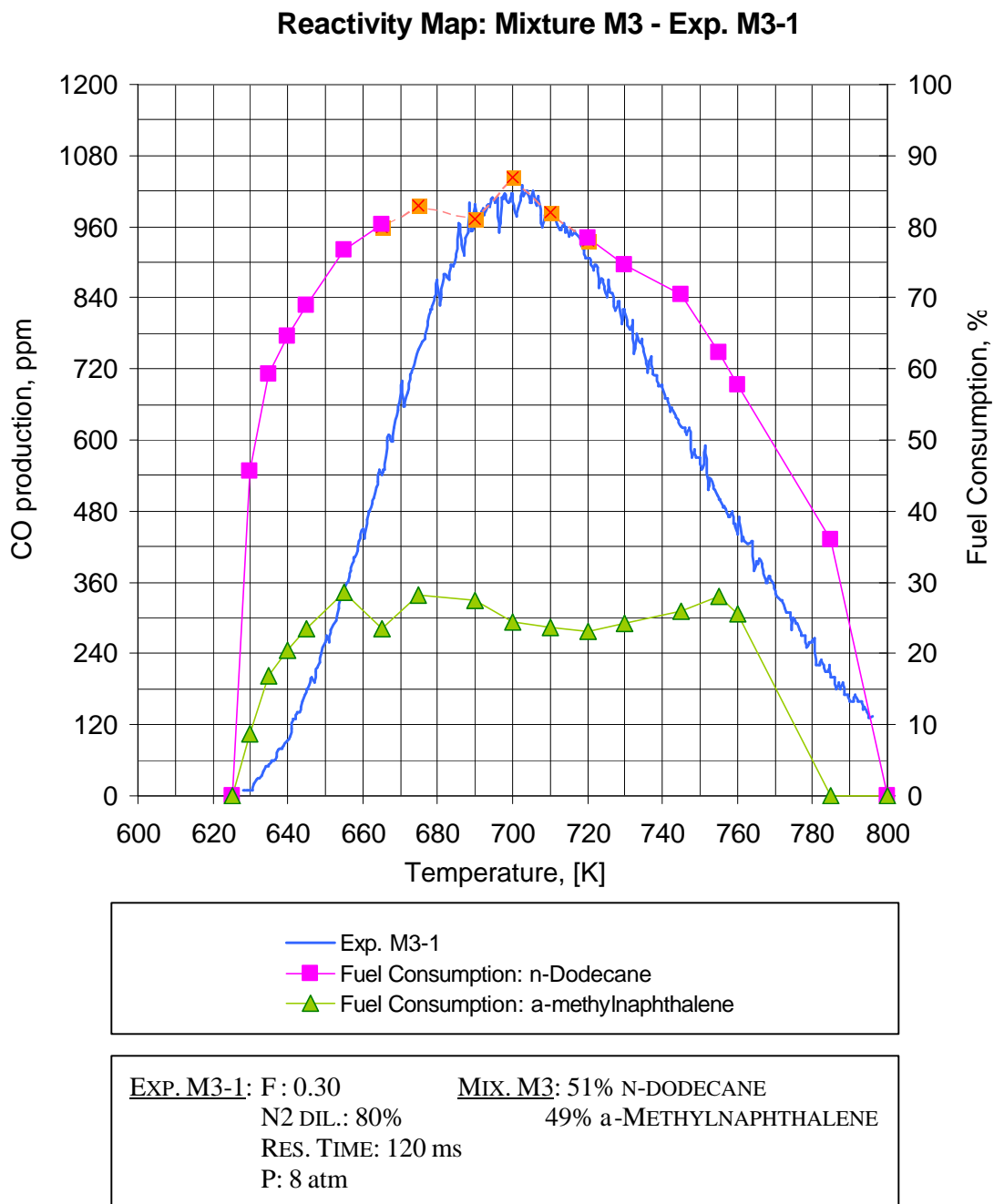
Figure 5.4 Reactivity Map and Fuel Consumption: Mixture M3, Exp. M3-1
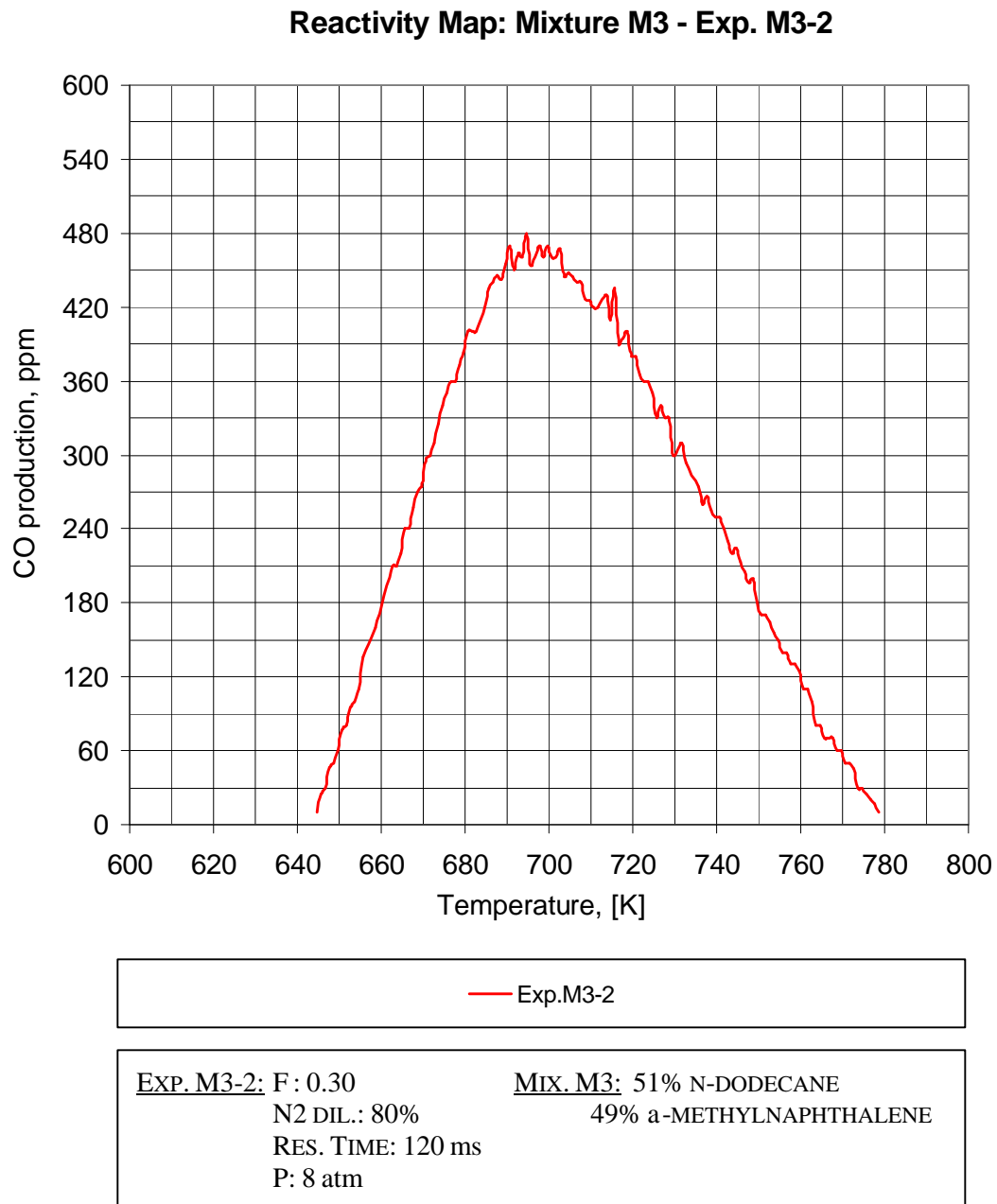
Figure 5.5 Reactivity Map and Fuel Consumption: Mixture M3, Exp. M3-2

Reactivity Map: Mixtures M4 and M5

Figure 5.6 Reactivity Map: Mixtures M4 and M5

Figure 5.7 Reactivity Map: Mixtures M6 and M7

Cetane Number - CO Peak Correlation

$y = 39.732x - 1359.5$
$R^2 = 0.99$

(45, 900) mixture M1
(45, 860) mixture M2
(45, 713) mixture M4
(38, 550) mixture M7
(37, 520) mixture M6
(45, 480) mixture M3
(88, 2200) n-dodecane
(56, 850) n-heptane
(48, 560) decalin

CO max, ppm
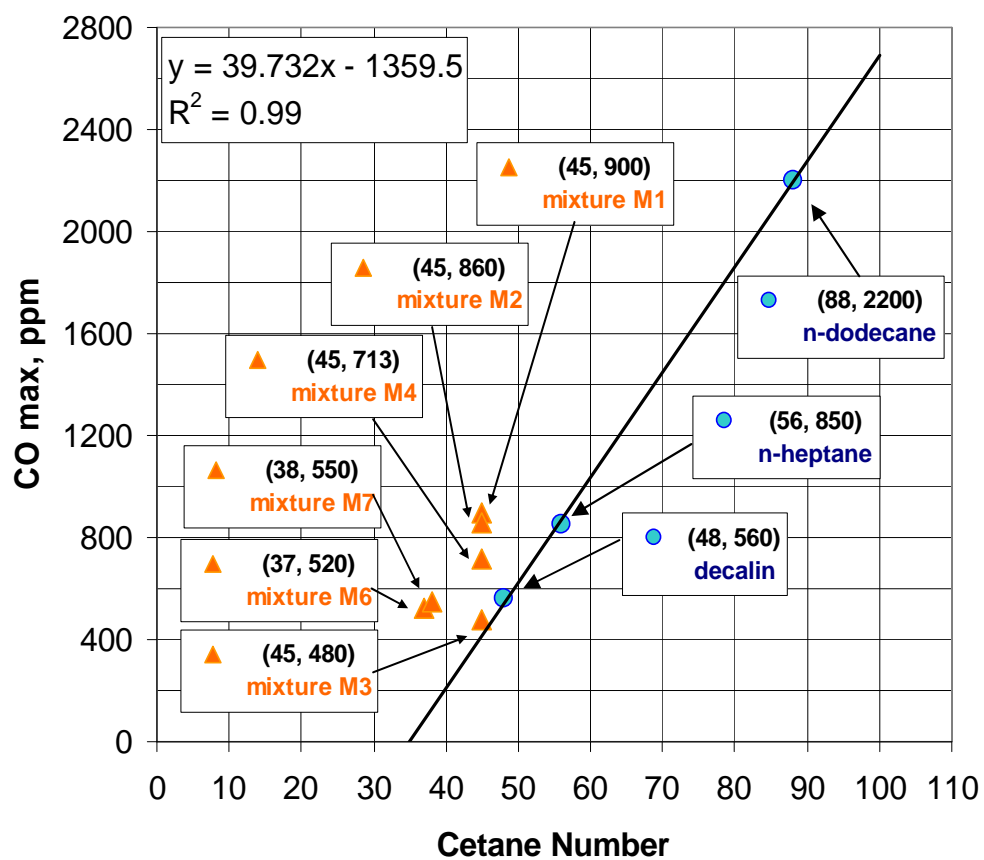
Cetane Number

Figure 5.8 Cetane Number – CO Peak Correlation: Mixtures

CHAPTER 6 – JP-8 AND JP-8 SURROGATE: RESULTS AND DISCUSSION

6.1 INTRODUCTION

The analysis of interactions controlling the ignition of the binary, ternary and larger mixtures presented in Chapter 5 as well as the results on the oxidation of pure hydrocarbons reported in Chapter 4 led to the synthesis of a multi-component surrogate for the aviation fuel JP-8. Due to its compositional reproducibility and tractability, the developed JP-8 surrogate is suitable for both well-controlled fundamental modeling and experimental studies in lieu of the otherwise complex and chemically undefined parent fuel.

In this Chapter a formulation strategy and procedure are described for blending pure hydrocarbons in such a way as to produce a surrogate that closely matches the reactivity profile of the parent fuel in the low and negative temperature regions. The blending Cetane numbers derived in Chapter 5 have been applied to predict the ignition behavior of the surrogate.

The oxidative behavior of the surrogate has been compared with that of JP-8 both qualitatively (reactivity maps graphical comparison) and quantitatively (through the Likelihood Index described in Section 3.8). Three sets of Controlled Cool Down experiments have been conducted in such a way as to test the goodness of the surrogate under different conditions of pressure and equivalence ratio. The exact experimental conditions for both fuel and surrogate are reported in the next sections. Finally, the conclusions of this surrogate development work are presented.

6.2 SURROGATE FUEL FORMULATION: STRATEGIC APPROACH

The process of selecting and blending the individual components for the JP-8 surrogate has been based on the following hierarchical strategy.

¦ Component number: The total number of components has been restricted to less than 6 in order to limit the mixture complexity.

¦ Component choice: the selected components will represent the three major hydrocarbon classes present in JP-8: alkanes, naphthenes, and aromatics. A maximum of two compounds can represent one hydrocarbon class. The component will be of high purity and will be selected to minimize the surrogate cost. Preferably, candidate components should have been studied kinetically.

¦ Component blending: the component species will be present in the surrogate in specific volumetric concentrations that result in a strict matching of the compound class composition of parent JP-8. Average JP-8 composition is reported by Edwards and Maurice (2001) (see Table 6.4 in Section 6.4).

¦ Reactivity Similarity: the component species will be chosen on the basis of their reactivity behavior to produce a surrogate blend with a reactivity map that matches the reactivity map of the parent JP-8 over the range of temperatures tested.

Following this strategy, six candidate fuels were selected, two for each hydrocarbons class present in JP-8. The oxidative behavior of these fuels, specifically n-dodecane, isocetane, methylcyclohexane, decalin, a-methylnaphthalene, and hexylbenzene has been described in detail in Chapters 4 and 5. While the majority of published studies on kerosene-type fuels approximate JP-8 as a blend of only one normal alkane – typically n-decane or n-dodecane – and one aromatic, a simple binary mixture proved to be an oversimplification. In fact, none of the binary mixtures reported in Chapter 5 reproduced JP-8 reactivity accurately (see Section 6.3). Recently, a twelve components surrogate has been used to develop a detailed model for JP-8 combustion, and a four components surrogate was used for a reduced model (Montgomery et al., 2002).

Considering first the alkane class, two components have been selected: n-dodecane and isocetane. Due to the scarcity of data, it is still debated whether the approximation of the alkane portion of JP-8 would be better with a normal or a branched alkane (Edwards, 2001). Together they represent approximately 60% of JP-8, and the ratio of iso-paraffins to n-paraffins is known to be approximately 2:1. In developing the JP-8 surrogate the total alkanes volumetric content of 60% has been increased to 62% to include the 2% of olefins in JP-8, while the proportion of isocetane to n-dodecane has been determined using the blending Cetane numbers and matching an approximate Cetane number for JP-8 of 45 ± 3 units. Considering the naphthenes, both methylcyclohexane and decalin are compounds typically representative of the aviation fuels, as explained in Chapter 4. The published data report a 20% volumetric content of

naphthenes in JP-8, with a ratio of 3:1 for monocyclic compounds to 2 and 3 ring compounds. Finally, considering the aromatic portion, an average of 18% is present in JP-8 and this percentage has been matched in the development of the surrogate. However, it should be noted that there are no strict specifications or the composition of JP-8 (as well as for the other aviation fuels), thus 18% is only an average value and the aromatic content can be as high as 25% (see Figure 1.8). Since the results of an investigation on the oxidative behavior of the two different aromatics initially considered, a-methylnaphthalene and hexylbenzene, did not highlight any significant difference, only a-methylnaphthalene has been selected to represent the aromatic class in the surrogate blend.

In the next sections the reactivity maps and LIs for JP-8 and the candidate surrogates are compared to identify the best surrogate. Then the oxidation behavior of the selected JP-8 surrogate under several different experimental conditions is compared to that of the parent fuel to show the suitability of the developed surrogate to represent the oxidative behavior of JP-8.

6.3 JP-8 OXIDATION

In this section the results of the oxidation of JP-8 are reported. The essential information for JP-8 – mainly hydrocarbon class composition – is listed in Table C.2 from the Certificate of Analysis reported by the supplier, Phillips Chemical Company. Three CCD experiments were conducted at different conditions of equivalence ratio (F = 0.3 and 0.4), and pressure (P = 8 atm and 12 atm). Reactivity and NTC behavior was clearly observed in all cases. The experimental conditions for all the runs with JP-8 are reported in Table 6.1. The results of the quantitative data analysis are listed in Table 6.2, while the reactivity maps are shown in Figures 6.1, 6.2, and 6.3.

Table 6.1 Summary of Experimental Conditions: JP-8 Oxidation

	EXP. J8-1	*EXP. J8-2*	*EXP. J8-3*
EQUIVALENCE RATIO	0.3	0.4	0.3
PRESSURE, [atm]	8.0	8.0	12.0
N_2 DILUTION, [%]	80	80	80
RESIDENCE TIME, [ms]	120	120	120
FUEL FLOW RATE, [ml/min]	1.05	1.40	1.05
FUEL MOLAR FRACTION, [ppm]	775	1030	775
FUEL CONCENTRATION [mol/m^3] @ 800K	0.0945	0.1259	0.1453

Table 6.2 Quantitative Data Analysis: JP-8 Oxidation

MEASURE	EXP. J8-1	EXP. J8-2	EXP. J8-3
MEAN, μ_1	257.86	337.42	414.61
SAMPLE VARIANCE, μ_2	28,049	57,389	88,598
SKEWNESS, μ_3	0.1728	0.1656	0.1517
START OF REACTIVITY, R_1, [K]	632	630	612
END OF REACTIVITY, R_2, [K]	755	763	786
START OF NTC, R_X, [K] (HORIZONTAL LOCATION)	692	694	690
START OF NTC, R_Y, [ppm] (VERTICAL LOCATION)	500	730	870

In Table 6.1 fuel concentration has been expressed for each experiment in terms of mol/m^3. This parameter is more significant than the fuel molar fraction when dealing with experiments conducted at different pressures. The three experiments produced consistent results on the oxidation of JP-8. When the fuel concentration is increased from Exp. J8-1 to Exp. J8-3, the maximum CO production, the mean, and the sample variance linearly increase too. Moreover, the 3rd order statistical moment is almost constant for all the experiments, proving how smooth the JP-8 temperature profiles are, at least compared with the case of "explosive" compounds such as methylcyclohexane. A small shift in the NTC regime start is noted in Exp. J8-3, as it can be expected at the higher pressure conditions. The overall reactivity extends over a narrow region, approximately 123 °C wide for Exp. J8-1. This behavior may seem counterintuitive since a much broader reactivity could be expected from a fuel that actually is a blend of several hundred

different compounds. Comparing the JP-8 temperature profile from Exp. J8-1 with that of a simple binary mixture of n-dodecane and isocetane (Exp. M1-2, Section 5.2), JP-8 reacted between 632 K and 755 K, while the mixture – with a fuel molar fraction of only 2/3 that of JP-8 – reacted between 628 K and 767 K. Therefore, the use of a binary mixture in lieu of JP-8 appears to be an oversimplification. As explained in Chapter 4 and 5, the addition of naphthenes, which are characterized by high reactivity over a narrow temperature range, to pure alkanes and aromatic mixtures results in a much better matching of the JP-8 oxidative behavior.

6.4 JP-8 SURROGATE DEVELOPMENT

As described in section 6.2, five candidate fuels were finally selected for the JP-8 surrogate: n-dodecane, isocetane, methylcyclohexane, decalin, and a-methylnaphthalene. Five possible surrogates have been designed and their volumetric composition is shown in Table 6.3. The composition of surrogate S1 was determined using the assumption of linear blending, while for the other candidates the optimal blending Cetane numbers determined in Section 5.7 were used. The five blends were oxidized in our PFR at the same experimental conditions (F = 0.3, P = 8 atm, t = 120 ms, fuel molar fraction = 775 ppm). Detailed numerical experimental results are listed in the Experimental Matrix in Appendix D for all surrogates.

The Likelihood Index has been used as the criteria for the selection of the best surrogate and it is reported in Table 6.3 for each candidate blend. In Figure 6.4 the JP-8 reactivity map is compared to those of surrogates S1, S3, and S5 (S2 and S4 are not shown for simplicity). Surrogate S1 with a LI of 0.72, does not match JP-8 reactivity and demonstrates that the linear blending assumption based on Cetane numbers is not valid for this blend. Between the other candidate blends, S5 has the highest LI (0.97) which is very close to unity. Therefore S5, a mixture of five components, appears to best match the reactivity of a complex fuel such as JP-8 without being too complex, and for this reason it was selected as the final JP-8 surrogate. Moreover, the number of hydrogen and carbon atoms for S5 (#C = 20.9, #H = 11.5) is very close to the values published for JP-8 (#C = 21, #H = 11, Edwards (2001)), indicating that the surrogate may be a good predictor of the soot levels of the parent fuel (Edwards and Maurice, 2001).

The volumetric content of S5 (26% n-dodecane, 36% isocetane, 14% methylcyclohexane, 6% decalin, and 18% a-methylnaphthalene) is listed in Table 6.4 together with the volumetric composition of the parent JP-8.

Table 6.3 JP-8 Surrogates Summary

SURROGATE #	VOLUMETRIC CONTENT, %					LIKELIHOOD INDEX
	N-DODECANE	ISOCETANE	METHYL CYCLOHEXANE	DECALIN	a-METHYL NAPHTHALENE	
S1	43	27	15	–	15	0.72
S2	32	30	20	–	18	0.94
S3	32	30	15	5	18	0.93
S4	30	32	15	5	18	0.94
S5	26	36	14	6	18	0.97

Table 6.4 JP-8 Volumetric Composition: Parent Fuel and Surrogate S5

HYDROCARBON CLASS	JP-8, VOL. %	JP-8 SURROGATE (S5), VOL. %
ALKANES	60.0%	36 % ISOCETANE
OLEFINS	2.0%	26 % N-DODECANE
NAPHTHENES	20.0%	14% METHYLCYCLOHEXANE 6% DECALIN
AROMATICS	18.0%	18% a-METHYLNAPHTHALENE

6.5 JP-8 AND JP-8 SURROGATE COMPARISON

As specified in Section 6.4, the selected JP-8 surrogate is composed of 26% n-dodecane, 36% isocetane, 14% methylcyclohexane, 6% decalin, and 18% a-methylnaphthalene and it has been designed to closely match the chemical class composition and reactivity behavior of the parent fuel. Considering the blending Cetane numbers listed in Table 5.12, this surrogate has been designed with a CN of 43.3. Three CCD experiments were conducted at different conditions of equivalence ratio (F = 0.3 and 0.4) and pressure (P = 8 atm and 12 atm) as was done for pure JP-8. Reactivity and NTC behavior was clearly observed in all cases. Experimental conditions for all the runs with JP-8 surrogate S5 are reported in Table 6.5. Results of quantitative data analysis are listed in Table 6.6, while reactivity maps are shown in Figures 6.5, 6.6, and 6.7.

Following the definition of Likelihood Index in Section 3.8, this surrogate closely matched JP-8 reactivity over the whole temperature range tested for all cases. In fact, the LI has been calculated to be 0.97 for all three experimental cases (see Table 6.7), demonstrating that this surrogate is suitable to represent JP-8 under different experimental conditions. From a qualitative point of view, Figures 6.8, 6.9, and 6.10 show the reactivity maps of both the surrogate and the parent fuel for the three cases investigated. In all the cases the temperature profile of the surrogate closely matches that of JP-8 in terms of both the reactivity parameters (start and end of reactivity, start of NTC regime) and the statistical measures (sample mean, variance, and skewness). Finally, Table 6.7 summarizes and compares the results of quantitative data analysis for JP-8 and the surrogate.

Table 6.5 Summary of Experimental Conditions: JP-8 Surrogate S5 Oxidation

	EXP. S5-1	*EXP. S5-2*	*EXP. S5-3*
EQUIVALENCE RATIO	0.3	0.4	0.3
PRESSURE, [atm]	8.0	8.0	12.0
N_2 DILUTION, [%]	80	80	80
RESIDENCE TIME, [ms]	120	120	120
FUEL FLOW RATE, [ml/min]	1.0	1.4	1.0
FUEL MOLAR FRACTION, [ppm]	753	1004	753
FUEL CONCENTRATION [mol/m^3] @ 800K	0.0918	0.1223	0.1377

Table 6.6 Quantitative Data Analysis: JP-8 Surrogate S5 Oxidation

MEASURE	*EXP. S5-1*	*EXP. S5-2*	*EXP. S5-3*
MEAN, μ_1	243.54	343.21	421.73
SAMPLE VARIANCE, μ_2	27,594	56,009	89,022
SKEWNESS, μ_3	0.1556	0.1493	0.1286
START OF REACTIVITY, R_1, [K]	632	632	620
END OF REACTIVITY, R_2, [K]	760	764	782
START OF NTC, R_X, [K] (HORIZONTAL LOCATION)	691	694	692
START OF NTC, R_Y, [ppm] (VERTICAL LOCATION)	490	750	860

Table 6.7 Quantitative Data Analysis: JP-8 & Surrogate S5 Comparison

		μ_1	μ_2	μ_3	R_1	R_2	R_X	R_Y	LI
EXP. #1	JP-8	257.8	28049	0.173	632	755	692	500	0.972
	S5	243.5	27594	0.156	632	760	691	490	
EXP. #2	JP-8	337.4	57389	0.166	630	763	694	730	0.975
	S5	343.2	56009	0.149	632	764	694	750	
EXP. #3	JP-8	414.6	88598	0.152	612	786	690	870	0.970
	S5	421.7	89022	0.129	620	782	692	860	

6.6 CONCLUSIONS

A chemical surrogate with a reproducible composition has been developed for the complex aviation fuel JP-8. The process of selecting and blending the individual hydrocarbon components has been based on a hierarchical selection strategy accounting for different factors, including pure component oxidative behavior, JP-8 volumetric hydrocarbon class composition, and fuel cost. Out of five possible surrogate candidates, a mixture of 26% n-dodecane, 36% isocetane, 14% methylcyclohexane, 6% decalin, and 18% a-methylnaphthalene proved to most closely match reactivity behavior of parent fuel. Comparison between surrogate and parent fuel reactivity profiles has been conducted both qualitatively and quantitatively through a graphical comparison and the application of Likelihood Index parameter. Three different sets of Controlled Cool Down experiments have been designed and conducted to test the goodness of the surrogate under different experimental conditions. System pressure (P = 8 and 12 atm) and equivalence ratio (F = 0.3 and 0.4) were varied, and in all cases the reactivity profiles of JP-8 and the surrogate closely matched over the whole range of temperature investigated. Based on these results, the developed surrogate is suitable to represent the oxidative behavior of the parent JP-8 fuel in the low and negative temperature regions. Due to its compositional reproducibility and tractability, the surrogate is suitable for both well-controlled fundamental modeling and experimental studies in lieu of the otherwise complex and chemically undefined JP-8.
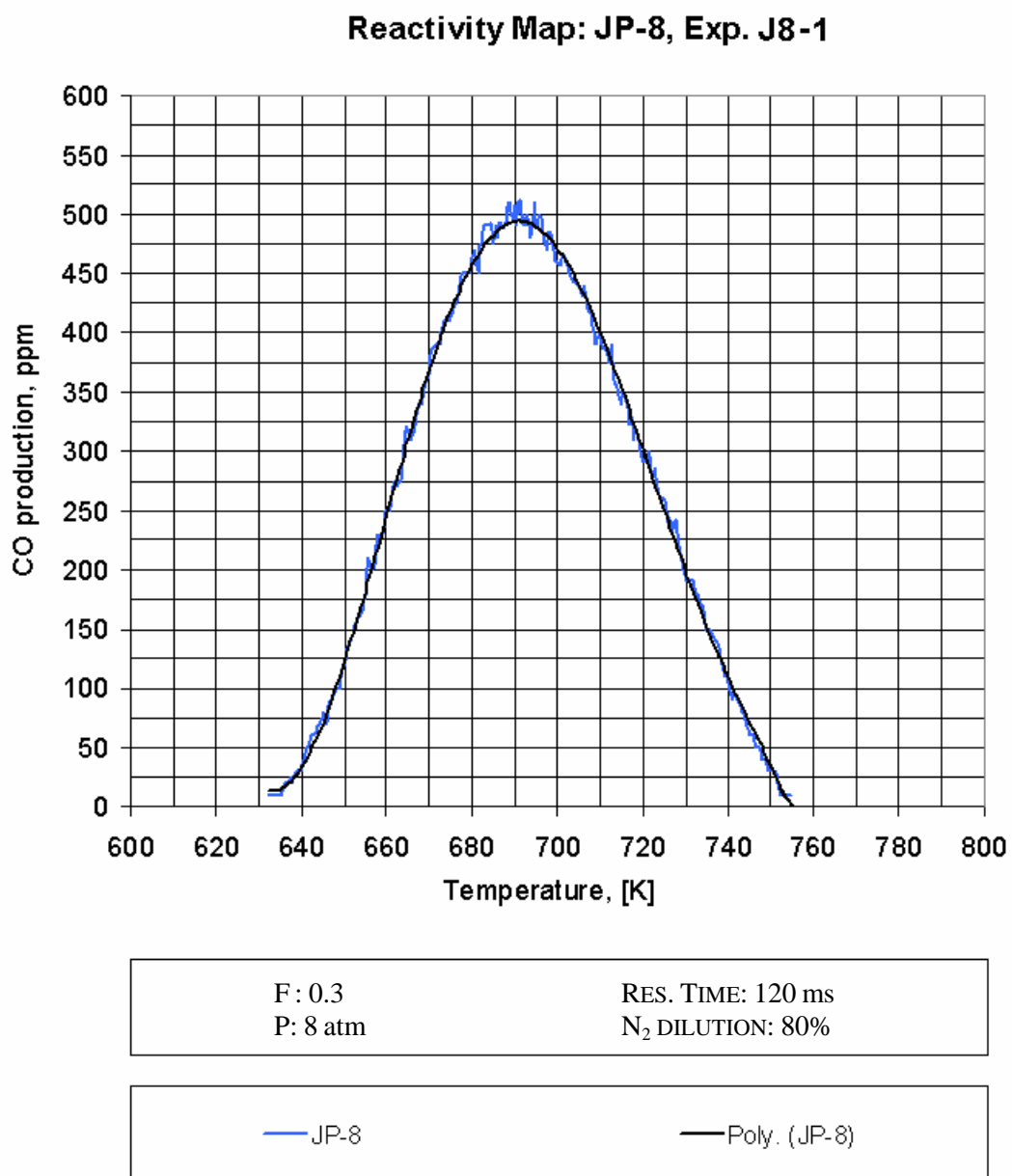
Figure 6.1 Reactivity Map and Polynomial Fit for JP-8, Exp. J8-1
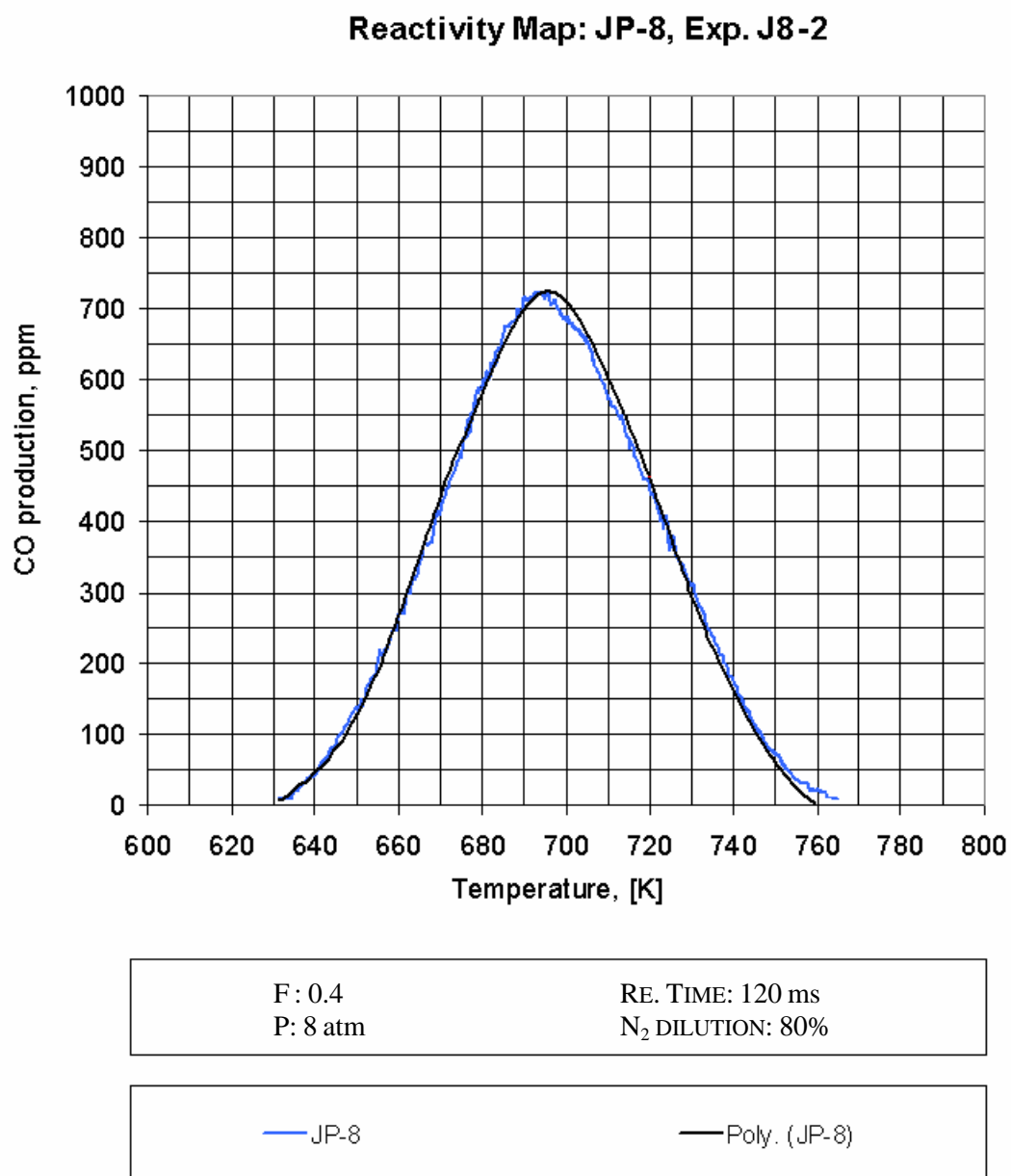
Figure 6.2 Reactivity Map and Polynomial Fit for JP-8, Exp. J8-2
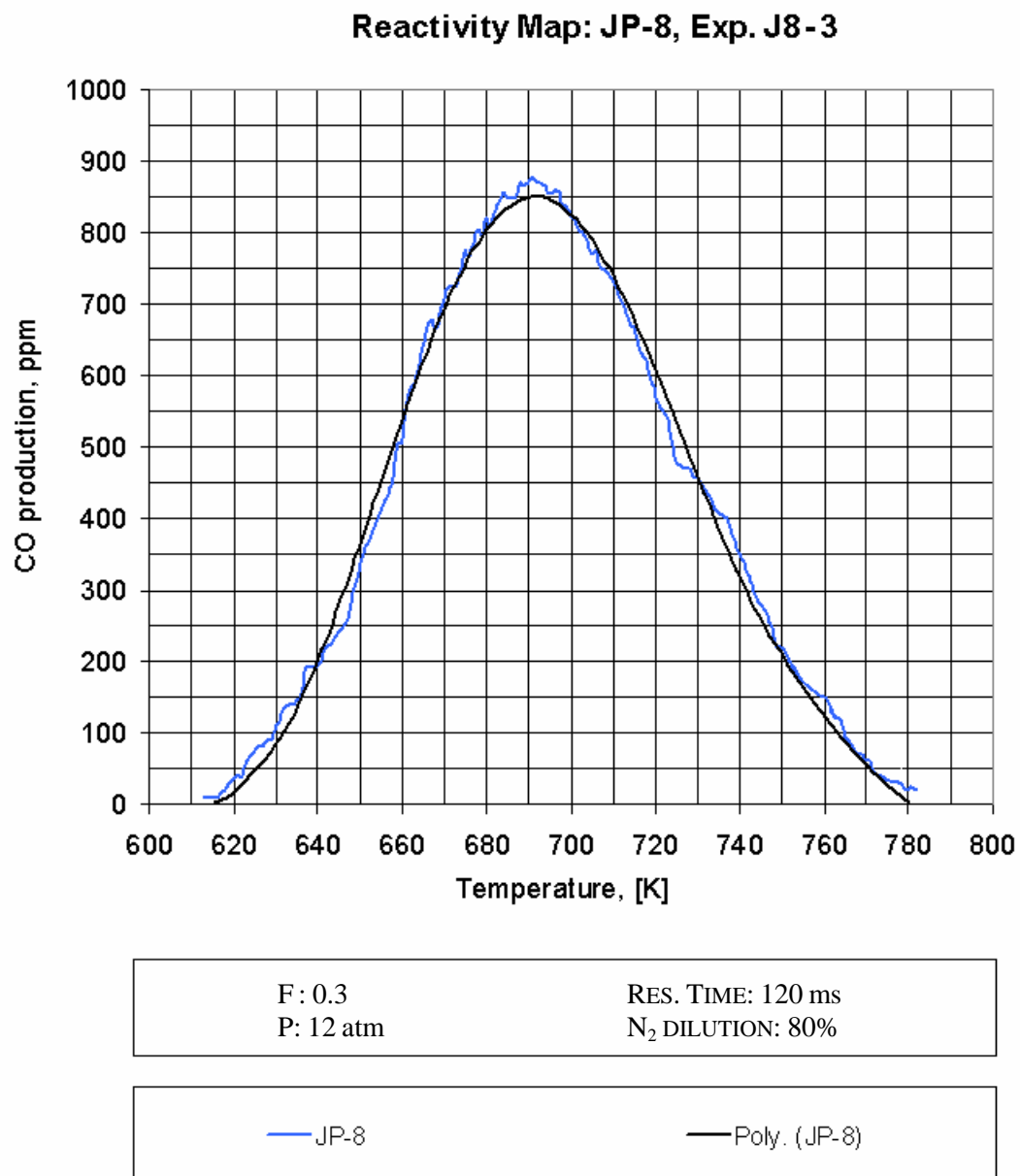
Figure 6.3 Reactivity Map and Polynomial Fit for JP-8, Exp. J8-3
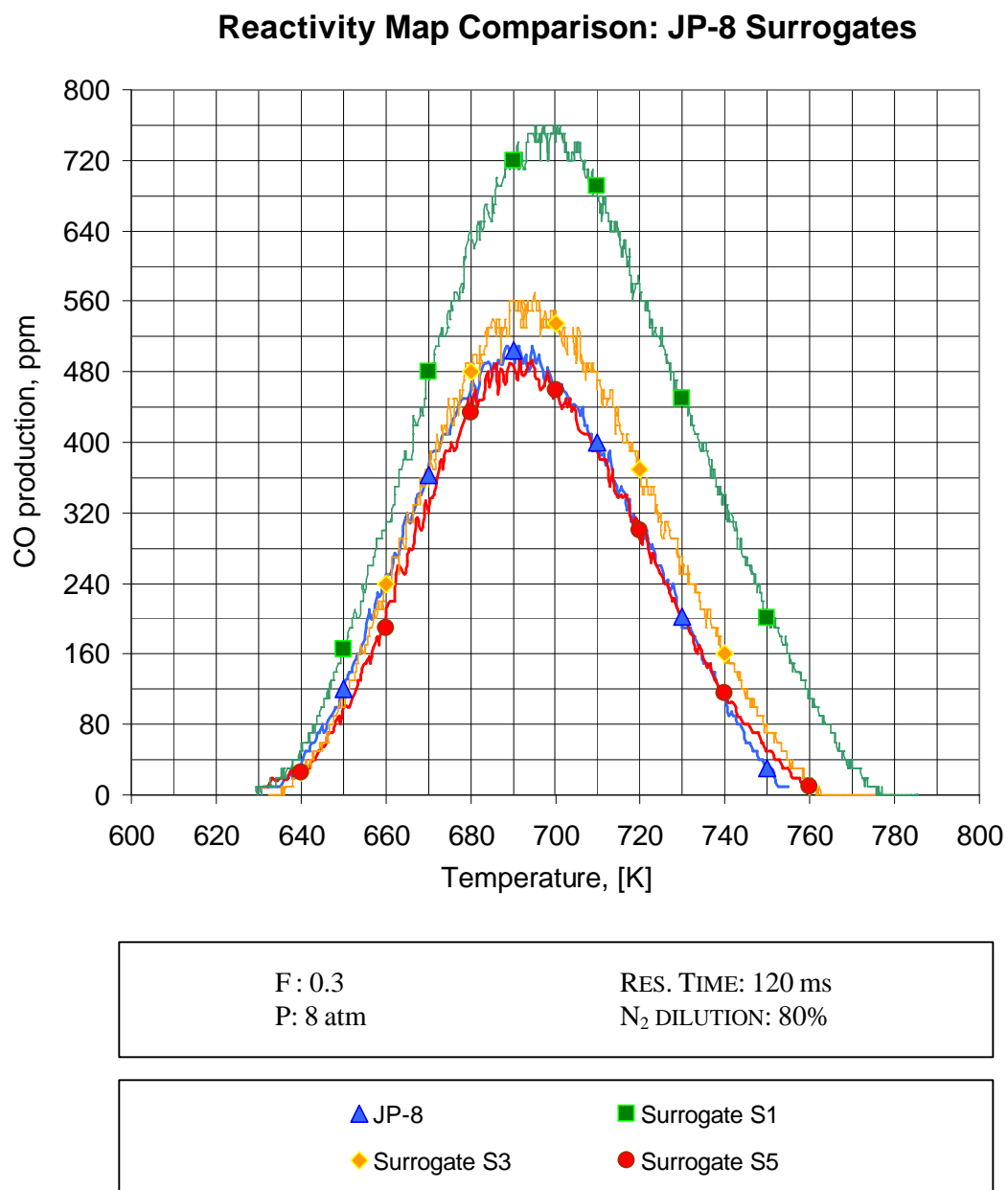
Figure 6.4 Reactivity Map Comparison: JP-8 Surrogates
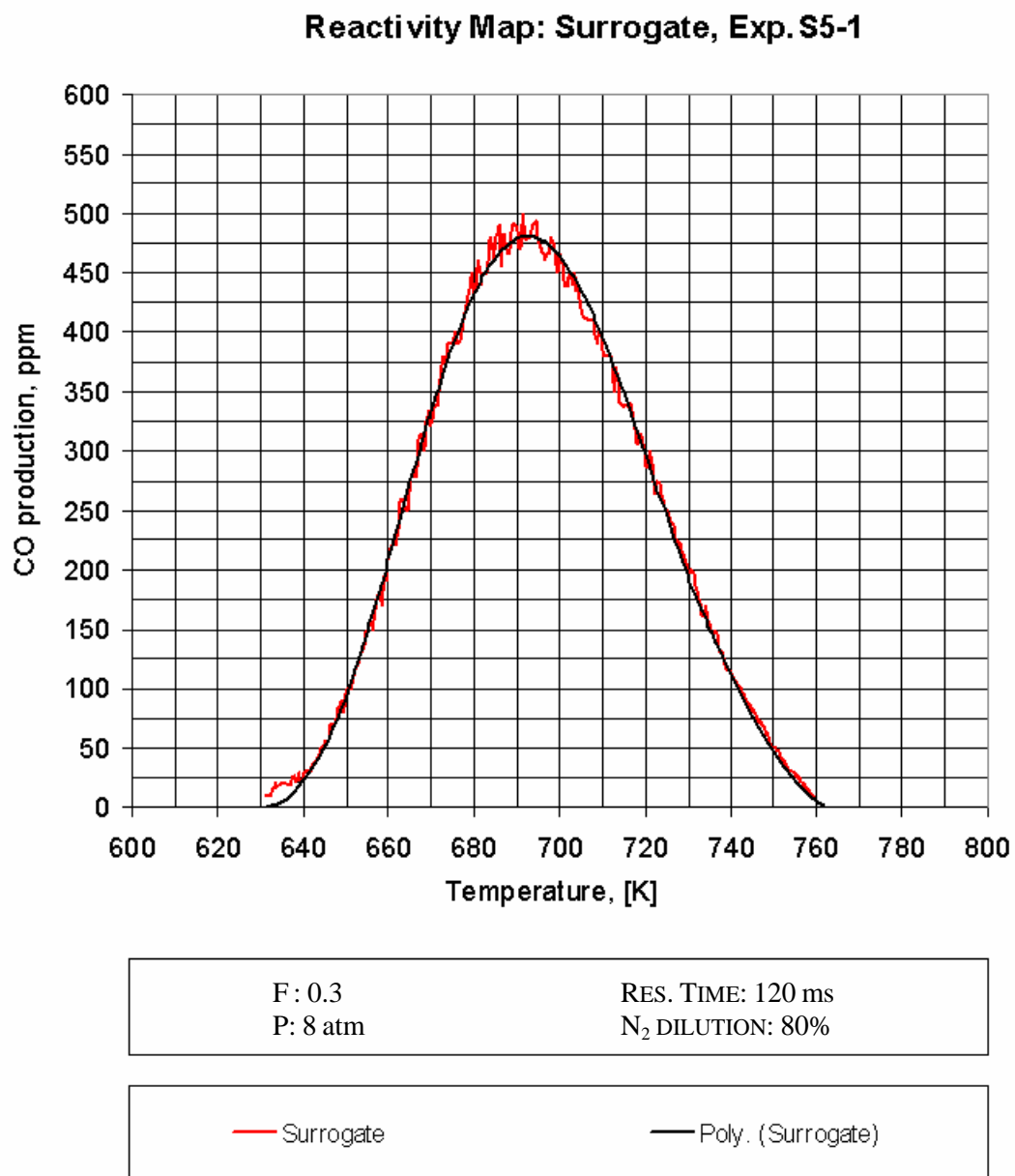
Figure 6.5 Reactivity Map and Polynomial Fit for Surrogate S5, Exp. S5-1
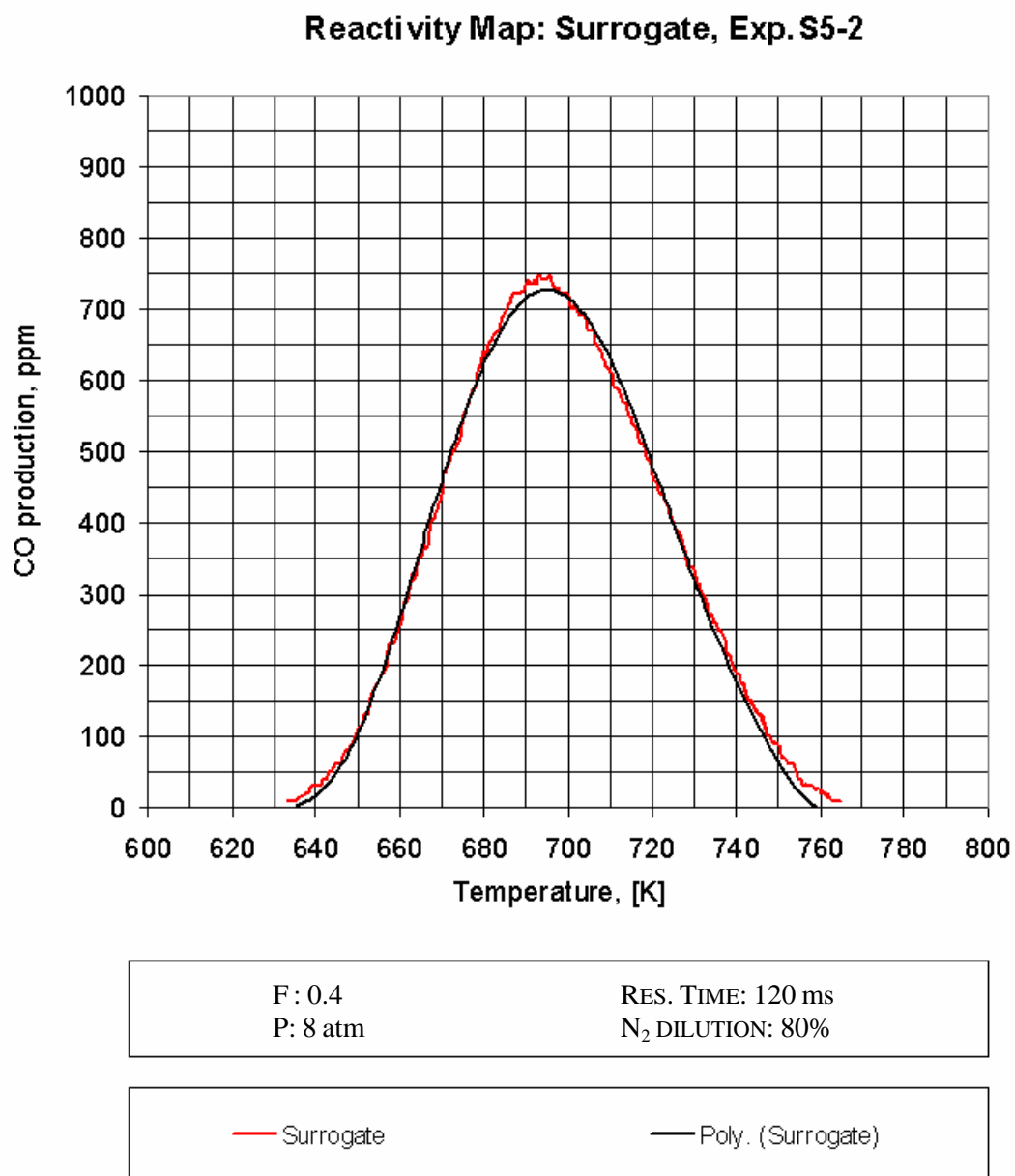
Figure 6.6 Reactivity Map and Polynomial Fit for Surrogate S5, Exp. S5-2
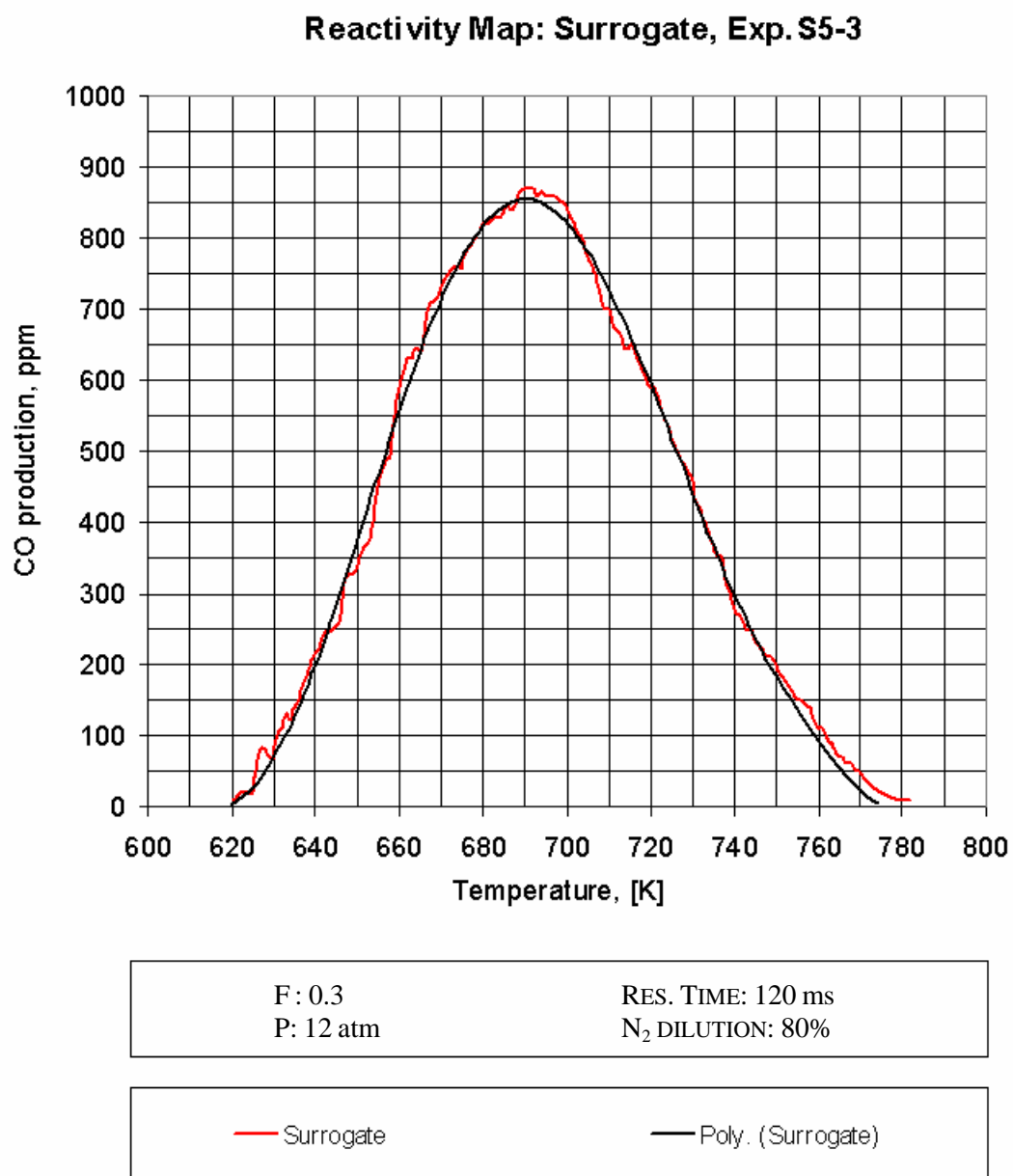
Figure 6.7 Reactivity Map and Polynomial Fit for Surrogate S5, Exp. S5-3

Reactivity Map Comparison: JP-8 & S5, Exp. #1

F : 0.3	RES. TIME: 120 ms
P: 8 atm	N_2 DILUTION: 80%
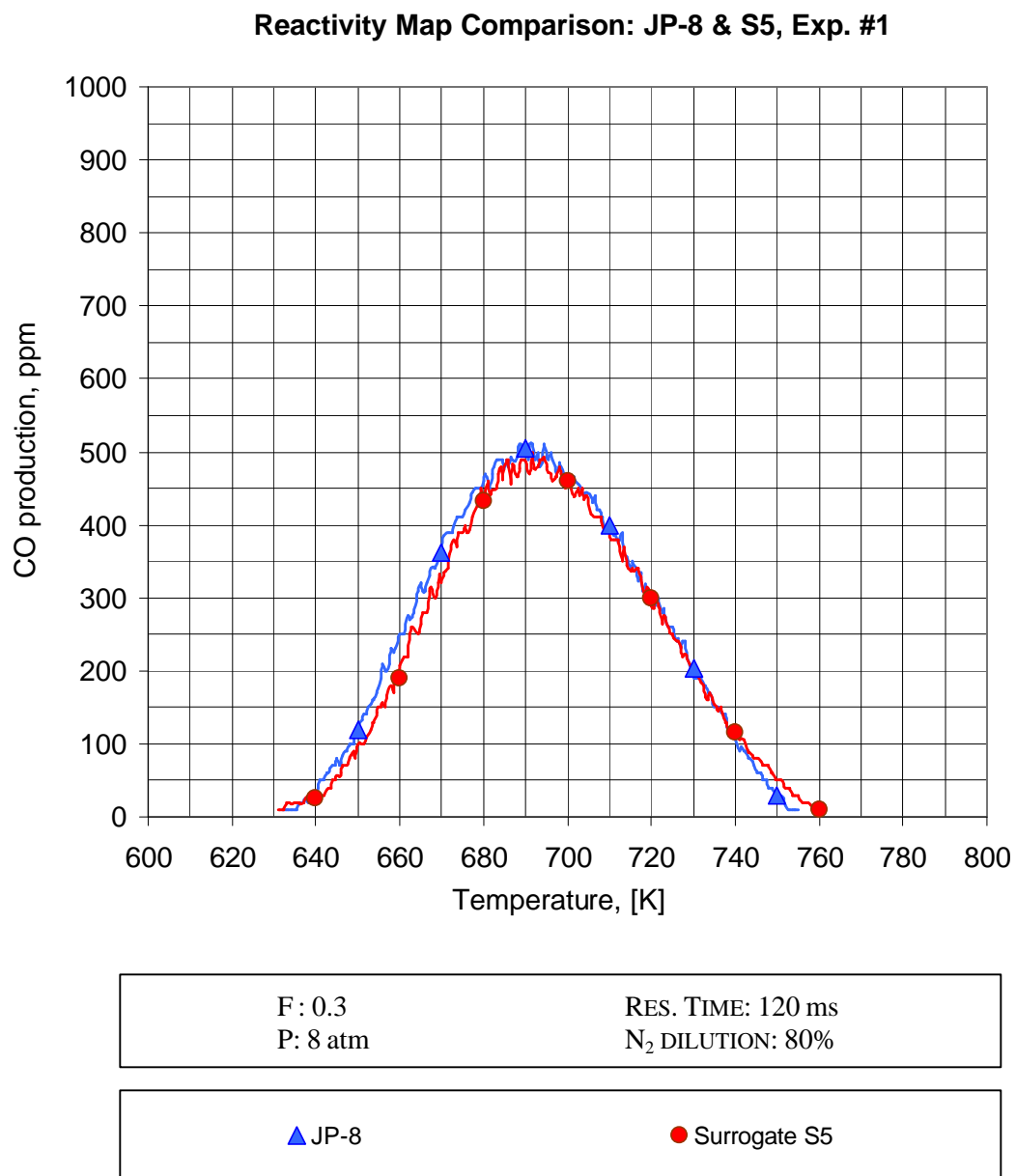
▲ JP-8　　　　　　　　　　● Surrogate S5

Figure 6.8 Reactivity Map Comparison: JP-8 & Surrogate S5, Exp. #1
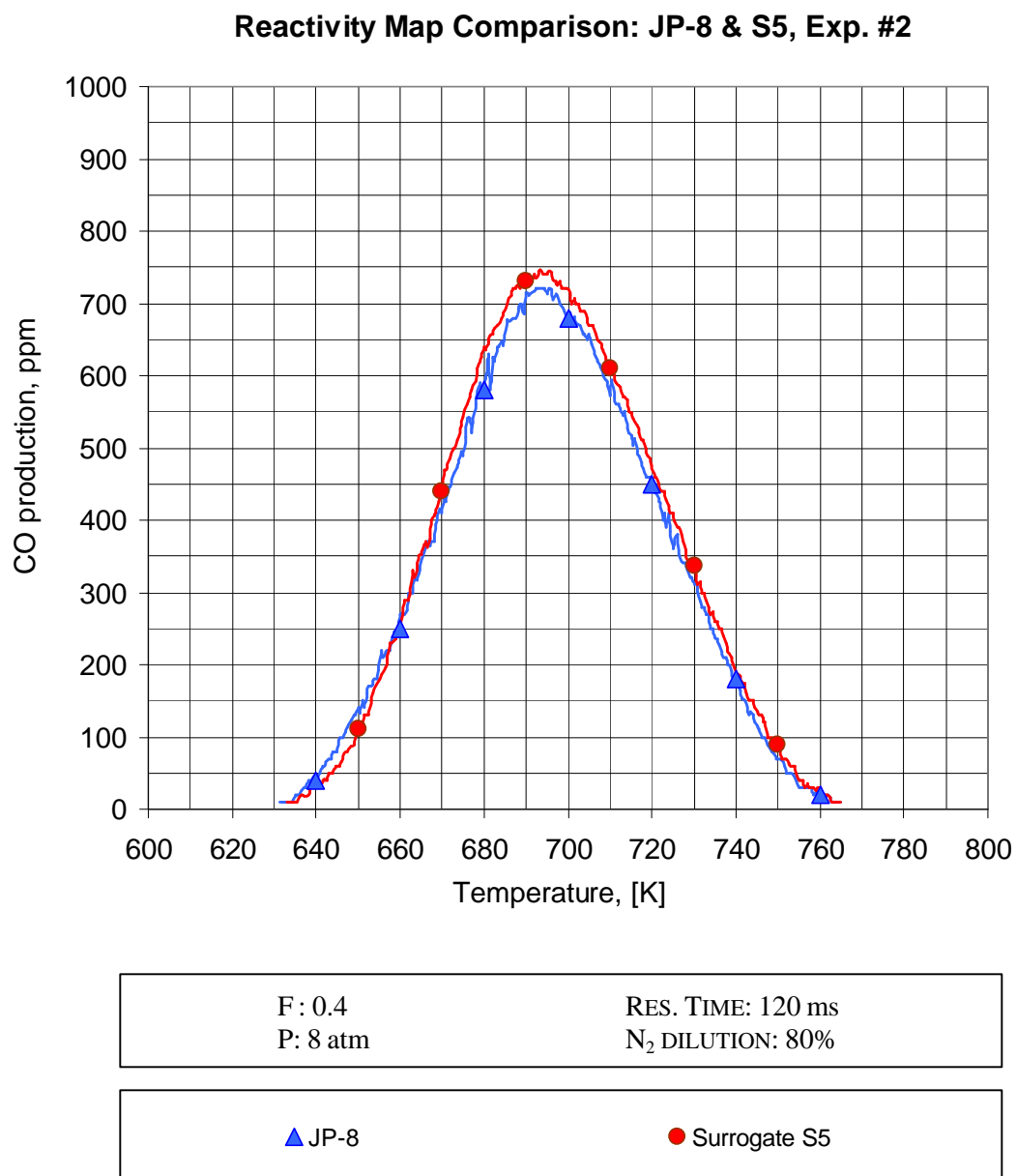
Figure 6.9 Reactivity Map Comparison: JP-8 & Surrogate S5, Exp. #2

Reactivity Map Comparison: JP-8 & S5, Exp. #3

F : 0.3	RES. TIME: 120 ms
P: 12 atm	N_2 DILUTION: 80%
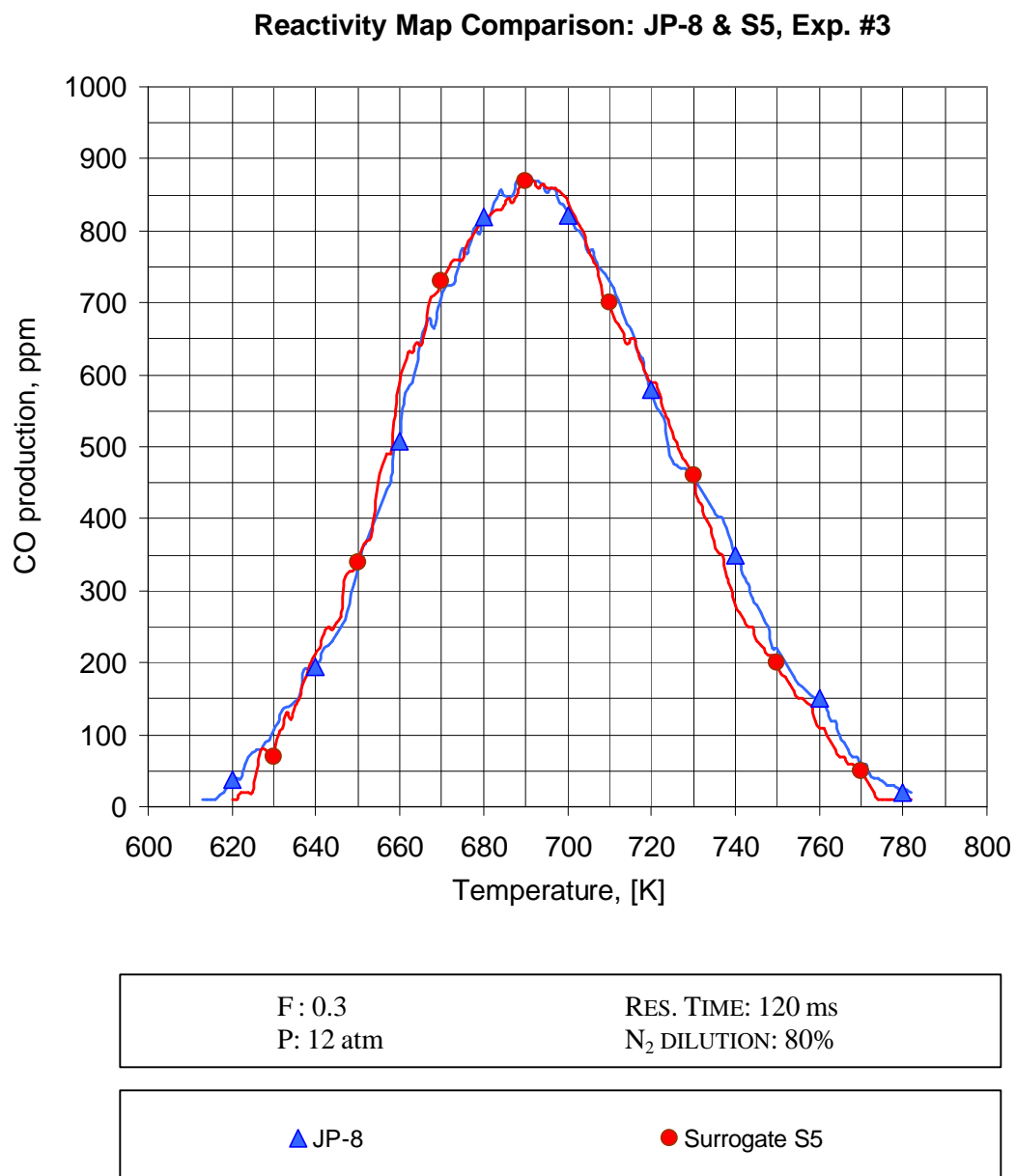
△ JP-8   ● Surrogate S5

Figure 6.10 Reactivity Map Comparison: JP-8 & Surrogate S5, Exp. #3

CHAPTER 7 – SUMMARY AND CONCLUSIONS

7.1 INTRODUCTION

This study investigated the autoignition oxidative behavior of several pure full boiling range hydrocarbon fuel components and their mixtures in the low and negative temperature regions with the final goal of developing a chemical surrogate for the military aviation fuel JP-8. The experimental study involved the measurement of reactivity maps under lean conditions for single fuels and binary, ternary, and larger mixtures using the Drexel Pressurized Flow Reactor.

The research results and findings are summarized in this Chapter. Recommendations of future work on JP-8 surrogate development and the antagonistic or synergistic effects of complex mixtures are also presented as the closure of this writing.

7.2 SUMMARY OF RESEARCH RESULTS

As one part of this research program, the oxidation of full boiling range fuels, specifically n-dodecane, isocetane, methylcyclohexane, decalin and a-methylnaphthalene, under lean conditions in the low and intermediate temperature regime (600 K to 800 K) and at elevated pressure (up to 12 atm) has been investigated. The experiments have been conducted in the well controlled Drexel Pressurized Flow Reactor. Due to the physical (boiling point) and chemical (autoignition reactivity) characteristics of some of the diesel compounds oxidized, the existing methods for fuel calibration and fuel delivery were redesigned in order to consistently deliver the required flow rates. The new calibration method is based on a double stage fuel injection into a

FTIR cell and the fuel delivery system is based on a high pressure syringe pump capable of delivering fuel with a resolution of 0.001ml/min. Both these two new methods have greatly increased system repeatability (CO mapping differences less then 5%) and decreased concentration variations during Controlled Cool Down experiments.

A parametric statistical data analysis method to perform the comparison of the reactivity maps obtained through two different CCD experiments has been implemented and developed. This method is based on several statistics and reactivity measures, including the first three moments (mean, variance, and skewness) of the data distributions as measures of location, shape and skewness of each temperature profile, as well as measures of reactivity start, end, and peak.

Clear and strong NTC behavior has been directly observed for pure n-dodecane and decalin. The three other pure compounds investigated resisted the ignition at the lean experimental condition tested, and their oxidative behavior was indirectly observed by blending them in binary mixtures with n-dodecane as a base fuel. The presence of n-dodecane accounted for the development of a radical pool large enough to initiate the oxidation of the other fuel, which would otherwise be unreactive at the tested conditions. Through fuel consumption mapping, an NTC regime was clearly observed for both fuels in the isocetane/n-dodecane mixture M1, while a-methylnaphthalene only showed low fuel consumption, almost constant over the entire temperature range, in the a-methylnaphthalene/n-dodecane mixture M3.

As a second part of this study, the oxidative behavior of several binary, ternary, and larger mixtures has been extensively investigated. The antagonistic and synergistic behavior of such complex mixtures has been observed by direct comparison of their

reactivity maps. Apart from the results of the oxidation of the three binary mixtures described above, two ternary and two larger mixtures have been designed and oxidized to investigate on the addition of aromatics and naphthenes. Considering the addition of an aromatic compound to a mixture of alkanes, no significant difference in the overall temperature profile was seen between the addition of hexylbenzene and a-methylnaphthalene. Moreover, both aromatics reacted synergistically with the other fuel in the blend, thus inhibiting the overall mixture reactivity. On the contrary, both of the naphthenes tested in a blend containing alkanes and aromatics, showed peculiar characteristics. Methylcyclohexane was extremely reactive (antagonistic effect), enhancing the overall reactivity of the mixture in the region across the NTC regime start, while the addition of decalin resulted in a small shift of the temperature profile towards lower temperatures, particularly by the NTC start point.

As a third and final part of this study, the results from the oxidation of both the single hydrocarbons and their mixtures were applied to develop a chemical surrogate for the military aviation fuel JP-8. The formulation strategy for the surrogate included the definition and application of a linear correlation between fuel Cetane numbers and the maximum CO production during a CCD experiment at fixed conditions. Through this correlation, optimal blending Cetane numbers have been calculated and then applied to calculate the surrogate composition. The JP-8 surrogate has also been tailored to closely match the hydrocarbon class composition of the parent fuel. A blend of 26% n-dodecane, 36% isocetane, 14% methylcyclohexane, 6% decalin, and 18% a-methylnaphthalene among a set of five surrogate candidates resulted in a close match to the JP-8 reactivity. Three different sets of Controlled Cool Down experiments were designed and conducted

to test the goodness of the surrogate under different experimental conditions. The system pressure (P = 8 and 12 atm) and the fuel to air equivalence ratio (F = 0.3 and 0.4) were varied and in all cases the reactivity profiles of JP-8 and surrogate closely matched over the whole range of temperature investigated, as shown by the Likelihood Index of 0.97 for all experiments. Therefore the developed surrogate proved to be suitable to represent the oxidative behavior of the parent fuel in the low and negative temperature regions. Due to its compositional reproducibility and tractability, the surrogate is suitable for both well-controlled fundamental modeling and experimental studies in lieu of the otherwise complex and chemically undefined JP-8.

7.3 RECOMMENDATIONS FOR FUTURE WORK

As discussed earlier in this report, the chemistry leading to autoignition for large hydrocarbons and their mixtures is very complex and still far from being exhaustively understood. Some recommendations for future work to this study are presented as follows.

1) In this study, the oxidative behavior of JP-8, JP-8 surrogate and all the other fuels and mixtures has been examined only in terms of reactivity maps. However, to gain insight into the autoignition chemistry of all these fuels and into the interactions between each fuel in complex mixtures, a detailed chemical analysis in terms of product species profiles should be conducted. Due to the complexity related to the chemistry of full boiling range fuels, however, a new more sensitive analysis technique needs to be developed. Gas chromatography coupled with Mass Spectrometry (GC-MS) would allow identifying and quantifying the product formation from fuel oxidation.

2) To date, chemical models are usually applied to alkanes and small aromatic compounds. A cooperative effort is ongoing with the group of Prof. Ranzi at Politecnico di Milano, to extend their semi-detailed model in order to model the oxidation of the developed JP-8 surrogate and, in turn, that of the real JP-8. The low and intermediate temperature mechanisms for the oxidation of isocetane, methylcyclohexane, and decalin need to be developed in order to apply the existing model to the JP-8 surrogate.

3) Regarding the synthesis of the JP-8 surrogate, other candidate compounds can be investigated. In particular the aromatic component, actually represented by a-methylnaphthalene only, may be replaced by a blend of two aromatics, an alkylbenzene and a bicyclic compound, to better match the JP-8 composition. In fact, even if the analysis of reactivity maps in this study did not show any significant difference between these two types of aromatics, their underlying chemistry may be different. Suggested hydrocarbon candidates are ethylbenzene or butylbenzene (less expensive than the investigated hexylbenzene) for the alkylbenzenic component, and a-methylnaphthalene for the bicyclic component.

4) Finally, the experimental methodology can be improved via the implementation of a computer controlled feedback based pressure regulation for the PFR. This would allow reduction in undesired system pressure fluctuations and, in turn, improvement in CO measurements.

LIST OF REFERENCES

AEO, (2001) - "Annual Energy Outlook 2002 With Projections to 2020", US Department of Energy and National Energy Information Center (Forrestal Building - Washington, DC 20585) DOE/EIA-0383(2002).

Barnard, J.A., Harwood, B.A., (1973a) - "Slow Combustion and Cool Flame Behavior in iso-Octane", Combustion and Flame, 21:345.

Barnard, J.A., Harwood, B.A., (1973b) - "The Spontaneous Combustion of n-Heptane", Combustion and Flame, 21:141.

Bartok, W., Sarofim, A.F., (1991) - "The Phenomenology of Modeling Combustion Chemistry", John Wiley & Sons Inc., New York.

Benson, S.W., (1981) - "The Kinetics and Thermochemistry of Chemical Oxidation with Application to Combustion and Flames", Progress in Energy & Combustion Science 7:125.

Bikas, G., Peters N., (2001) - "Kinetic Modeling of n-Decane Combustion and Autoignition", Combustion and Flame 126:1456-1475.

Blin-Simiand, N., Jorand, F., Sahetchian, K., Kerhoas, L., Malosse, C., Einhorn, J., (2001) - "Hydroperoxides with Zero, One, Two or More Carbonyl Groups Formed During the Oxidation of n-Dodecane" Combustion and Flame 126:1524-1532.

Bozzelli, J.W., Dean, A.M, (1990) - "Chemical Activation Analysis of the Reaction of C_2H_5 with O_2", Journal of Physical Chemistry, 94:3313-3317.

Brezinsky, K., Linteris, G.T., Litzinger, T.A., Glassman, I., (1986) - "High Temperature Oxidation of n-Alkyl Benzenes", Proceedings of the Combustion Institute, 21, pp. 833-840.

Briker, Y., Ring, Z., Iacchelli, A., McLean, N., Rahimi, P.M., Fairbridge, C., Malhotra, R., Coggiola, M.A., Young, S.E., (2001) - "Diesel Fuel Analysis by GC-FIMS: Aromatics, n-Paraffins, and Isoparaffins", Energy and Fuels, 15:1:23-37.

Chevron, (2000) - "Aviation Fuels Technical Review (FTR-3)", Chevron Product Company, Chevron USA Inc..

Chevron, (1998) - "Diesel Fuels Technical Review (FTR-2)", Chevron Product Company, Chevron USA Inc..

Coordinating Research Council, (1983) - "Handbook of Aviation Fuel Properties", Rept. 530, Coordinating Research Council Atlanta, GA.

Dagaut, P., Reuillon, M., Boettner, J-C, Cathonnet, M., (1994) - "Kerosene Combustion at Pressures up to 40 Atm: Experimental Study and Detailed Chemical Kinetic Modeling", Proceedings of the Combustion Institute, 21, p. 919.

Dagaut, P., Cathonnet, M., Ristori, A., (2001) - "The Oxidation of n-Hexadecane - Experimental and Detailed Kinetic Modeling", Combustion and Flame 125:1128-1137.

Defense Logistic Agency, (1998) - "Survey of Jet Fuels (1990-1996)", Defense Energy Support Center, Ft. Belvoir, VA.

EDA, (2001) - "Exploratory Data Analysis - Engineering Statistics Handbook", Statistical Engineering Division, National Institute of Standards and Technology, USA.

Edwards, T., (1993) - "USAF Supercritical Hydrocarbons Fuels Interests", AIAA Paper 93-0807.

Edwards, T., (2001) - ""Real" Kerosene Aviation and Rocket Fuels: Composition and Surrogates", ESSCI 2001-61, presented at the 2001 Fall Technical Meeting, Eastern State Section of the Combustion Institute, Hilton Head, SC.

Edwards, T., Maurice, L.Q., (2001) - "Surrogate Mixtures to Represent Complex Aviation and Rocket Fuels" Journal of Propulsion and Power, 17:2:461-466.

Griffiths, J.F., Heck, S.M., Pritchard, H.O., (1998) - "Cetane number vs. structure in paraffin hydrocarbons" – Journal Chemical Society, Faraday Transcript, 94:12:1725-1727.

Guibet, J.C., Faure-Birchem, E., (1999) - "Fuels and Engines: Technology, Energy, Environment" – Institut Francais du Petrole Publications - Editions Technip, Paris.

Kaiser, E.W., Siegel, W.O., Cotton, D.F., Anderson, R.W., (1992) - "Effect of Fuel Structure on Emission from a Spark-Ignited Engine -2- Naphthene and Aromatic Fuels" Environmental Science and Techonolgy, 26:1581-1586.

Khan, A.R., (1998) - "Oxidation of Industry Standard Fuels and Blends of Primary Reference Fuels in the Low and Negative Temperature Coefficient Regions", M.S. Thesis, Drexel University, Philadelphia, PA.

Knox, J.H., Wells, C.H.J., (1963) - "Slow Oxidation of Ethane and Ethylene in the Gas Phase", Transactions of the Faraday Society, 59:2786-2801.

Koert, D.N., (1990) - "Effects of Pressure on Hydrocarbon Oxidation Chemistry", Ph.D. Thesis, Drexel University, Philadelphia, PA.

Koert, D.N., Cernansky, N.P., (1992) – "A Flow Reactor for the Study of Homogeneous Gas-Phase Oxidation of Hydrocarbons at Pressures up to 20 atm (2 MPa)", Measurement Science and Technology, 3:6:607-613

Kowalski, S., (1993) – "A Study of the Low and Intermediate Temperature Oxidation Chemistry of a Primary Reference Fuel Blend and Two Gasolines at High Pressure", M.S. Thesis, Princeton University, NJ.

Lenhert, D.B., (2002) - Personal Communications.

Leppard, W.R., (1989) - "A Comparison of Olefin and Paraffin Autoignition Chemistries: A Motored Engine Study", SAE Trans. 98:892081.

Lignola, P.G., Reverchon, E., Piro, R., (1984) - "Dynamics of Combustion Processes of n-Heptane and iso-Octane and Their Mixtures and Knocking", Proceedings of the Combustion Institute, 20, p. 123.

Lignola, P.G., Reverchon, E., (1986) - "Dynamics of n-Heptane and iso-Octane Combustion Processes in a Jet Stirred Flow Reactor Operated Under Pressure", Combustion and Flame, 64:177.

Martel, C.R., 2000 - "Molecular Weight and Average Composition of JP-4, JP-5, JP-8 and Jet A", Chemical Propulsion Information Agency Airbreathing Propulsion Manual, Columbia, MD.

Maurice, L.Q., Lindstedt, R.P., (2000) - "Detailed Chemical-Kinetic Model for Aviation Fuels", Journal of Propulsion and Power, 16:2:187-195.

Maurice, L.Q., Lander, H., Edwards, T., Harrison, W.E. III, (2001) - "Advanced Aviation Fuels: a Look Ahead Via a Historical Perspective" Fuel 80:747-756.

Montgomery, C.J., Cannon, S.M., Mawid, M.A., Bekar, B., (2002) - "Reduced Chemical Kinetic Mechanisms for JP-8 Combustion", AIAA Paper 2002-0336.

Owen, K., Coley, T., (1995) - "Automotive Fuels Reference Book", 2nd edition, Society of Automotive Engineers Inc., Warrendale, PA.

Pilling, M.J., (1997) - "Comprehensive Chemical Kinetics 35: Low-Temperature Combustion and Autoignition" Elsevier, New York.

Ramotowski, M.J., (1992) - "The Oxidation of Propane and n-Butane at Elevated Pressure in the Region of Negative Temperature Coefficient", M.S. Thesis, Drexel University, Philadelphia, Pa.

Rose, J.W., Cooper, J.R., (1977) - "Technical Data on Fuel – 7th ed." The British National Committee, World Energy Conference, Scottish Academic Press.

Rose, J.W., Cooper, J.R., (1955) - "Technical Data on Fuel – 5th ed." The British National Committee, World Energy Conference, Scottish Academic Press.

Roubaud, H., Minetti, R., Sochet, L.R., (2000) - "Oxidation and Combustion of Low Alkylbenzenes at High Pressure: Comparative Reactivity and Autoignition" Combustion and Flame 121:535-541.

Roubaud, A., Lemaire, O., Minetti, R., Sochet, L.R., (2000) - "High Pressure Auto-ignition and Oxidation Mechanism of *o*-xylene, *o*-ethyltoluene, and *n*-butylbenzene between 600 and 900 K" Combustion and Flame 123:561-571.

Sahetchian, K., Champoussins, J.C., Brun, M., Levy, N., Blin-Simiand, N., Aligrot, C., Jorand,. F., Socoliuc, M., Heiss, A., Guerassi, N., (1995) - "Experimental Study and Modeling of Dodecane Ignition in a Diesel Engine", Combustion and Flame 103:207-220.

Salooja, K.C., (1965) - "Studies of Combustion Processes Leading to Ignition of Aromatic Hydrocarbons", Combustion and Flame, 9:121-130.

Sarofim, A.F., Eddings, E.G., Yan, S., Violi, A., and Granata, S., Faravelli, T., Ranzi, E., (2002) - "Experimental Formulation and Kinetic Modeling for JP-8 Surrogate Mixtures" 2nd Mediterranean Combustion Symposium, Sharm El Sheick, Egypt.

Scacchi, G., Glaude, P.A., Battin-Leclerc, F., Fournet, R., Warth, V., Côme, G.M., (2000) - "Construction and Simplification of a Model for the Oxidation of Alkanes", Combustion and Flame 122:451-462.

Schulz, W.D., Heneghan, S.P., Locklear, S.L., Geiger, D.L., Anderson, S.D., (1993) - "Static Tests of Jet Fuel Thermal and Oxidative Stability", Journal of Propulsion and Power, 9:1:5-9.

Semenov, N.N., (1935) - "Chemical Kinetics and Chain Reactions", Oxford University Press, London.

Shaddix, C.R., Brezinsky, K., Glassman, I., (1997) - "Analysis of Fuel Decay Routes in the High-Temperature Oxidation of a-Methylnaphthalene" Combustion and Flame 108:139-157.

Schobert, H., (1990) - "The Chemistry of Hydrocarbon Fuels", Butterworths, London.

Solomons, T.W.G., (1996) - "Organic Chemistry" 6th ed., John Wiley & Sons Inc., New York.

Song, C., Hsu, C.S., Mochida, I., (2000) - "Chemistry of Diesel Fuels", Taylor & Francis, New York.

Stephens, M.A., (1974) - "EDF Statistics for Goodness of Fit and Some Comparisons", Journal of the American Statistical Association, 69:730-737.

Tukey, J., (1977) - "Exploratory Data Analysis", Addison-Wesley, Reading, MA.

US Army Tank-Automotive RD&E Center, (2000) - "Fuel Users Guide – Average Survey Data", Fuels and Lubricants Team, Warren, MI.

Wagner, A.F., Slagle, I.R., Sarzynski, D., Gutman, D., (1990) - "Experimental and Theoretical Studies of the $C_2H_5 + O_2$ Reaction Kinetics", Journal of Physical Chemistry, 94:1853-1868.

Wilk, R.D., Koert, D.N, Cernansky, N.P., (1989) - "Low-Temperature Carbon Monoxide Formation as a Means of Assessing the Autoignition Tendency of Hydrocarbons and Hydrocarbon Blends", Journal of Energy & Fuels, 3:292.

Wood, C.P., (1989) – "The Development and Application of Surrogate Blends in Simulating the Combustion Performance of Distillate Aviation Fuels", M.S. Thesis, Department of Mechanical Engineering, University of California, Irvine.

Wood, C.P., McDonell, V.G., Smith, R.A., Samuelsen, G.S., (1989) -"Development and Application of a Surrogate Distillate Fuel", Journal of Propulsion and Power, 5:4:399-405.

Zeelenberg, A.P., Bickel, A.F., (1961) - "Slow Oxidation of Hydrocarbons in the Gas Phase – Part I – Reactions during the Induction Period of Isobutane Oxidation", Journal of Chemical Society, 4014-4019.

Zeppieri, S., Brezinsky, K., Glassman, I., (1997) - "Pyrolysis Studies of Methylcyclohexane and Oxidation Studies of Methylcyclohexane and Methylcyclohexane/Toluene Blends", Combustion and Flame, 108:266-286.

APPENDIX A – CETANE NUMBER FOR PURE HYDROCARBONS

As explained in Chapter 1, Cetane Number is a measure of how readily a distillate fuel auto-ignites under diesel engine conditions. The Cetane Numbers for several hydrocarbons, grouped by their class, are reported in Table A.1. Most of these data have been collected by Rose and Cooper in the 70s and there is agreement among the scientific communities that they are still valid today. However, it is useful to remember that usually the Cetane Number is known with an uncertainty of ± 3 units. In Table A.1 the empirical formula for each compound are also reported. Finally, the last column includes the sources for the data.

Table A.1 Cetane Number of Pure Hydrocarbons

EMPIRICAL FORMULA	CLASS	HYDROCARBON	CETANE NUMBER	SOURCE
C_7H_{16}	N-PARAFFINS	N-HEPTANE	56	1,2,4
C_8H_{18}	N-PARAFFINS	N-OCTANE	64	2,4
$C_{10}H_{22}$	N-PARAFFINS	N-DECANE	76	1,3
″	″	″ ″	77	2,4
$C_{12}H_{26}$	N-PARAFFINS	N-DODECANE	80	1
″	″	″ ″	88	2,4
″	″	″ ″	82	2
$C_{13}H_{28}$	N-PARAFFINS	N-TRIDECANE	88	1
$C_{14}H_{30}$	N-PARAFFINS	N-TETRADECANE	93	1
″	″	″ ″	96	2,4
$C_{15}H_{32}$	N-PARAFFINS	N-PENTADECANE	95	1,3
$C_{16}H_{34}$	N-PARAFFINS	N-HEXADECANE	100	1
$C_{17}H_{36}$	N-PARAFFINS	N-HEPTADECANE	105	1
$C_{18}H_{38}$	N-PARAFFINS	N-OCTADECANE	110	1
″	″	″ ″	103	2,4

C$_{19}$H$_{40}$	N-PARAFFINS	N-NONADECANE	110	1
C$_{20}$H$_{42}$	N-PARAFFINS	N-EICOSANE	110	1,3
C$_6$H$_{14}$	ISO-PARAFFINS	2-METHYLPENTANE	33	1
C$_8$H$_{18}$	ISO-PARAFFINS	2,2,4-TRIMETHYLPENTANE	12	1
C$_{12}$H$_{26}$	ISO-PARAFFINS	4,5-DIETHYLOCTANE	20	1,3
C$_{12}$H$_{26}$	ISO-PARAFFINS	3-EHTYLDECANE	48	1,3
C$_{12}$H$_{26}$	ISO-PARAFFINS	4,5-DIETHYLOCTANE	20	1
C$_{13}$H$_{28}$	ISO-PARAFFINS	2,5-DIMETHYLUNDECANE	58	1
C$_{13}$H$_{28}$	ISO-PARAFFINS	4-PROPYLDECANE	39	1
C$_{13}$H$_{28}$	ISO-PARAFFINS	5-BUTYLNONANE	53	1
C$_{16}$H$_{34}$	ISO-PARAFFINS	5-BUTYLDODECANE	45	1
C$_{16}$H$_{34}$	ISO-PARAFFINS	2,2,4,4,6,8,8-HEPTAMETHYLNONANE	15	2,3
C$_{16}$H$_{34}$	ISO-PARAFFINS	7,8-DIMETHYLTETRADECANE	40	1
C$_{18}$H$_{38}$	ISO-PARAFFINS	8-PROPYLPENTADECANE	48	1,3
C$_{20}$H$_{42}$	ISO-PARAFFINS	9,10-DIMETHYLOCTANE	59	1,3
C$_8$H$_{16}$	OLEFINS	1-OCTENE	40	2,4
C$_8$H$_{16}$	OLEFINS	DI-ISOBUTYLENE	10	1
C$_{10}$H$_{20}$	OLEFINS	1-DECENE	60	2,4
C$_{12}$H$_{24}$	OLEFINS	7-DODECENE	71	2,4
C$_{14}$H$_{28}$	OLEFINS	1-TETRADECENE	79	1
"	"	" "	83	2,4
C$_{16}$H$_{32}$	OLEFINS	1-HEXADECENE	88	1
"	"	" "	84	2,4
C$_{17}$H$_{34}$	OLEFINS	7-BUTYLTRIDECENE	36	1
C$_{18}$H$_{36}$	OLEFINS	1-OCTADECENE	90	2,4
C$_{18}$H$_{36}$	OLEFINS	8-PROPYL-8-PENTADECENE	45	1
C$_6$H$_{12}$	NAPHTHENES	CYCLOHEXANE	13	1
C$_7$H$_{14}$	NAPHTHENES	METHYLCYCLOHEXANE	20	1,2,4
C$_{10}$H$_{18}$	NAPHTHENES	DECALIN	42	2,4
"	"	" "	48	1,3
C$_{12}$H$_{22}$	NAPHTHENES	BICYCLOHEXYL	53	1
"	"	" "	47	3
C$_{12}$H$_{24}$	NAPHTHENES	3-CYCLOHEXYLHEXANE	36	1,3
C$_{13}$H$_{24}$	NAPHTHENES	N-PROPYLDECALINE	35	1
C$_{13}$H$_{18}$	NAPHTHENES	N-PROPYLTETRALINE	8	1
C$_{14}$H$_{26}$	NAPHTHENES	N-BUTYLDECALINE	31	1
C$_{14}$H$_{20}$	NAPHTHENES	N-BUTYLTETRALINE	18	1
C$_{18}$H$_{34}$	NAPHTHENES	N-OCTYLDECALINE	31	1

$C_{18}H_{28}$	NAPHTHENES	N-OCTYLTETRALINE	18	1
$C_{19}H_{38}$	NAPHTHENES	1-METHYL-3-DODECYLCYCLOHEXANE	70	1
$C_{20}H_{40}$	NAPHTHENES	2-CYCLOHEXYLTETRADECANE	57	1
$C_{11}H_{16}$	AROMATICS	N-PENTYLBENZENE	8	1,2,3,4
$C_{11}H_{10}$	AROMATICS	a-METHYLNAPHTHALENE	0	1,3
$C_{12}H_{18}$	AROMATICS	N-HEXYLBENZENE	26	1,2,4
$C_{12}H_{10}$	AROMATICS	DIPHENYLE	21	1,3
$C_{13}H_{20}$	AROMATICS	N-HEPTYLBENZENE	35	1
$C_{13}H_{12}$	AROMATICS	DIPHENYLMETHANE	11	1
$C_{14}H_{14}$	AROMATICS	1,2-DIPHENYLETHANE	1	1
$C_{14}H_{16}$	AROMATICS	1-N-BUTYLNAPHTHALENE	6	1
$C_{14}H_{22}$	AROMATICS	N-OCTYLBENZENE	31	1
$C_{14}H_{22}$	AROMATICS	2-PHENYLOCTANE	33	1
$C_{15}H_{24}$	AROMATICS	N-NONYLBENZENE	50	1,2,3,4
$C_{16}H_{26}$	AROMATICS	N-OCTYLXYLENE	20	1
$C_{17}H_{28}$	AROMATICS	2-PHENYLUNDECANE	51	1
$C_{18}H_{24}$	AROMATICS	2-N-OCTYLNAPHTHALENE	3	1
$C_{18}H_{30}$	AROMATICS	N-DODECYLBENZENE	68	1
$C_{18}H_{30}$	AROMATICS	4-PHENYLDODECANE	42	1
$C_{20}H_{34}$	AROMATICS	N-TETRADECYLBENZENE	72	1
$C_{20}H_{34}$	AROMATICS	2-PHENYLTETRADECANE	49	1

Sources:
[1] *Rose, J.W., Cooper, J.R., (1977) - "Technical Data on Fuel" 7th edition, The British National Committee, World Energy Conference, London.*

[2] *Song, C., Hsu, C.S., Mochida, I., (2000) - "Chemistry of Diesel Fuels" Taylor & Francis, New York.*

[3] *Chevron, (1998) – "Diesel Fuels Technical Review (FTR-2)", Chevron Products Company, Chevron USA Inc..*

[4] *Schobert, H., (1990) - "The Chemistry of Hydrocarbon Fuels", Butterworths, London.*

APPENDIX B – FTIR DOUBLE INJECTION CALIBRATION METHOD

B.1 INTRODUCTION

This appendix includes the details of the calculations developed for the FTIR Double Injection calibration method presented in Chapter 4 and the Standard Operation Procedures. Based on these calculations an Excel Spreadsheet (shown in section B.3) has been developed in order to automatically obtain the calibration curve and the actual fuel flow rate required for the experiment.

The following calculations show how to apply the Law of Ideal Gases to obtain the ideal value of pressure rise inside the cell after the fuel syringe injection, supposing that the value of the fuel density does not depend on temperature. Indeed, the fuel density at the specific experimental conditions is unknown. Nevertheless even if these equations can not be applied to obtain the actual flow rate, they are still useful to evaluate the quality of the calibration.

$$P \cdot V = N \cdot Ru \cdot T \tag{B.1}$$

$$N = \frac{m_{injected-fuel}}{MW_{fuel}} = \frac{r_{fuel}\left[\frac{kg}{m^3}\right] \cdot V_{inj.fuel}[m^3]}{MW_{fuel}\left[\frac{kg}{kmol}\right]} = \frac{r_{fuel} \cdot V_{inj.fuel}}{MW_{fuel}}[kmol] \tag{B.2}$$

Plugging equation (B.2) into equation (B.1) and solving for P, we find an equation useful for calculating the pressure rise inside the FTIR cell (or inside the calibration cylinder).

$$P[Pa] = \frac{N \cdot Ru \cdot T}{V_{cell}} = \frac{r_{fuel}\left[kg \Big/ m^3\right] \cdot V_{inj.fuel}\left[m^3\right]}{MW_{fuel}\left[kg \Big/ kmol\right]} \cdot \frac{Ru\left[\dfrac{kg \cdot m^2}{s^2 \cdot kmol \cdot k}\right] \cdot T[K]}{V_{cell}\left[m^3\right]}$$

(B.3)

$$P[Pa] = \frac{r_{fuel} \cdot V_{inj.fuel} \cdot Ru \cdot T}{MW_{fuel} \cdot V_{cell}}\left[kg \Big/ m \cdot s^2\right]$$

(B.4)

Equation (B.4) demonstrates that, in order to obtain a larger pressure rise inside the cell when injecting the same volume of fuel, the only parameter that it can easily be changed is the cell temperature T.

It is instructive to compare the effect of changing the temperature on the fuel vaporization, and, in turn, on the overall efficiency of the calibration process. Injecting 10 µl of n-dodecane into the cylinder (see Figure B.1) at ambient temperature (T ~ 30 °C) resulted in a pressure rise of approximately 0.8 torr while the ideal ?P calculated using B.4 is 1.7 torr. Repeating the same injection, but with the cylinder heated to 260 °C, the observed pressure rise was 2.6 torr, while the ideal ?P is 2.9 torr. The increase in the ideal pressure rise, and in turn in the injection method resolution, is in the order of ~50%. Moreover the actual value is much closer to the ideal case when the cell temperature is higher than the fuel boiling point, that means T = 260 °C. Similar results are obtained injecting 5 µl of n-dodecane, as reported in Table B.1.

Table B.1 Temperature Effect on Fuel Calibration: n-Dodecane Calibration

VOLUME INJECTED [μl]	TEMPERATURE [°C]	?P ACTUAL [torr]	?P IDEAL [torr]
5	30	0.45	0.70
5	260	1.20	1.20
10	30	0.80	1.70
10	260	2.60	2.90

B.2 STANDARD OPERATING PROCEDURES

This section includes the Standard Operating Procedures which have been developed for the new Double Injection Calibration method. The numbers of the valves refer to the device schematic presented in Figure B.1.

Operating Procedures: $T_{CYLINDER} = T_{FUEL\ BOILING\ POINT} + \sim 30\ °C$

$T_{FTIR\ CELL} = 175\ °C$

$P \sim 5\text{-}8$ torr

$V_{CYLINDER} \sim 500$ ml

$V_{FTIR\ CELL} \sim 600$ ml

Cylinder Injection Time: < 5 s

FTIR Cell Injection Time: < 5 s

1st Stage: • Evacuate the whole system (open 8) and then close all valves

• Record the Cylinder and the FTIR Cell pressures

(open 1 and 6 and measure P1 & P2)

• Inject fuel into the Cylinder with a syringe and measure

Cylinder $?P_1$

• Refill (open 9) only the Cylinder with nitrogen up to 760 torr

2nd Stage: • Injection from the Cylinder to the FTIR Cell (open 3 and 5)

• Measure and record FTIR Cell $?P_2$

• Close the Cylinder valve (close 5) and backfill only the FTIR

Cell up to 760 torr (open 4)

• Close 3, 4 and 1 and measure and record spectrum absorbance

• Clean and purge the system using nitrogen (open 3, 4, 5, 6, and 8).

B.3 FTIR CALIBRATION SHEET

The FTIR Calibration Sheet is an Excel spreadsheet that is used during the calibration process (see Section 3.6) to calculate the relationship between the fuel absorbance at two particular peaks and the fuel concentration. Two peaks are considered for each calibration, and the final flow rates should coincide. The spreadsheet is shown in Figures B.2 and B.3. All the cells in italic font represent data that have to be entered by the user during the different steps of the calibration process. The spreadsheet is based on the following equations (the cell labels refer to cells in Figures B.2 and B.3, while the functions *slope* and *intercept* are available in Excel):

Cell F11: $\qquad D11 - C11 \qquad\qquad\qquad\qquad\qquad\qquad$ (B.5)

Cell G11: $\qquad \dfrac{G1 \cdot B11 \cdot 10^9 \cdot 8314.51 \cdot [273.15 + G3]}{G5 \cdot G7 \cdot 10^{-6} \cdot 7.5006168 \cdot 10^3} \qquad$ (B.6)

Cell H11: $\qquad \dfrac{F11}{760} \cdot 10^6 \qquad\qquad\qquad\qquad\qquad\quad$ (B.7)

Cell F18: $\qquad \dfrac{H11 \cdot G8}{G7 + G8} \qquad\qquad\qquad\qquad\qquad$ (B.8)

Cell G18: $\qquad \dfrac{D18 - C18}{E11 - D11} \cdot H11 \qquad\qquad\qquad\quad$ (B.9)

Cell G28: $\qquad SLOPE\big[(G18 : G22), (C27 : C31)\big] \qquad$ (B.10)

Cell I28: $\qquad SLOPE\big[(G18 : G22), (E27 : E31)\big] \qquad$ (B.11)

Cell G29: $\qquad INTERCEPT\big[(G18 : G22), (C27 : C31)\big] \qquad$ (B.12)

Cell I29: $\qquad INTERCEPT\big[(G18 : G22), (E27 : E31)\big] \qquad$ (B.13)

Cell G31: $\dfrac{B5 - G29}{G28}$ (B.14)

Cell I31: $\dfrac{B5 - I29}{I28}$ (B.15)

Cell G40: $SLOPE\big[(A39 : A50), (C39 : C50)\big]$ (B.16)

Cell I40: $SLOPE\big[(A39 : A50), (E39 : E50)\big]$ (B.17)

Cell G41: $INTERCEPT\big[(A39 : A50), (C39 : C50)\big]$ (B.18)

Cell I41: $INTERCEPT\big[(A39 : A50), (E39 : E50)\big]$ (B.19)

Cell G43: $\dfrac{G40 - G31}{G41}$ (B.20)

Cell I343: $\dfrac{I40 - I31}{I41}$ (B.21)
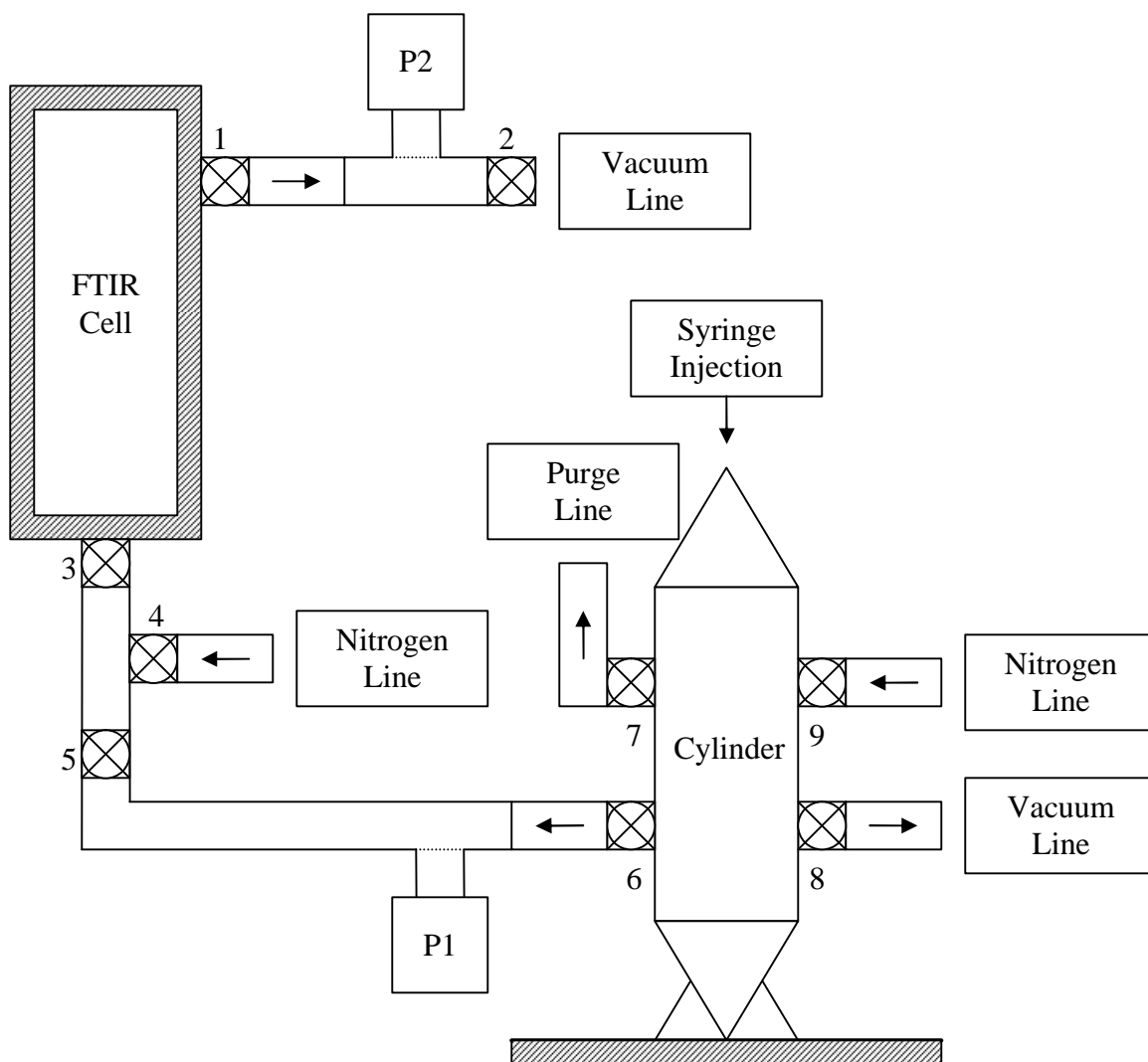
Figure B.1 Double Injection Calibration Apparatus

	A	B…E	F	G	H
1	Run by:		Fuel Density:	800	[kg/m3]
2	Time:	12:00			
3	Date:		Temperature:	280	[°C]
4	Fuel:	JP-8			
5	Desired PPM:	775	MW fuel:	153	[kg/kmol]
6	File Location:	fuelcal*.spc			
7	File Name:		Volume TANK:	500	[ml]
8			Volume FTIR:	600	[ml]

	A	B	C	D	E	F	G	H
9	sample	Vol Inj.	P TANK	P TANK	P TANK	?P	?P TANK	PPM
10	#	[µl]	Initial	Final 1	Final 2	TANK	Ideal	TANK
11	1	5	31	32.9	790	1.9	1.8	2500
12	2	7.5	31.1	33.9	791	2.8	2.7	3684
13	3	10	31	34.6	790	3.6	3.6	4737
14	4	12.5	31.2	35.6	791	4.4	4.5	5789
15	5	2.5	30.8	32	790	1.2	0.9	1579

	A	B	C	D	E	F	G
16	sample	Vol Inj.	P FTIR	P FTIR	P FTIR	PPM FTIR	PPM FTIR
17	#	[µl]	Initial	Final 1	Final 2	Ideal	Actual
18	1	5	6.2	301	760	1364	973
19	2	7.5	6.3	301.8	761	2010	1438
20	3	10	6.2	301.4	760	2584	1851
21	4	12.5	6.4	301.9	761	3158	2265
22	5	2.5	5.7	301.3	763	861	616

Figure B.2 FTIR Calibration Sheet – Part I

184

	A	B	C	D	E	F	G	H	I
25	sample	Peak	Peak 1	Peak	Peak 2	Absorbance Interpolated Values			
26	#	Wave1	Absorb	Wave2	Absorb				
27	1	2881.8	0.3176	1468.4	0.1121	Peak 1	Peak1	Peak 2	Peak2
28	2	2881.8	0.5281	1468.4	0.1857	Slope	2541	Slope	7348
29	3	2881.8	0.7034	1468.4	0.2448	Intercept	94.90	Intercept	78.40
30	4	2881.8	0.8386	1468.4	0.2924				
31	5	2881.8	0.2222	1468.4	0.0788	Absorb	1.0968	Absorb	0.3815
32	6	2881.8		1468.4					
33	7	2881.8		1468.4					
34	8	2881.8		1468.4					
35	9	2881.8		1468.4					
36	10	2881.8		1468.4					

	A	B	C	D	E	F	G	J	K
37	Flow	Peak	Peak 1	Peak	Peak 2	Flow Rate Interpolated Values			
38	ml/min	Wave1	Absorb	Wave2	Absorb				
39	0.70	2881.8	0.1908	1468.4	0.0654	Peak 1	Peak1	Peak 2	Peak2
40	0.70	2881.8	0.1959	1468.4	0.0674	Slope	3.6284	Slope	10.382
41	0.70	2881.8	0.1961	1468.4	0.0685	Intercept	-0.005	Intercept	0.0073
42	0.80	2881.8	0.2199	1468.4	0.0760				
43	0.80	2881.8	0.2233	1468.4	0.0776	Flow Rate	0.975	Flow Rate	0.991
44	0.80	2881.8	0.2211	1468.4	0.0768				
45	0.90	2881.8	0.2526	1468.4	0.0839				
46	0.90	2881.8	0.2515	1468.4	0.0850				
47	1.00	2881.8	0.2760	1468.4	0.0939				
48	1.00	2881.8	0.2769	1468.4	0.0959				
49	1.05	2881.8	0.2914	1468.4	0.1013				
50	1.05	2881.8	0.2884	1468.4	0.1017				

Figure B.3 FTIR Calibration Sheet – Part II

APPENDIX C – LIQUID FUELS AND REACTANT GASES

The experiments reported in this work were performed using gas phase mixtures of oxygen, nitrogen, and fuel. The high pressure (2200 psig), extra dry, oxygen was delivered via a bank of four 200 lb cylinders supplied by BOC Gases with a 2.6^{TM} grade. The minimum certified purity for this grade is 99.6%. The liquid nitrogen was delivered via a bank of four NILG 165 350 IR tanks supplied by BOC Gases. The nitrogen delivery system has been redesign to support on-line tank switching capability. Four Swagelock-Whitey SS-26VM8-F8 stainless steel integral bonnet needle valves with a pressure rating of 6000 psig have been added to the original design. Each valve controls the nitrogen flow to/from one tank allowing replacing any empty or low-pressure tank at any moment during an experiment. This capability is particularly useful for experiments conducted at elevated pressure since a tank pressure of at least 2 atm higher than the reactor pressure is required to ensure a constant flow during the experiment. In fact, any fluctuation in the nitrogen flow would result into a change of the reactor pressure and, in turn, into unreliable values of CO production. A schematic of the nitrogen delivery system is presented in Figure C.1. Finally, all the fuels used in this work are listed in Table C.1, including the fuel supplier, the fuel identification number (CAS #), the purity grade and the cost. All the reported fuel costs are quotations as of January 2002. Due to the elevated cost of isocetane, for this fuel two quotations have been listed in Table C.1, one from Sigma-Aldrich (the actual supplier) and the other from TCI America .

All the liquid fuels where supplied by Sigma-Aldrich, not including JP-8 which was supplied by Phillips Chemical Company. The essential information for JP-8 (hydrocarbon class, tests) is listed in Table C.2 from the Certificate of Analysis reported by Phillips Chemical Company – Specialty Chemicals Division.

Table C.1 List of Liquid Fuels and Suppliers

FUEL	CAS #	SUPPLIER	GRADE	COST
N-HEPTANE	142-82-5	ALDRICH	99%	$30 /l
N-DODECANE	112-40-3	ALDRICH	99+% ANHYDROUS	$160 /l
2,2,4,4,6,8,8 HEPTAMETHYLNONANE	4390-04-9	ALDRICH	98%	$450 /l
2,2,4,4,6,8,8 HEPTAMETHYLNONANE	4390-04-9	TCI	96+% GC	$460 /l
METHYLCYCLOHEXANE	180-87-2	ALDRICH	99+% ANHYDROUS	$80 /l
DECALIN (MIX. OF TRANS & CIS)	91-17-8	ALDRICH	98%	$55 /l
a-METHYLNAPHTHALENE	90-12-0	ALDRICH	95%	$130 /l
HEXYLBENZENE	1077-16-3	ALDRICH	97%	$1200 /l
JP-8	–	PHILLIPS CHEMICAL COMPANY	–	$65 /l

Table C.2 JP-8 Certificate of Analysis – Phillips Chemical Company

TEST	RESULT	SPECIFICATION	METHOD
SPECIFIC GRAVITY 60/60 °F	0.7955	0.775-0.840	ASTM D-4052
API GRAVITY	46.4	37.0-51.0	ASTM D-1298
TOTAL SULFUR, WT%	0.01	0.30 MAX	ASTM D-2622
MERCAPTAN SULFUR, WT%	0.0001	0.002 MAX	ASTM D-3227
FLASH POINT, °F	124	100 MIN	ASTM D -93
FREEZE POINT, °F	-53.5	-53 MAX	ASTM D-2386
SMOKE POINT, mm	27	25.0 MIN	ASTM D-1322
VISCOSITY, cst @-20°C	6.9	8 MAX	ASTM D-445
HYDROGEN CONTENT, WT%	14.89	13.4 MIN	ASTM D-3701
MSEP	98	70 MIN	ASTM D-3948
NET HEAT OF COMBUSTION (Btu/lb)	18,649	18,400 MIN	ASTM D-3338
PARTICULATES (mg/l)	0.5	1 MAX	ASTM D-2276
DISTILLATION POINTS, °F	RESULT	SPECIFICATION	METHOD
ISP	341	–	ASTM D-86
10%	364	401 MAX	ASTM D-86
50%	398	–	ASTM D-86
90%	456	–	ASTM D-86
EP	504	572 MAX	ASTM D-86
HYDROCARBON TYPE, VOL%	RESULT	SPECIFICATION	METHOD
AROMATICS	16.1	25 MAX	ASTM D-319
OLEFINS	1.	5 MAX	ASTM D-319
SATURATES	82.9	–	ASTM D-319
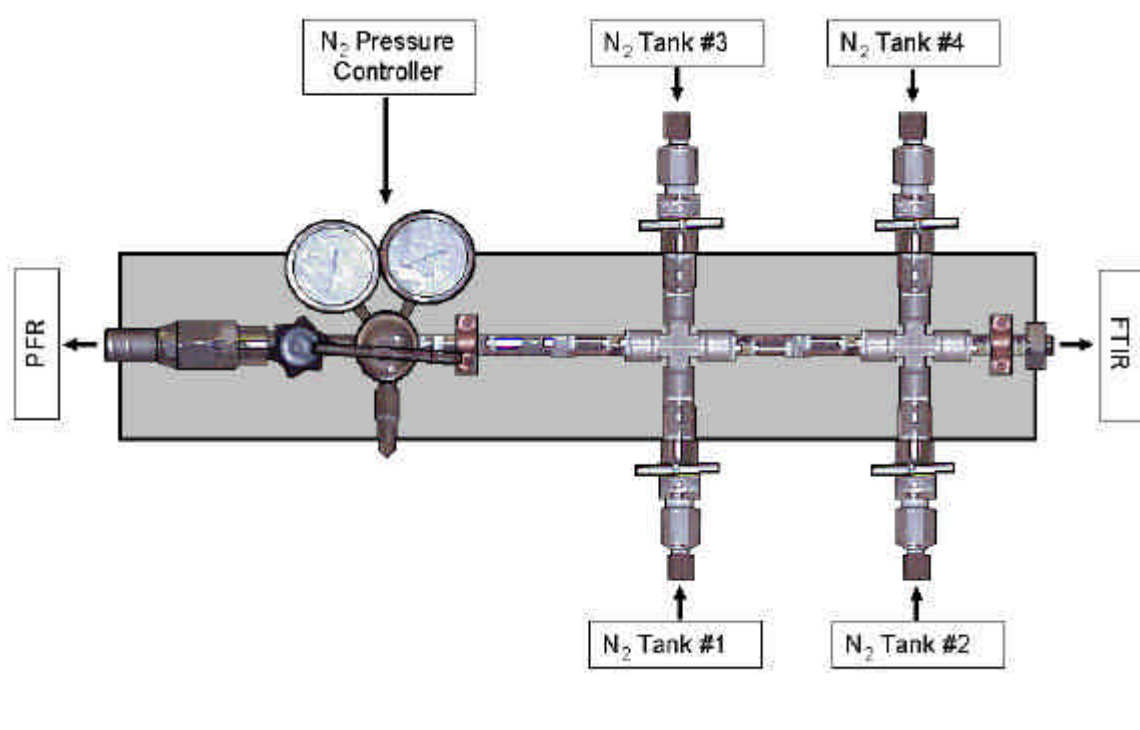
Figure C.1 Nitrogen Delivery System

APPENDIX D – EXPERIMENTAL MATRIX

Table D.1 Experimental Matrix

# EXPERIMENT	NH-1	NH-2	ND-1	ND-2	ND-3	MN-1	MN-2	MN-3	MN-4	MN-5	MC-1	MC-2	MC-3	MC-4
Fuel	N-HEPTANE	N-HEPTANE	N-DODECANE	N-DODECANE	N-DODECANE	aMETHYLNAPHTHALENE	aMETHYLNAPHTHALENE	aMETHYLNAPHTHALENE	aMETHYLNAPHTHALENE	aMETHYLNAPHTHALENE	METHYLCYCLOHEXANE	METHYLCYCLOHEXANE	METHYLCYCLOHEXANE	METHYLCYCLOHEXANE
# C ATOMS	7	7	12	12	12	11	11	11	11	11	7	7	7	7
# H ATOMS	16	16	26	26	26	10	10	10	10	10	14	14	14	14
CETANE NUMBER	56	56	88	88	88	0	0	0	0	0	20	20	20	20
CETANE NUMBER (BLENDING)	–	–	90	90	90	0	0	0	0	0	36	36	36	36
PRESSURE, [atm]	8	8	8	8	8	8	8	8	8	12	8	8	8	8
EQUIVALENCE RATIO	0.4	0.4	0.3	0.25	0.2	0.3	0.3	0.5	0.7	0.7	0.3	0.4	0.6	0.7
RESIDENCE TIME [ms]	100	100	120	120	120	120	175	120	215	250	120	120	120	120
NITROGEN DILUTION, [%]	85	85	80	80	80	80	70	80	65	65	80	80	70	65
NITROGEN FUEL, [%]	20	20	20	20	20	20	20	20	20	20	20	20	20	20
OXYGEN, [%]	16	16	16	16	16	16	16	16	16	16	16	16	16	16
R_X, [K]	705	705	703	693	694	–	–	–	–	–	–	–	–	–
R_Y, [ppm]	945	950	1660	1270	750	–	–	–	–	–	–	–	–	–
R_1, [K]	636	623	~610	~613	624	–	–	–	–	–	–	–	–	–
R_2, [K]	768	770	>800	~800	792	–	–	–	–	–	–	–	–	–
FUEL MOLAR FRACTION, [ppm]	1144	1144	680	567	454	932	1398	1553	3798	3798	1199	1598	3588	4878
FUEL VOL. FLOW RATE, [ml/min]	1.48	1.48	1.10	0.85	0.60	0.80	0.80	1.50	2.20	2.20	1.05	1.50	2.00	2.50

# EXPERIMENT		# C ATOMS	# H ATOMS	CETANE NUMBER	CETANE NUMBER (BLENDING)	PRESSURE, [atm]	EQUIVALENCE RATIO	RESIDENCE TIME [ms]	NITROGEN DILUTION, [%]	NITROGEN FUEL, [%]	OXYGEN, [%]	R_X, [K]	R_Y, [ppm]	R_1, [K]	R_2, [K]	FUEL MOLAR FRACTION, [ppm]	FUEL VOL. FLOW RATE,[ml/min]
IC-1	ISOCETANE	16	34	15	33	8	0.7	180	65	15	16	–	–	–	–	2906	2.40
DC-1	DECALIN	10	18	48	–	8	0.3	120	80	20	16	696	560	656	724	868	0.80
DC-2	DECALIN	10	18	48	–	8	0.4	120	80	20	16	700	850	651	726	1157	1.10
J8-1	JP-8	11	21	–	–	8	0.3	120	80	20	16	692	500	632	755	775	1.05
J8-2	JP-8	11	21	–	–	8	0.4	120	80	20	16	694	730	630	763	1030	1.40
J8-3	JP-8	11	21	–	–	12	0.3	120	80	20	16	690	870	612	786	775	1.05
S1-1	SURROGATE S1	11.4	21.4	45	53	8	0.3	120	80	20	16	698	750	630	775	751	1.00
S2-1	SURROGATE S2	11.1	20.2	37	45	8	0.3	120	80	20	16	700	520	640	767	780	1.00
S3-1	SURROGATE S3	11.3	20.5	38	46	8	0.3	120	80	20	16	695	550	635	765	767	1.00
S4-1	SURROGATE S4	11.4	20.7	37	46	8	0.3	120	80	20	16	694	560	634	761	760	1.00
S5-1	SURROGATE S5	11.5	20.9	34	45	8	0.3	120	80	20	16	691	490	632	760	753	1.00
S5-2	SURROGATE S5	11.5	20.9	34	45	8	0.4	120	80	20	16	694	750	632	764	1004	1.40
S5-3	SURROGATE S5	11.5	20.9	34	45	12	0.3	120	80	20	16	692	860	620	782	753	1.00

# Experiment	Mixture	# C Atoms	# H Atoms	Cetane Number	Cetane Number (Blending)	Pressure, [atm]	Equivalence Ratio	Residence Time [ms]	Nitrogen Dilution, %	Nitrogen Fuel, [%]	Oxygen, [%]	R_X, [K]	R_Y, [ppm]	R_1, [K]	R_2, [K]	Fuel Molar Fraction, [ppm]	Fuel Vol. Flow Rate, [ml/min]
M1-1	Mixture M1	14.1	30.3	44		8	0.3	120	70	20	16	697	1050	603	798	870	1.00
M1-2	Mixture M1	14.1	30.3	44		8	0.3	120	80	20	16	694	460	628	767	580	1.00
M2-1	Mixture M2	8.2	17	45		8	0.3	120	70	20	16	706	2200	630	771	1516	1.05
M2-2	Mixture M2	8.2	17	45		8	0.3	120	80	20	16	700	1150	641	754	1011	1.05
M3-1	Mixture M3	11.4	16.3	45		8	0.3	120	70	20	16	700	1030	627	>800	1220	0.90
M3-2	Mixture M3	11.4	16.3	45		8	0.3	120	80	20	16	696	480	642	780	814	0.90
M4-1	Mixture M4	13.1	24.8	45		8	0.3	120	80	20	16	694	600	626	783	652	1.00
M5-1	Mixture M5	13.6	27.6	45		8	0.3	120	80	20	16	694	570	621	779	614	1.00
M6-1	Mixture M6	11.1	20.2	37		8	0.3	120	80	20	16	700	520	640	767	780	1.00
M7-1	Mixture M7	11.3	20.5	37		8	0.3	120	80	20	16	695	550	635	765	767	1.00
M8-1	Mixture M8	11.4	21.4	45		8	0.3	120	80	20	16	698	750	630	775	751	1.00
M9-1	Mixture M9	11.7	21.8	45		8	0.3	120	80	20	16	696	700	624	776	784	1.00